

# Methods of Improving the Performances of HF Digital Radio Systems

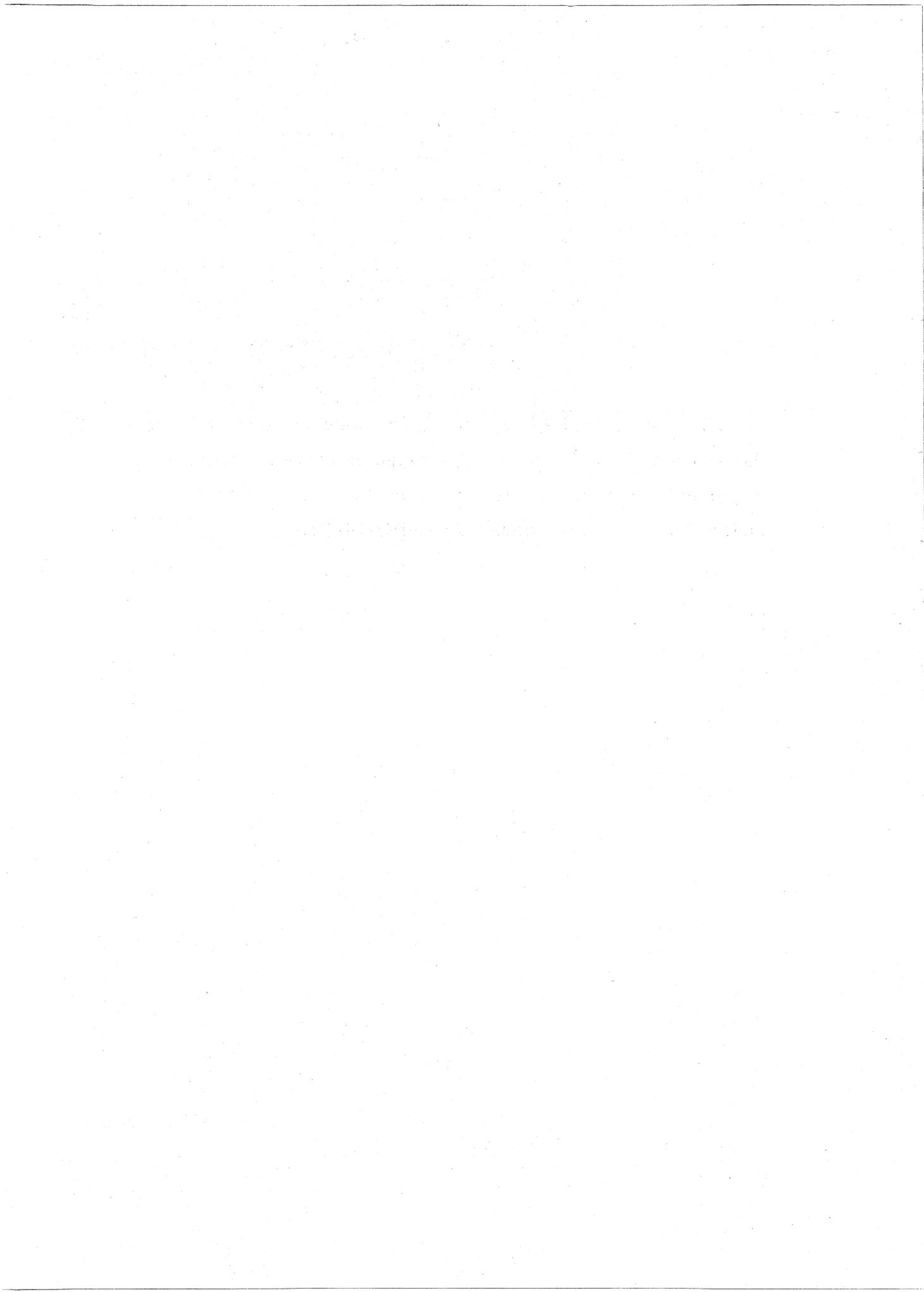
C.C. Watterson



**U.S. DEPARTMENT OF COMMERCE**  
**Juanita M. Kreps, Secretary**

Henry Geller, Assistant Secretary  
for Communications and Information

October 1979



## PREFACE

The work described in this report was done for and with the support of the U.S. Army Communications-Electronics Engineering Installation Agency, Fort Huachuca, Arizona, under Project Order Number CCC-PO-14-78.



## TABLE OF CONTENTS

	<u>Page</u>
PREFACE	iii
LIST OF FIGURES	vi
LIST OF TABLES	vii
ABSTRACT	1
1. INTRODUCTION	1
2. HF DIGITAL RADIO SYSTEMS	3
3. TRANSMITTER	9
3.1 Error Coder	9
3.2 Modulator	10
3.3 HF Transmitter	29
3.4 Transmitting Antenna	31
4. HF CHANNEL	35
4.1 Propagation Characteristics	35
4.2 Channel Model	39
5. RECEIVER	46
5.1 Receiving Antenna	46
5.2 HF Receiver	47
5.3 Demodulator	49
5.4 Error Decoder	68
5.5 Diversity Operation	72
5.6 Performance Monitoring and Prediction	74
6. SYSTEM PERFORMANCES	76
6.1 Additive Distortions	77
6.2 Multiplicative Distortions	90
6.3 Nonlinear Distortions	108
7. PERFORMANCE IMPROVEMENTS	113
7.1 System Design	113
7.2 System Operation	121
8. SUMMARY AND CONCLUSIONS	122
9. RECOMMENDATIONS	127
10. ACKNOWLEDGEMENTS	127
11. REFERENCES	127

## LIST OF FIGURES

<u>Figure</u>	<u>Page</u>
1. Basic HF digital radio system.	4
2. Examples of amplitudes of trains of complex pulses.	14
3. Examples of single-filter complex keying values.	17
4. Orthonormal parabolic cylinder waveforms.	21
5. Pulse distributions in frequency and time with M-ary ASK, PSK, and APSK.	22
6. Pulse distributions in frequency and time with binary FSK.	25
7. Pulse distributions in frequency and time with binary CPK.	27
8. Typical HF exciter.	30
9. Hypothetical ionograms.	36
10. Maximum differential delay versus relative operating frequency for HF channels.	38
11. Maximum differential delay versus distance for HF channels.	38
12. HF channel model.	40
13. Path-gain spectrum.	43
14. Hypothetical channel scatter function.	43
15. Typical HF receiver.	48
16. Portions of demodulators for pulse train $\lambda$ .	50
17. Characteristics of matched-filter system with binary PSK under ideal conditions.	53
18. Matrices for soft decoding of a (25,16) block code.	70
19. Bit-error-probability performances of matched-filter ASK, PSK, FSK, and CPK systems over a slow, frequency-flat, Rayleigh-fading channel with white thermal noise.	80
20. Bit-error-probability performances of matched-filter coherent binary and quaternary PSK systems over slow, frequency-flat, independently Rayleigh-fading diversity channels with independent white thermal noise and maximal-ratio combining.	87
21. Bit-error-probability performances of nonmatched-filter, frequency-multiplexed, time-differentially coherent, quaternary PSK systems with and without (25,16) soft error-correcting coding over a slow, frequency-flat, Rayleigh-fading channel with white thermal noise.	89

<u>Figure</u>	<u>Page</u>
22. Perspective plot of the magnitude of the response of a detector with guard time to a rectangular pulse.	93
23. Contour plot of the magnitude of the response of a detector with guard time to a rectangular pulse.	94
24. Perspective plot of the magnitude of a hypothetical detector response with zero total derivatives as well as zeros at the locations of undesired pulses in a system with frequency-multiplexed pulse trains.	98
25. Example of coherence multiplicative distortions in the succeeding demodulator pulse samples in a single-filter ASK, PSK, or APSK system with $K_{\lambda}(l) = 1$ in the absence of additive and crosstalk multiplicative distortions.	99
26. Bit-error-probability performances of nonmatched-filter, frequency-multiplexed, time-differentially coherent, quaternary PSK systems over a frequency-flat, Rayleigh-fading channel.	102
27. Bit and block error-probability performances of the USC-10, ACQ-6, and MX-190 frequency-multiplexed, time-differentially coherent, quaternary PSK modems over a two-path, frequency-selective, Rayleigh-fading channel.	109

#### LIST OF TABLES

<u>Table</u>	<u>Page</u>
1. Permutations of N bits	11
2. Keying methods for various bit-decision methods	58
3. Channel and equipment distortions	78



# METHODS OF IMPROVING THE PERFORMANCES OF HF DIGITAL RADIO SYSTEMS

Clark C. Watterson\*

The bit-error-probability performances of HF digital radio systems with respect to channel and equipment additive, multiplicative, and nonlinear distortions are evaluated with respect to the nine system design features that affect the performances. The system design features are the fundamental pulse waveform, the keying method (ASK, PSK, APSK, FSK, and CPK), the multiplexing method (frequency and concentric multiplexing), the type of demodulator filter (matched and nonmatched non-adaptive filters and quasi-static and dynamic adaptive filters), the detection method (coherent, partially coherent, differentially coherent, and noncoherent), the transmitter power, the antennas, diversity, and error coding. Spectral efficiency (information rate/signal bandwidth) is also evaluated. The best combination of system design features is determined.

Key Words: Adaptive filtering, additive distortion, APSK, ASK, bit error probability, bit error rate, channel model, coding, coherent, CPK, detection, differentially coherent, digital, distortion, diversity, error rate, fading, FSK, HF, ionosphere, keying, modem, multipath, multiplexing, multiplicative distortion, noncoherent, nonlinear distortion, partially coherent, performance, PSK, radio, spectral efficiency.

## 1. INTRODUCTION

For a number of decades, HF ionospheric radio has been a reasonably simple and effective method of communicating over a very large range of distances: from less than 100 miles (the upper limit of the range of VHF and UHF line-of-sight radio) to many thousands of miles (world-wide). HF radio has been particularly useful where cable communication is impossible or impractical: for communication with aircraft, ships, and other mobile units; and for communication with temporary and remote

---

\*The author is with the Institute for Telecommunication Sciences, National Telecommunications and Information Administration, U.S. Department of Commerce, Boulder, Colorado 80303.

ground stations.

In recent years, the rapid development of SHF satellite radio has provided an alternate method of communication with mobile units and remote ground stations over the same large range of distances. Because SHF satellite radio can be competitive in cost and is usually superior in performance and reliability, it almost certainly will replace HF ionospheric radio as the predominant mode of long-distance communication with mobile units and remote ground stations.

Despite its usual superiority, however, SHF satellite radio is greatly inferior to HF ionospheric radio in one respect: in military communications under wartime conditions, it is (or probably will be) much more susceptible to destruction by an enemy. For this reason, the armed forces need to retain an efficient and reliable capability in HF ionospheric radio as a backup to the more vulnerable SHF satellite radio. It is therefore important to improve the performance and reliability of HF ionospheric radio communication.

During the past three decades, the development and use of transistors and integrated circuits has substantially improved the weight, power requirements, and reliability of HF radio equipment. However, little has been done to reduce or overcome the performance degradations imposed by multipath, fading, interference, and other types of channel distortions characteristic of HF radio. While the general replacement of AM (amplitude modulation) with SSB (single sideband) has improved analog voice communications, essentially no improvements have been made in signal processing techniques in digital communications: The same FSK (frequency-shift keying) and PSK (phase-shift keying) techniques introduced some decades ago are still in universal use, and despite the development of effective error-detecting/correcting coding techniques, the armed forces have made little use of this improvement in HF digital radio systems.

The performance and reliability of HF digital radio can be very substantially improved by the development and use of a number of improved signal processing techniques. The present availability of integrated circuits

in general and microprocessors in particular make the application of such techniques very practical. With this in mind, the purpose of the present report is to present general and detailed descriptions of HF digital radio systems that include classifications and descriptions of system design features, HF ionospheric channel characteristics, and the types of channel and equipment distortions that degrade system performance; to relate the equipment design features to the various types of channel and equipment distortions to determine the best methods of improving system performance; and to present suitable conclusions and recommendations.

## 2. HF DIGITAL RADIO SYSTEMS

The functional form of a basic HF digital radio system is illustrated in Figure 1. The system consists of three major parts: the transmitter on the left, the HF ionospheric channel at the top, and the receiver on the right. In general, the transmitter consists of an error coder, a modulator, an HF transmitter, and an antenna, while the receiver consists of an antenna, an HF receiver, a demodulator, and an error decoder. Unlike the other parts of the transmitter and receiver, the error coder and error decoder are optional; most military HF digital radio systems at present do not use them.

Regardless of its actual format, the digital information to be transmitted can be viewed as a binary sequence of information bits,  $b_1(i)$ , with values of zero or one that occur at a constant rate,  $f_1$ . With error coding, the transmitter input binary information sequence,  $b_1(i)$ , is delivered to an encoder. The encoder uses the information bits to generate additional check bits in a manner determined by an encoding algorithm. The information and check bits are combined to form an encoder output binary data sequence,  $b_2(j)$ , that is delivered to the modulator. The binary data sequence,  $b_2(j)$ , has values of zero or one that occur at a constant rate,  $f_2$ , that is greater than  $f_1$  because of the introduction of the check bits.

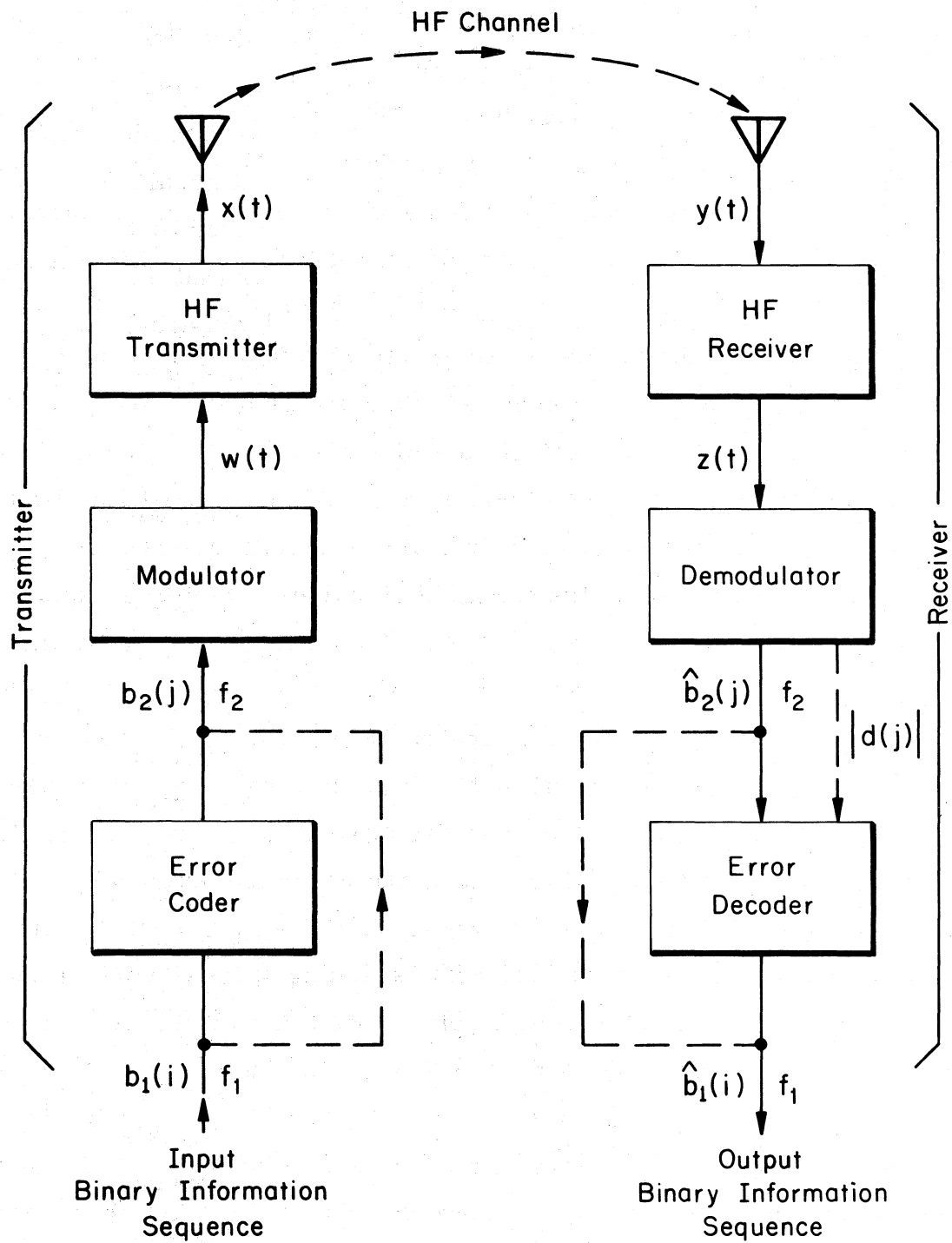


Figure 1. Basic HF digital radio system.

When error coding is not used, the information bits are delivered directly to the modulator, as shown by the dashed line in Figure 1.

The modulator generates one or more trains of IF pulses that are multiplexed and transmitted simultaneously over separate subchannels. The pulses may have any shape and time spacing, but usually are adjoining rectangular pulses. Each pulse is keyed or selected by the data sequence from a set of two or more pulse waveforms that differ in amplitude, phase, frequency, or other waveshape characteristics. In nearly all systems, the number of selectable pulse waveforms is an integral power of two. Each keyed or selected pulse via its distinctive waveform then carries an integral number of data bits, usually one or two.

The one or more trains of low-level keyed IF pulses,  $w(t)$  in Figure 1, are delivered by the modulator to an HF transmitter. The HF transmitter frequency translates the trains of IF pulses (which are usually generated in the ELF band) to the desired frequency in the HF band, and filters and amplifies the resulting trains of HF pulses to a suitably higher power level. The higher power trains of HF pulses,  $x(t)$ , are delivered by the HF transmitter to the transmitting antenna which radiates them. The radiated trains of HF pulses constitute the HF transmitted signal.

The HF transmitted signal travels to the receiving antenna by reflection from the ionosphere. Because the HF signal generally propagates to the receiving antenna over several fading paths (involving one or more reflections from several layers in the ionosphere), it arrives at the receiving antenna in a distorted form. The receiving antenna also receives noise and sometimes interference (unwanted signals) in the same frequency band as the signal that constitute additional channel distortion components. The aggregate (signal and distortion components),  $y(t)$  in Figure 1, is delivered by the antenna to an HF receiver that is tuned to the signal band. The receiver amplifies the aggregate to a higher power level suitable for subsequent processing, it filters the aggregate to exclude out-of-signal-band noise and interference, and it frequency-translates the aggregate to restore nominally the signal pulse trains to

the intermediate frequencies at which they were generated in the modulator. The amplified, filtered, and frequency-translated aggregate,  $z(t)$ , is delivered by the HF receiver to the demodulator.

In the demodulator, the trains of distorted IF signal pulses are separated by suitable band-pass filters. Each train of pulses is then sampled (detected) at the pulse rate to obtain an estimate of the amplitude, the phase, or the amplitude and phase of each signal pulse. In general, each pulse sample differs from the true value of the signal pulse because of the various types of signal distortion that are introduced by the channel and equipment. Each pulse sample is delivered to a bit decider which, for each data bit carried by the pulse, decides whether a zero or one bit was transmitted. The data-bit decisions are delivered at the output of the demodulator. Regardless of the data-bit format, the decisions can be viewed as a binary data sequence,  $\hat{b}_2(j)$ , of zero or one values that occur at a constant rate,  $f_2$ . Ideally, the binary data sequence at the demodulator output,  $\hat{b}_2(j)$ , is identical to the binary data sequence at the modulator input,  $b_2(j)$  in Figure 1. Practically, however, it differs [is an estimate of  $b_2(j)$ ], because of binary errors introduced in the bit-decision process by the channel and equipment distortions.

In an HF digital radio system that does not incorporate error coding, the binary data sequence from the demodulator,  $\hat{b}_2(j)$ , is delivered directly as the receiver output binary information sequence,  $\hat{b}_1(i)$ , as shown by the dashed line in Figure 1. In a system that does incorporate error coding,  $\hat{b}_2(j)$  is delivered to a decoder, as illustrated. The magnitudes of the pulse samples,  $|d(j)|$ , that are obtained in the demodulator sometimes are also delivered to the decoder. The decoder then processes  $\hat{b}_2(j)$ , and sometimes  $|d(j)|$ , using a suitable decoding algorithm, to detect and correct binary errors. The decoder delivers the receiver output binary information sequence,  $\hat{b}_1(i)$ , that is an estimate of the transmitter input binary information sequence,  $b_1(i)$ . In general,  $\hat{b}_1(i)$  differs from  $b_1(i)$  because of uncorrected errors. However,  $\hat{b}_1(i)$  has a lower error probability with error coding than without, except at high error probab-

ities; i.e., the error coding improves the overall system performance.

In some duplex (two-way) systems with error detection, the receiver via the return transmitter-receiver link may ask for a repeat of some portion of the transmission when errors are detected.

Some HF digital radio systems use space diversity to improve the system performance. With space diversity, the receiver in the basic system of Figure 1 is expanded to include two or more parallel antennas and HF receivers that drive a single demodulator designed for such multiple inputs.

The sources of signal distortion that produce bit errors are:

#### Sources of Signal Distortion

- (1) Transmitter
  - (a) Modulator
  - (b) HF transmitter
- (2) HF channel
- (3) Receiver
  - (a) HF receiver
  - (b) Demodulator

In general, each source may introduce several types of distortion. The distortions introduced by the transmitter are usually small and not significant. The HF channel distortions can be substantial, however, and are of primary importance. While the distortions introduced by the receiver may not be larger than the distortions introduced by the transmitter, their effects on system bit-error-probability performance can be much greater under some channel conditions, and their presence should not be ignored. The system performance is dependent not only on the types and magnitudes of the distortions, but is also dependent on the system design features: the fundamental pulse waveform, the type of keying, the multiplexing technique, the receiver filtering, the bit-decision (detection) method, the transmitter power, the antennas, the

order and type of diversity, and the type of error coding.

The signal distortions introduced by the transmitter and receiver (equipment distortions) can be classified as follows:

#### Types of Equipment Distortion

- (1) Additive
  - (a) Noise
    - (i) Thermal
    - (ii) Quantizing
  - (b) Interference (internal)
- (2) Multiplicative
  - (a) Time scatter (frequency selective)
    - (i) Synchronization
    - (ii) Filtering
  - (b) Frequency scatter (time selective)
    - (i) Doppler correction
    - (ii) AGC (automatic gain control)
- (3) Nonlinear

Synchronization distortion and filtering distortion are classified as time-scatter distortions because synchronization distortion is produced by a nonoptimum allowance for or correction of the signal delay or translation in time, while filtering distortion is produced by a nonoptimum spreading or stretching of the signal pulses in time by the filtering. In an analogous way, Doppler-correction distortion is produced by a nonoptimum allowance for or correction of signal Doppler shift or translation in frequency, while AGC distortion is produced when the AGC modulates the signal, generates sidebands, and thus spreads the signal in frequency.

The channel distortions are classified later.

The preceding brief preliminary description of a basic HF digital radio system is expanded with more detailed descriptions and evaluations in the following three sections: the transmitter design features and

distortions in Section 3, the HF channel characteristics and distortions in Section 4, and the receiver design features and distortions in Section 5. The effects of the system design features on system performance are then determined in Section 6 for the various types of channel and equipment distortions. The optimum system design features are selected in Section 7, and suitable conclusions and recommendations are presented in Sections 8 and 9. In doing this, the goal was to be as comprehensive as possible, so as to include all factors that have a significant effect on HF digital system performance, but at the same time, to keep the descriptions as brief as practical for the present purpose of evaluating methods of improving HF digital radio system performance.

### 3. TRANSMITTER

#### 3.1 Error Coder

With error coding, the transmitter input binary information sequence,  $b_1(i)$ , is delivered to the encoder at rate  $f_1$ . The encoder combines the information bits with additional check bits, according to some coding algorithm, and delivers a binary data sequence,  $b_2(j)$ , at rate  $f_2 > f_1$ , as illustrated in Figure 1, p. 4. The coding ratio,

$$r_c = \frac{f_1}{f_2} < 1, \quad (1)$$

is one measure of the efficiency of the coding technique.

There are two major types of error codes:

#### Types of Error Codes

- (1) Block
- (2) Convolutional

In a block code, successive sets of  $n_i$  adjacent information bits in  $b_1(i)$  are each combined with  $n_c$  check bits to form a block (set) of size

$$n_b = n_i + n_c \text{ bits} \quad (2)$$

In each block, the  $n_c$  check bits are generated from the  $n_i$  information bits according to the encoding algorithm, and are combined with the unaltered information bits to form the block of  $n_b$  bits. If the information bit sequence,  $b_1(i)$ , contains independent bits, then the successive encoded blocks in the output data sequence,  $b_2(j)$ , are independent.

In a convolutional code, the generation of each bit in the encoder output data sequence,  $b_2(j)$ , is determined by the previous  $n_c$  check bits, as well as  $n_i$  of the most recent information bits, according to the encoding algorithm. The convolutional code then has a constraint length,  $n_b$ . However, unlike the block code, each data bit in  $b_2(j)$  is dependent on all preceding data bits, even with independent information bits in  $b_1(i)$ . However, the dependence decreases for an increasing number of past data bits beyond the constraint length,  $n_b$ .

Because error encoders are digital equipments, they introduce no distortion.

### 3.2 Modulator

The modulator generates one or more trains of IF pulses. When more than one train of pulses is used, the several trains, numbered

$$\lambda = 0, 1, 2, \dots, \Lambda-1 \quad (3)$$

are transmitted simultaneously over separate subchannels, using either frequency multiplexing or concentric multiplexing. With frequency multiplexing, the pulse trains have different center frequencies, and with concentric multiplexing, the pulse trains have a common center frequency, as explained later. The input binary data sequence,  $b_2(j)$ , is commutated in the modulator to the  $\Lambda$  generators of the IF pulse trains. Each generator receives a binary sequence,  $b_{3\lambda}(k)$  for the  $\lambda$ th generator, with a recurrence rate that is  $1/\Lambda$  times the recurrence rate of  $b_2(j)$ . In the  $\lambda$ th IF pulse-train generator, each successive set of  $N$  adjacent bits in

$b_{3\lambda}(k)$  is used in effect to select one of

$$M = 2^N \quad (4)$$

different available pulse waveforms for transmission. Let

$$m = 0, 1, 2, \dots, M \quad (5)$$

be an integer that numbers the available pulse waveforms. Then each of the  $M$  available pulse waveforms

corresponds to one of  $M$  possible permutations of the  $N$  bits, as

Table 1. Permutations of  $N$  bits

illustrated by the examples in

Table 1. Consequently, each transmitted pulse, by means of its distinctive waveform, carries

$N$  bits of data. In nearly all HF

digital radio systems,  $N$  is an

integer (usually one or two)

and will be so considered in

this report.

m	N = 1	N = 2	N = 3
0	0	00	000
1	1	01	001
2		11	011
3		10	010
4			110
5			111
6			101
7			100

The  $\Lambda$  trains of IF pulses generated by the modulator constitute the real IF bandpass signal output from the modulator. The real bandpass signal can be specified by

$$\psi(t) = \text{Re}[w(t)\exp(j2\pi f_r t)] \quad (6)$$

where  $f_r$  is an arbitrary reference frequency, usually in or near the IF signal band, and

$$w(t) = w'(t) + jw''(t) \quad (7)$$

is the complex envelope of the signal. The real band-pass signal then is

$$\psi(t) = w'(t)\cos(2\pi f_r t) - w''(t)\sin(2\pi f_r t) \quad (8)$$

which contains two quadrature reference (carrier) components,  $\cos(2\pi f_r t)$  and  $\sin(2\pi f_r t)$ , multiplied (amplitude modulated) by two real baseband functions,  $w'(t)$  and  $w''(t)$ , that are the components of the complex envelope,  $w(t)$  in (7). If  $w_\lambda(t)$  is the complex envelope of the  $\lambda$ th pulse train relative to  $f_r$ , then

$$w(t) = \sum_{\lambda=0}^{\Lambda-1} w_\lambda(t) \quad . \quad (9)$$

In the remainder of the report, the signal and the channel and equipment processing imposed on it will be described by complex-envelope functions.

All of the  $\Lambda$  pulse trains,  $\{w_\lambda(t)\}$ , are obtained by frequency multiplexing or concentrically multiplexing a set of  $\Lambda$  basic pulse trains,  $\{\bar{w}_\lambda(t)\}$ . The basic pulse trains are generated from a common set of  $M$  available basic pulse waveforms,  $\{p_m(t)\}$ , each of which is generally complex and, in practice, of finite duration. Let

$$p_m(t) = a_m(t) \exp[j\alpha_m(t)] \quad (10)$$

be the  $m$ th available basic pulse waveform, where  $a_m(t)$  and  $\alpha_m(t)$  are the real amplitude and phase components, and  $P_m(f)$ , the Fourier transform of  $p_m(t)$ , is centered on  $f_c = 0$ . Then for each basic pulse train, successive sets of  $N$  bits in  $b_{3\lambda}(k)$  are used to select basic pulse waveforms from  $\{p_m(t)\}$  to form the  $\lambda$ th basic pulse train,

$$\bar{w}_\lambda(t) = \sum_{\ell} p_{m_\lambda(\ell)}(t - \ell T) \quad , \quad (11)$$

where  $\ell$  is an integer that numbers the pulses, and  $T$  is the time spacing of adjacent pulses. The subscript  $m$  for the  $m$ th available pulse in (10) is replaced by  $m_\lambda(\ell)$  in (11) to indicate the value of  $m$  is generally different in each basic pulse train and changes with  $\ell$ .

There are an infinite variety of pulse waveforms from which  $M$  basic

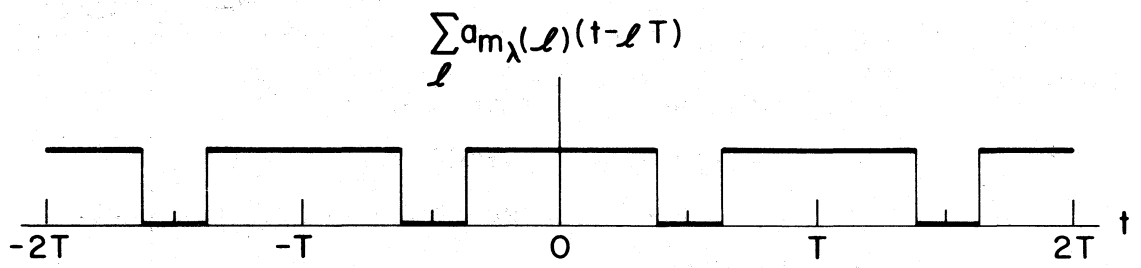
pulse waveforms,  $\{p_m(t)\}$ , can be chosen for use in an HF digital radio system. The possible designs of  $\{p_m(t)\}$  can be classified in terms of the pulse duration,  $\tau_p$ , relative to the adjacent pulse spacing,  $T$ :

#### Types of Pulse Waveforms

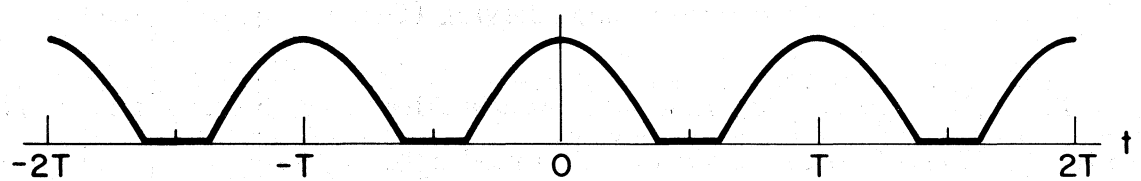
- (1) Spaced ( $\tau_p < T$ )
- (2) Adjoining ( $\tau_p = T$ )
- (3) Overlapping ( $\tau_p > T$ )

Examples of the three types of pulse waveforms are illustrated by their amplitude components in Figure 2. In the examples, the pulse amplitude function is the same for all illustrated values of  $\ell$ . This is not necessary, of course; the  $M$  members may have different amplitude functions. For each pulse amplitude function,  $a_m(t)$ , there is an infinite variety of phase functions that might be used for  $\alpha_m(t)$ . Most past and present HF digital radio systems use adjoining pulses with rectangular amplitude functions and constant phase functions, primarily because they are easiest to generate. However, other pulse functions can provide better overall system performance.

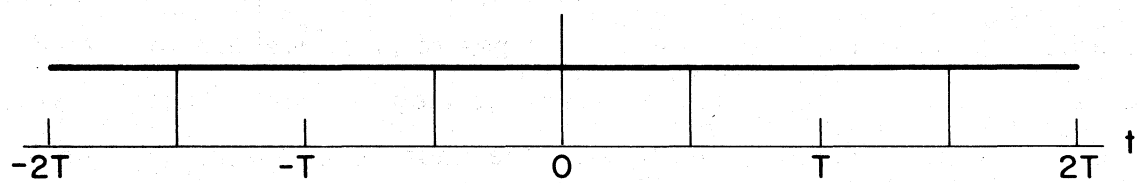
In the generation of each basic pulse train,  $\bar{w}_\lambda(t)$  in (11), when  $N$  adjacent data bits in  $b_{3\lambda}(k)$  are used in effect to select one of  $M$  available pulse waveforms,  $p_m(t)$ , for transmission, the selection can be viewed as a keying process: the data bits in effect key (switch) the values of one or more waveform parameters to change the pulse waveform, or key (select) one of  $M$  stored waveforms. The possible methods of keying a pulse can be classified as follows:



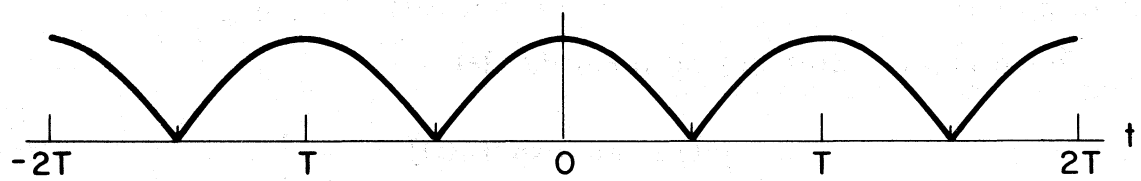
(a) Spaced Rectangular Pulses



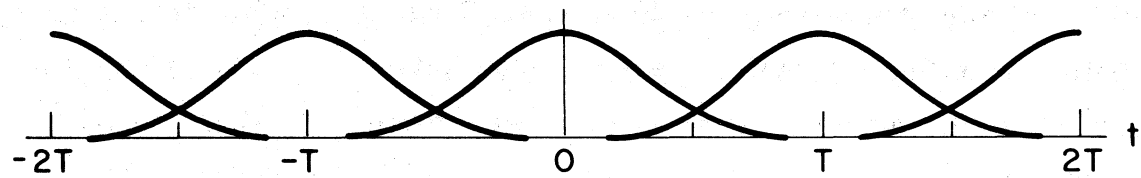
(b) Spaced Nonrectangular Pulses



(c) Adjoining Rectangular Pulses



(d) Adjoining Nonrectangular Pulses



(e) Overlapping Nonrectangular Pulses

Figure 2. Examples of amplitudes of trains of complex pulses.

## Keying Methods

- (1) Single filter
  - (a) Amplitude-scale keying (ASK)
  - (b) Phase-shift keying (PSK)
  - (c) Amplitude-and-phase-shift keying (APSK)
- (2) Multiple filter
  - (a) Frequency-shift keying (FSK)
  - (b) Concentric-pulse keying (CPK)

The two major keying methods, single filter and multiple filter, refer to the number of filters used in the demodulator to separate each train of pulses from the other  $\Lambda-1$  pulse trains and from noise and interference that is outside the signal pulse train frequency band. Any of the keying methods may be used with any of the types of pulse waveforms listed earlier. It is convenient and desirable to view the single-filter keying methods as fundamental, and to view the multiple-filter keying methods as modifications of one single-filter keying method: ASK. Therefore, the single-filter keying methods will be described first, and then the multiple-filter keying methods will be considered.

In the single-filter keying methods, let

$$p(t) = a(t)\exp[j\alpha(t)] \quad (12)$$

be a generally complex fundamental pulse waveform, where  $a(t)$  and  $\alpha(t)$  are real amplitude and phase functions. Then in each single-filter keying method, the fundamental pulse waveform,  $p(t)$ , is modified in  $M$  different ways to form the set of  $M$  basic pulse waveforms,  $\{p_m(t)\}$ . With amplitude-scale keying,

$$p_m(t) = k_m p(t) = k_m a(t)\exp[j\alpha(t)] \quad , \quad \text{ASK} \quad , \quad (13)$$

where  $k_m$  is one of  $M$  different positive real keying numbers. With ASK, the  $m$ th basic pulse waveform,  $p_m(t)$ , is therefore obtained by multiplying

the fundamental pulse waveform,  $p(t)$ , with a positive real number,  $k_m$ , that scales its amplitude component,  $a(t)$ . The term "amplitude-shift keying" is often used, but generally is incorrect because  $a(t)$  is not shifted by the addition of  $k_m$ , but is scaled by the multiplication of  $k_m$ . When rectangular pulses are used, "amplitude-shift keying" can be correctly used if a rectangular time function,  $k_m(t)$ , with a duration and timing identical to  $a(t)$ , is added to  $a(t)$  to shift it only during the pulse period,  $\tau_p$ . This is not possible with nonrectangular pulse waveforms, however.

With phase-shift keying,

$$p_m(t) = \exp(j\kappa_m) p(t) = a(t) \exp\{j[\alpha(t) + \kappa_m]\} \quad , \quad \text{PSK} \quad , \quad (14)$$

where

$$-\pi < \kappa_m \leq \pi \quad \text{radians} \quad (15)$$

is one of  $M$  different real phase keying values. With PSK, the  $m$ th basic pulse waveform,  $p_m(t)$ , is therefore obtained by multiplying the fundamental pulse waveform,  $p(t)$ , with a unit-magnitude complex number that shifts its phase component,  $\alpha(t)$ , by an amount  $\kappa_m$ .

With amplitude-and-phase-shift keying,

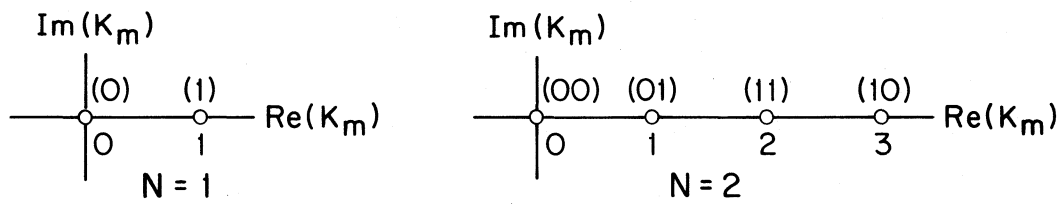
$$p_m(t) = K_m p(t) = k_m a(t) \exp\{j[\alpha(t) + \kappa_m]\} \quad , \quad \text{APSK} \quad , \quad (16)$$

where

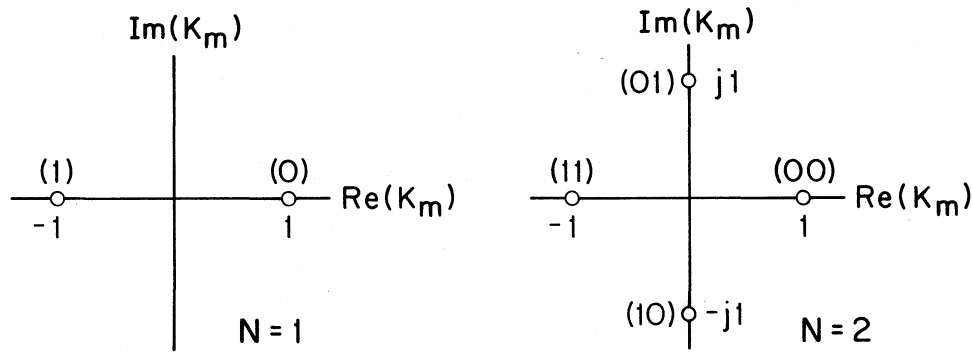
$$K_m = k_m \exp(j\kappa_m) \quad (17)$$

is one of  $M$  different complex numbers. With APSK, the  $m$ th basic pulse waveform,  $p_m(t)$ , is therefore obtained by multiplying the fundamental pulse waveform,  $p(t)$ , with a complex number,  $K_m$ , that in general scales its amplitude component,  $a(t)$ , and shifts its phase component,  $\alpha(t)$ . It can be seen that ASK and PSK are special cases of APSK: with ASK,  $\kappa_m = 0$  for all  $m$ , and with PSK,  $k_m = 1$  for all  $m$ .

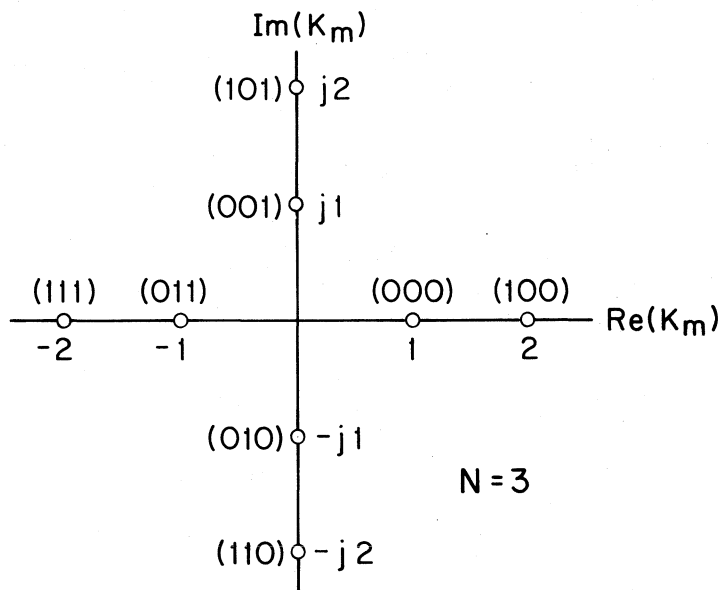
The three single-filter keying methods are illustrated in Figure 3. For each of the three keying methods, the  $M = 2^N$  possible keying values,



(a) Amplitude - Scale Keying (ASK)



(b) Phase - Shift Keying (PSK)



(c) Amplitude - and - Phase - Shift Keying (APSK)

Figure 3. Examples of single-filter complex keying values.

$\{K_m\}$ , are illustrated by circles in the complex plane for various values of  $N$ , the number of bits/pulse. The numbers in parentheses are the permutations of the  $N$  data bits corresponding to each keying value. For  $N > 1$ , the permutations are usually assigned to the keying values so that the most closely spaced pairs of keying values differ in only one bit; otherwise the system performance would be poorer. In Figure 3(a), the  $N=1$  example is simple on-off keying. In Figure 3(b), the  $N=1$  example is binary (bi-phase) PSK, while the  $N=2$  example is quaternary (four-phase) PSK. In Figure 3(c), the  $N=3$  example makes use of two amplitudes and four phases. The  $N=3$  example can be extended to  $N=4$  by incorporating eight additional complex keying values with magnitudes of 1 and 2 at angles of  $\pm 45^\circ$  and  $\pm 135^\circ$ , or also by forming a square  $4 \times 4$  matrix of keying values centered on  $K_m = 0$ . For any  $N$ , the choice of keying values is arbitrary, but the best performance is usually obtained when the spacing of the values is maximized for a given average power of the keying values.

In the single-filter keying methods, the successive keying values in each train of pulses form a generally complex  $M$ -ary sequence,  $K_\lambda(\ell)$ , where  $\lambda$  specifies the pulse train and  $\ell$  numbers the pulses in the train. For each value of  $\ell$ ,  $K_\lambda(\ell)$  may have any one of the  $M$  values in  $\{K_m\}$ . The  $\lambda$ th basic pulse train,  $\bar{w}_\lambda(t)$  in (11), then becomes

$$\bar{w}_\lambda(t) = \sum_{\ell} K_\lambda(\ell) p(t-\ell T) \quad , \quad \text{ASK, PSK, APSK} \quad . \quad (18)$$

In some PSK and APSK systems, the direct keying sequence,  $K_\lambda(\ell)$ , is replaced by a phase-differential keying sequence,  $K_{\lambda\Delta}(\ell)$ . Three types of phase-differential keying are possible: time-differential (TD) keying, which can be used with single or multiple frequency-multiplexed or concentrically multiplexed pulse trains; frequency-differential (FD) keying, which can be used only with multiple frequency-multiplexed pulse trains; and concentric-differential (CD) keying, which can be used only with multiple concentrically multiplexed pulse trains.

In time-differential keying, which is widely used in PSK systems, the direct keying sequence,  $K_\lambda(t)$ , is replaced by the time-differential keying sequence,

$$K_{\lambda\Delta}(t) = K_\lambda(t) \exp[j\kappa_{\lambda\Delta}(t-1)] \quad , \quad \text{TD} \quad ; \quad (19)$$

i.e., the  $t$ th value in the direct keying sequence,  $K_\lambda(t)$  [generated from  $b_{3\lambda}(k)$ ], is advanced in phase by  $\kappa_{\lambda\Delta}(t-1)$ , the phase of the preceding differential keying value, to generate  $K_{\lambda\Delta}(t)$ , which is used to key the  $t$ th pulse.

In frequency-differential keying and concentric-differential keying, which are little used, the direct keying sequence,  $K_\lambda(t)$ , is replaced by the frequency-differential or concentric-differential keying sequence,

$$K_{\lambda\Delta}(t) = K_\lambda(t) \exp[j\kappa_{(\lambda-1)\Delta}(t)] \quad , \quad \text{FD, CD} \quad ; \quad (20)$$

i.e., the  $t$ th value in the direct keying sequence,  $K_\lambda(t)$ , is advanced in phase by  $\kappa_{(\lambda-1)\Delta}(t)$ , the phase of the concurrent differential keying value in the adjacent  $(\lambda-1)$ th basic pulse train, to generate  $K_{\lambda\Delta}(t)$ , which is used to key the  $t$ th pulse in the  $\lambda$ th basic pulse train. The  $\lambda = 0$  pulse train can carry no frequency-differentially keyed or concentric-differentially keyed data, although it still might carry data that is directly or time-differentially keyed. A distinction is made between frequency-differential and concentric-differential keying because they result in different system performances under some channel conditions.

The  $\lambda$ th pulse train,  $w_\lambda(t)$  in (9), is obtained by frequency multiplexing or concentrically multiplexing the pulses in the  $\lambda$ th basic pulse train,  $\bar{w}_\lambda(t)$  in (18). If  $m_\lambda$  specifies the multiplexing operation for  $\bar{w}_\lambda(t)$ , then

$$w_\lambda(t) = \sum_{\ell} m_\lambda [K_\lambda(\ell) p(t-\ell T)] = \sum_{\ell} K_\lambda(\ell) m_\lambda [p(t-\ell T)] \quad . \quad (21)$$

With frequency multiplexing, the basic pulse trains are frequency translated so that the center frequencies of their spectrums have equal

adjacent spacings,  $F$ . Given the fundamental pulse waveform,  $p(t)$ ,  $F$  is chosen so that the  $\Lambda$  trains of pulses in  $w(t)$  can be adequately separated by suitable filtering in the demodulator. With frequency multiplexing, (21) becomes

$$w_{\lambda}(t) = \sum_{\ell} K_{\lambda}(\ell) \exp\{j2\pi[\lambda - (\Lambda - 1)/2] Ft\} p(t - \ell T) \quad (22)$$

when the spectrum of  $w(t)$  is centered on  $f_c = 0$ .

With concentric multiplexing, the spectrums of the  $\Lambda$  pulse trains,  $\{w_{\lambda}(t)\}$ , have a common center frequency,  $f_c = 0$ . Concentric multiplexing can be illustrated with parabolic cylinder functions (Jahnke et al., 1960). Let the fundamental pulse waveform be a real Gaussian function,

$$p(t) = \exp\left[-c\Lambda\pi\left(\frac{t}{T}\right)^2\right] \quad (23)$$

Then (21) becomes

$$w_{\lambda}(t) = \frac{(2c\Lambda)^{1/4}}{(\lambda! T)^{1/2}} \sum_{\ell} K_{\lambda}(\ell) H_{e\lambda}\left[2\sqrt{c\Lambda\pi}\frac{(t - \ell T)}{T}\right] p(t - \ell T) \quad (24)$$

where

$$H_{e\lambda}(x) = (-1)^{\lambda} \exp\left(\frac{x^2}{2}\right) \frac{d^{\lambda}}{dx^{\lambda}} \exp\left(-\frac{x^2}{2}\right) \quad (25)$$

is the  $\lambda$ th Hermite polynomial. Given  $\Lambda$  and  $T$ , the parameter  $c$  can be adjusted to control the overlapping of successive pulses. The  $\Lambda$  concentric pulse waveforms for  $\ell = 0$  in (24) are illustrated in Figure 4 for  $c = 2$ ,  $\Lambda = 8$ , and  $K_{\lambda}(0) = 1$ . Because the  $\Lambda$  parabolic cylinder waveforms are an orthonormal set, the  $\Lambda$  pulse trains,  $\{w_{\lambda}(t)\}$ , can be separated by matched filters in the demodulator.

With single-filter keying (ASK, PSK, and APSK) and frequency multiplexing, the pulses in the  $\Lambda$  trains in  $w(t)$  are distributed in frequency and time as illustrated in Figure 5(a) for  $\Lambda = 4$  pulse trains. Each rectangle represents one pulse carrying  $N$  bits of data, as shown. The effective

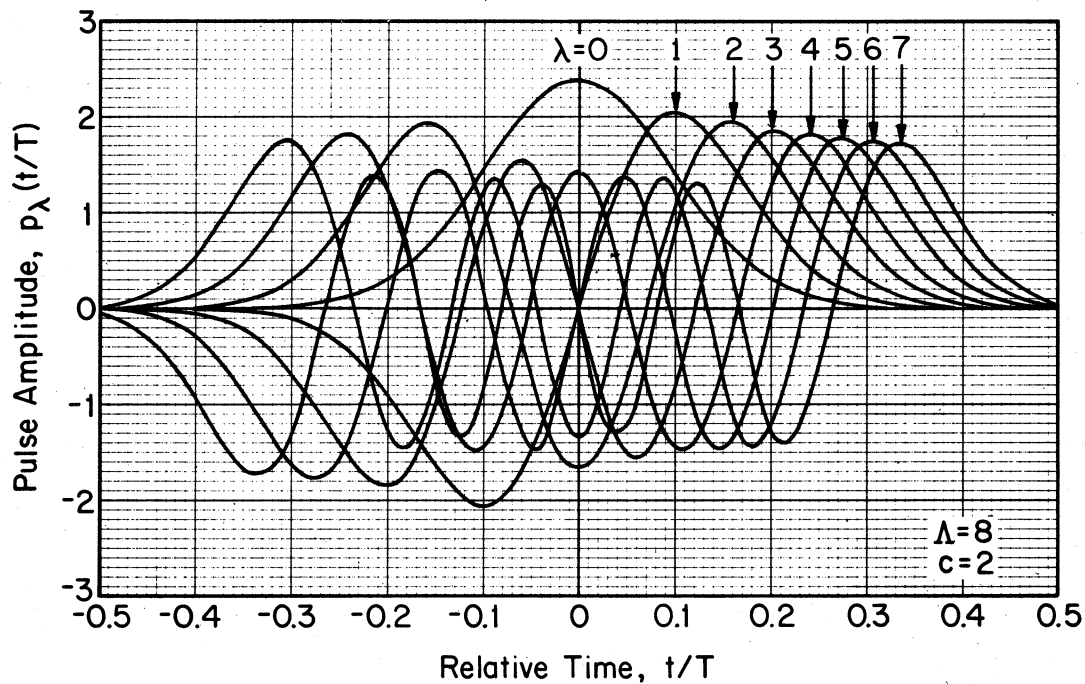


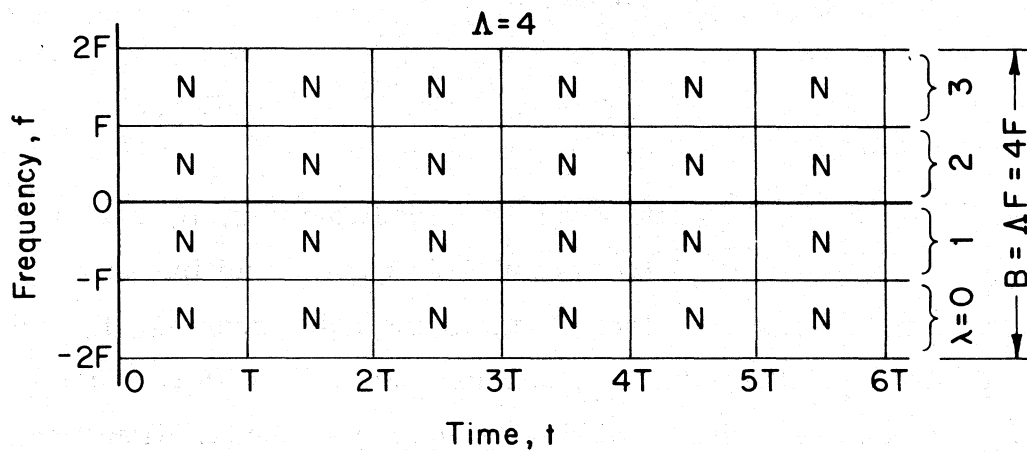
Figure 4. Orthonormal parabolic cylinder waveforms.

bandwidth of each pulse is  $F$ , the height of each rectangle, while the effective duration of each pulse is  $T$ , the width of each rectangle.

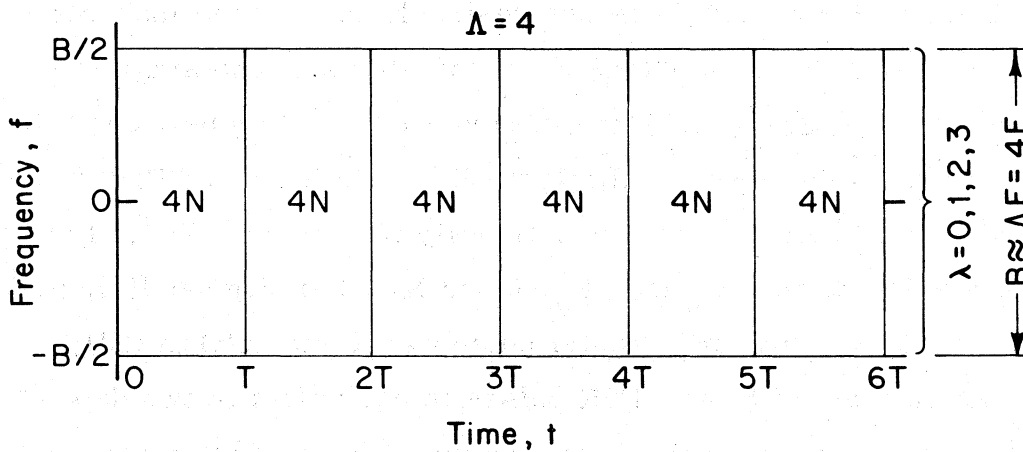
Let the spectral efficiency of the signal,  $w(t)$ , be defined as the ratio of the information rate,  $f_1$ , carried by  $w(t)$ , to the bandwidth of  $w(t)$ . Then with single-filter keying and frequency multiplexing, Figure 5(a) shows that  $w(t)$  carries  $f_2 = \Lambda N/T$  data bits/second in a bandwidth  $B = \Lambda F$ . Therefore, the spectral efficiency with single-filter keying and frequency multiplexing is

$$\eta_f = \frac{r_c N}{FT} \quad , \quad \text{ASK, PSK, APSK} \quad . \quad (26)$$

With single-filter keying and concentric multiplexing, the pulses in the  $\Lambda$  trains in  $w(t)$  have a common center frequency,  $f_c = 0$ , as described in the discussion of (23)-(25). Consequently, their spectrums occupy some central portion or all of a frequency band,  $B$ , centered on  $f = 0$ , as



(a) Frequency-Multiplexed Pulse Trains



(b) Concentrically-Multiplexed Pulse Trains

Figure 5. Pulse distributions in frequency and time with M-ary ASK, PSK, and APSK.

illustrated in Figure 5(b) for  $\Lambda = 4$  pulse trains. Each rectangle represents  $\Lambda$  pulses, concentric in frequency and time, that carry  $\Lambda N$  data bits. Figure 5(b) and (1) show that the spectral efficiency with single-filter keying and concentric multiplexing is

$$\eta_c = \frac{\Lambda r_c N}{BT} \approx \frac{r_c N}{FT} , \quad \text{ASK, PSK, APSK} . \quad (27)$$

The signal bandwidth with concentric multiplexing,  $B$ , may be smaller or larger than the signal bandwidth with frequency multiplexing,  $\Lambda F$ , for the same number of bits/pulse,  $N$ , the same pulse spacing,  $T$ , and the same number of pulse trains,  $\Lambda$ , because generally different basic pulse waveforms are used with the two multiplexing methods. However, if comparable care is given to the design of the basic pulse waveforms in the two multiplexing methods,  $B \approx \Lambda F$  in (27), and  $\eta_c \approx \eta_f$  with single-filter (ASK, PSK, and APSK) keying.

It is informative and therefore desirable to view the multiple-filter keying methods (FSK and CPK) as modifications of one single-filter keying method: binary ASK (on-off keying). FSK can be viewed as a modification of frequency-multiplexed binary ASK, and CPK can be viewed as a modification of concentrically multiplexed ASK. In both cases, the binary ASK keying values,  $K_0 = 0$  and  $K_1 = 1$  in Figure 3(a), p. 17, may be used with any fundamental pulse waveform,  $p(t)$  in (12).

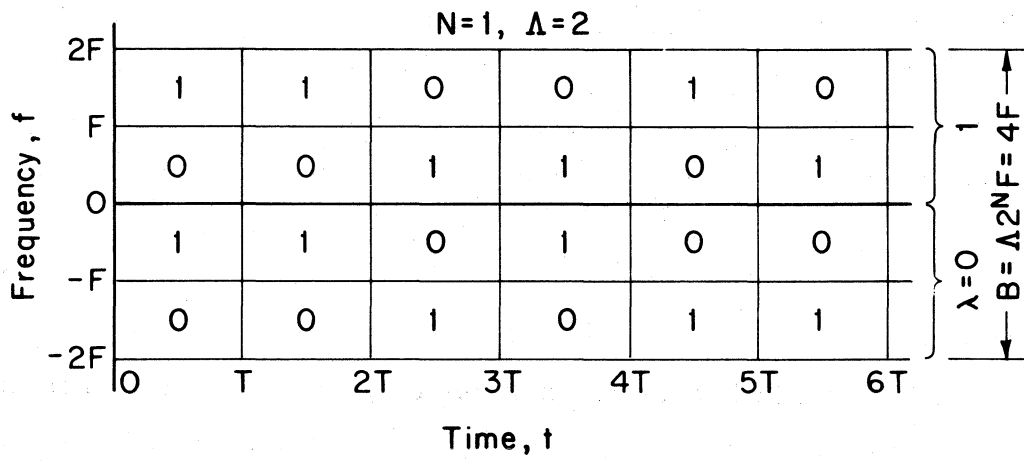
A single train of binary FSK pulses is equivalent to two dependent (redundant) frequency-multiplexed trains of binary ASK pulses, one of which is on while the other is off; i.e., the on-off keying sequence on one binary ASK pulse train is complemented (zeros and ones interchanged) to key the second binary ASK pulse train. When adjoining rectangular pulses are used, and  $FT$  is not an integer, the keying sequence on each binary ASK pulse train in effect is adjusted by a suitable amount on each succeeding pulse if phase continuity is desired at the pulse transition times. However, this is not usually desirable with pulses other than adjoining rectangular pulses.

Figure 6(a) illustrates the frequency and time distributions of the pulses in  $\Lambda = 2$  trains of frequency-multiplexed binary FSK pulses. The lowest two rows of rectangles represent the two binary ASK pulse trains that comprise the  $\lambda = 0$  train of binary FSK pulses, while the upper two rows of rectangles represent the two binary ASK pulse trains that comprise the  $\lambda = 1$  train of binary FSK pulses. The rectangles labeled 1 represent on states (energy present), and the rectangles labeled 0 represent off states (no energy). In each pulse interval,  $T$ , in each binary FSK pulse train,  $\lambda$ , the selected pulse-waveform number,  $m$ , is determined by which of the two frequency-multiplexed binary ASK pulse trains is on. In effect, each on pulse carries  $N = 1$  data bit, as shown, while the off pulses each carry zero data bits. The on-pulse density in the frequency-time domain is one-half.

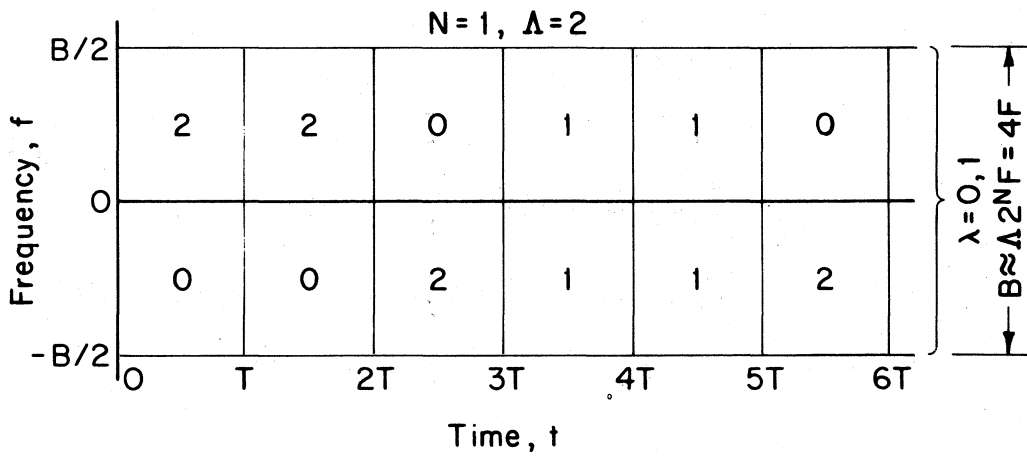
Frequency-multiplexed binary FSK, illustrated in Figure 6(a), can be extended to frequency-multiplexed  $M$ -ary FSK. Each train of  $M$ -ary FSK pulses is equivalent to  $M$  dependent frequency-multiplexed trains of binary ASK pulses, one of which is on while the other  $M-1$  are off for each pulse number,  $\ell$ . For each pulse number,  $\ell$ , in each  $M$ -ary FSK pulse train,  $\lambda$ , the selected pulse-waveform number,  $m$ , is determined by which one of the  $M$  frequency-multiplexed binary ASK pulse trains is on. In effect, as with binary FSK, each on pulse carries  $N$  data bits, while the off pulses carry zero data bits. The on-pulse density in the frequency-time domain is  $1/M$ . Therefore, the spectral efficiency with FSK and frequency multiplexing is

$$\eta_f = \frac{r_c N}{2^{N_{FT}}} , \quad \text{FSK} \quad . \quad (28)$$

Several trains of  $M$ -ary FSK pulses may also be concentrically multiplexed, as illustrated in Figure 6(b) for  $\Lambda = 2$  trains of binary FSK pulse trains. Each row of rectangles represent  $\Lambda = 2$  concentrically multiplexed binary ASK pulse trains. The number in each rectangle specifies the number of concentric pulses that are on in that rectangle, where the 0-1



(a) Frequency-Multiplexed Pulse Trains



(b) Concentrically-Multiplexed Pulse Trains

Figure 6. Pulse distributions in frequency and time with binary FSK.

pattern in the two frequency-multiplexed binary FSK pulse trains in Figure 6(a) are repeated in the two concentrically multiplexed binary FSK pulse trains in Figure 6(b). Each rectangle of area  $BT/M$  in Figure 6(b) carries an average of  $\Lambda N/M$  data bits, so the spectral efficiency with FSK and concentric multiplexing is

$$\eta_c = \frac{\Lambda r_c N}{BT} \approx \frac{r_c N}{2^{N_{FT}}} , \quad \text{FSK} . \quad (29)$$

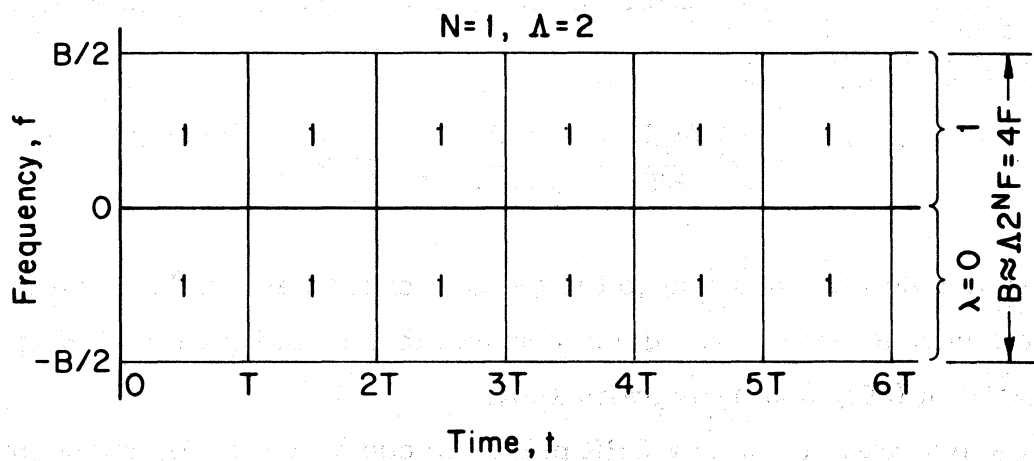
If comparable care is given to the designs of the basic pulse waveforms in the frequency-multiplexed and concentrically multiplexed FSK systems,  $B \approx \Lambda 2^{N_F}$  in (29), and  $\eta_c \approx \eta_f$  with FSK.

A single train of  $M$ -ary CPK pulses is equivalent to  $M$  dependent concentrically multiplexed trains of binary ASK pulses, one of which is on while the other  $M-1$  are off for each pulse number,  $\iota$ . For each pulse number,  $\iota$ , in each  $M$ -ary CPK pulse train,  $\lambda$ , the selected pulse-waveform number,  $m$ , is determined by which one of the  $M$  concentrically multiplexed binary ASK pulse trains is on. In effect, each on pulse carries  $N$  data bits, while the off pulses carry zero data bits. Several trains of CPK pulses, like several trains of FSK pulses, may be frequency multiplexed or concentrically multiplexed. Frequency multiplexing of CPK pulse trains is illustrated in Figure 7(a) for  $\Lambda = 2$  trains of binary CPK pulse trains. The spectral efficiency with CPK and frequency multiplexing is

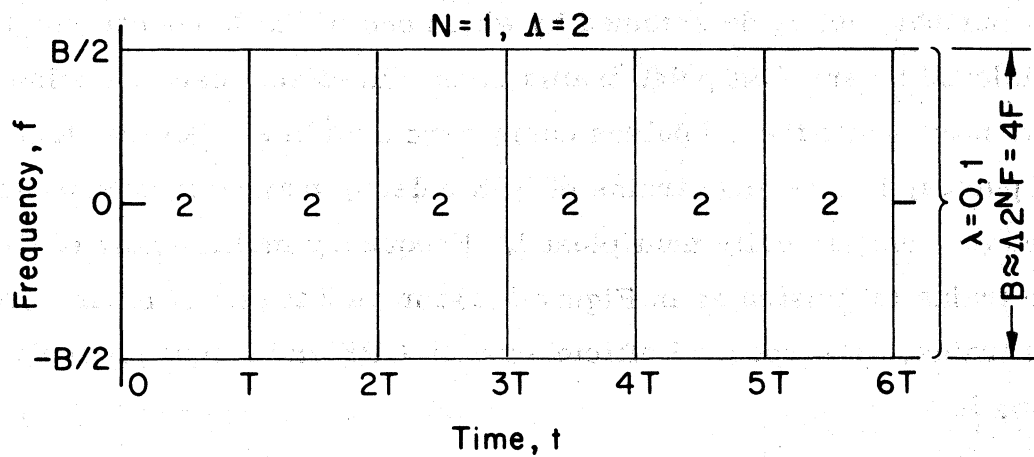
$$\eta_f = \frac{\Lambda r_c N}{BT} \approx \frac{r_c N}{2^{N_{FT}}} , \quad \text{CPK} . \quad (30)$$

Concentric multiplexing of CPK pulse trains is illustrated in Figure 7(b) for  $\Lambda = 2$  trains of binary CPK pulse trains. The spectral efficiency with CPK and concentric multiplexing is

$$\eta_c = \frac{\Lambda r_c N}{BT} \approx \frac{r_c N}{2^{N_{FT}}} , \quad \text{CPK} . \quad (31)$$



(a) Frequency-Multiplexed Pulse Trains



(b) Concentrically-Multiplexed Pulse Trains

Figure 7. Pulse distributions in frequency and time with binary CPK.

A comparison of the spectral efficiencies in (28)-(31) for the multiple-filter keying methods (FSK and CPK) with the spectral efficiencies in (26)-(27) for the single-filter keying methods (ASK, PSK, and APSK) shows that the single-filter keying methods have spectral efficiencies that are  $\sim 2^N = M$  times greater.

Of all of the single-filter and multiple-filter keying methods, binary FSK with adjoining rectangular pulses is most commonly used in HF digital communication systems, with frequency multiplexing when more than one train of pulses is used. Binary and quaternary PSK with adjoining rectangular pulses is second most commonly used, also with frequency multiplexing when more than one train of pulses is used. Other pulse waveforms, other keying methods, and concentric multiplexing are less frequently or rarely used.

In nearly all applications,  $w(t)$  in effect is used to generate a real IF signal,  $\psi(t)$  in (8), p. 11, which is then delivered by the modulator to the HF transmitter for suitable frequency translation to and amplification in the HF band. It is possible, however, to use a double-modulation process in which  $w(t)$  is first used to generate  $\psi(t)$  at a suitably low IF, and then  $\psi(t)$ , rather than being frequency translated to the HF band, is used in turn to modulate the amplitude or phase of a higher IF carrier that is frequency translated to the HF band. While such double-modulation techniques are useful and commonly used in the UHF and SHF bands, they are little used in HF digital communication because their performance is poorer under HF channel conditions. Therefore, double modulation will not be considered further in this report.

The modulator can introduce all of the types of equipment distortion listed on p. 8 except synchronization distortion and Doppler-correction distortion (the latter because it is assumed that any frequency error introduced by the modulator can be compensated or corrected by the Doppler-correction circuit in the demodulator). The modulator always introduces thermal noise; quantizing noise is unavoidably introduced when the modulator incorporates digital processing, as most modern modulators do;

and internal interference (120-Hz power-supply ripple, clocking transients, etc.) is always present. Any filters that are used in the modulator can introduce filtering distortion, the variations in signal level imposed by any AGC circuit introduce at least a small amount of frequency-scatter distortion, and nonlinear distortion is always present. All of the modulator distortions are usually small enough to have negligible effect on the system performance, however, and therefore may be ignored.

### 3.3 HF Transmitter

The one or more trains of low-level keyed IF pulses (the signal) generated in the modulator are delivered to the HF transmitter for frequency translation and amplification. The transmitter typically consists of a low-level HF exciter followed by an HF power amplifier of one or more tuned stages. The exciter translates the signal to the desired frequency in the HF band, and the power amplifier increases the signal power to the desired amount.

A typical HF exciter is illustrated in Figure 8. It consists of an input first-IF amplifier followed by a first frequency converter, a fixed-tuned band-pass higher frequency second-IF amplifier, a second frequency converter, and a tunable output band-pass HF pre-amplifier. The second local-oscillator frequency is adjusted to obtain the desired HF transmitter signal frequency. The band-pass filtering in the second-IF amplifier and the output HF pre-amplifier suppress the unwanted sideband generated by each frequency converter, suppress the local-oscillator components if the balancing of the frequency converters is inadequate, and also suppress any undesired out-of-signal-band higher order intermodulation productions generated by the converters that are not good approximations of true multipliers. The amplification provided by the HF exciter may be controlled manually or by an AGC circuit.

The HF power amplifier which the HF exciter drives may use nonlinear (class-C) tuned amplifier stages when the signal has an envelope

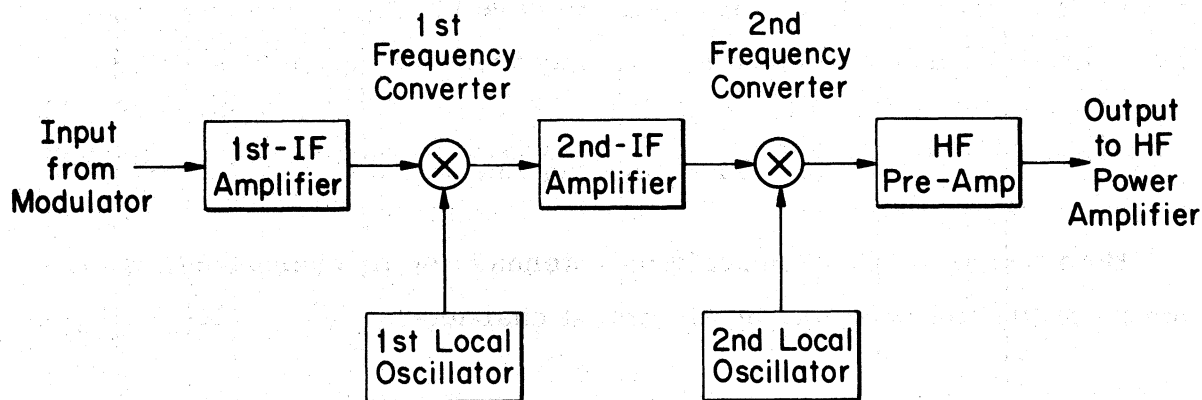


Figure 8. Typical HF exciter.

whose magnitude is constant, because the nonlinear (harmonic) distortion is suppressed by the band-pass filtering. The signal has a constant-magnitude envelope only when a single pulse train is used, and then only when PSK or FSK modulation is used with adjoining rectangular pulses. Otherwise, the power amplifier must be essentially linear (class-A, push-pull class-AB, or push-pull class-B stages) to minimize nonlinear distortion of the filtered signal.

It can be seen that the HF transmitter performs three interleaved primary functions:

#### HF Transmitter Functions

- (1) Frequency translation
- (2) Filtering
- (3) Amplification

In performing these functions, the HF transmitter can introduce all of the types of equipment distortion listed on p. 8 except quantizing noise (provided all-analog circuits are used), synchronization distortion, and Doppler-correction distortion (because it is assumed that any frequency error introduced by the local oscillators in Figure 8 can be compensated or corrected by the Doppler-correction circuit in the demodulator). The HF transmitter

distortions are usually small enough to have negligible effect on the system performance, however, and may therefore be ignored.

### 3.4 Transmitting Antenna

Both transmitting and receiving antennas can be characterized in terms of the following major electrical characteristics:

#### Antenna Characteristics

- (1) Size (in wavelengths)
- (2) Gain
- (3) Bandwidth
- (4) Steering

The electrical size of an antenna can be specified in terms of its maximum dimension in wavelengths: small if less than 0.1 wavelengths, medium for 0.1 to 1.0 wavelengths, and large if more than 1.0 wavelengths. For a given electrical size, the physical size is inversely proportional to frequency. The gain of an antenna relative to a half-wavelength dipole can be rated low up to 3 dB, medium from 3 to 8 dB, and high for more than 8 dB. The bandwidth of an antenna (with fixed tuning) can be rated in terms of the ratio of its high and low 3-dB frequencies: small for ratios up to 1.1, medium for ratios up to 2, and large for higher ratios. The azimuthal electrical or mechanical steering capabilities of an antenna can be rated as none, partial, or complete (360°).

The types of antennas that are commonly used in HF transmitting and receiving applications (Jasik, 1961) are:

## Types of Antennas

- (1) Dipole
- (2) Whip
- (3) Long wire
- (4) V
- (5) Rhombic
- (6) Broadside (curtain)
- (7) End fire (Yagi)
- (8) Log periodic
- (9) Wire /cap/notch (aircraft)

A dipole antenna is typically one-half wavelength in size, horizontally polarized, and easy to install. It has a broad bidirectional azimuthal pattern with low gain. A dipole antenna has a narrow bandwidth, is usually not tuned, and consequently is restricted to a single narrow frequency band in transmitting operation. Mechanically steerable dipoles are practical at frequencies above about 10 MHz, but are rarely used.

A vertical whip antenna, usually used on a vehicle, is physically small and simple to install. It has an omnidirectional, low-gain pattern which is usually desirable in mobile applications. However, it has a small bandwidth, requires tuning to change frequency in the HF band, and can be inefficient (lossy) in the lower frequency end of the HF band.

A long-wire antenna is medium to large in size and usually easy to install. The number of radiation-pattern lobes increases with the length, with the strongest lobes of a straight wire nearest its axis. The strongest lobe gain increases with antenna length and ranges from low to medium. An unterminated long-wire antenna has a small bandwidth, requires tuning, cannot be steered, and has a radiation pattern that changes with frequency.

A V antenna is formed from two straight long-wire antennas that are driven at the apex of the V. The angle of the V is chosen so that the major lobes of the two long-wire legs reinforce each other. A V antenna is medium to large in size, with a gain that ranges from low to medium-large.

An unterminated V antenna has a bidirectional pattern, narrow bandwidth, and requires tuning. A V antenna with proper resistive terminations is unidirectional, has a medium to large bandwidth, but is not practical to steer.

A rhombic antenna, formed by joining two V antennas at their open ends, is driven at one end and terminated by a suitable resistance at the other end. It is large in size, typically several wavelengths per side, and has a unidirectional pattern. It usually has a large gain and medium to large bandwidth, but cannot be steered.

A broadside antenna is formed in general from a matrix (curtain) of driven elements, usually dipoles, in a vertical plane. The elements are driven in phase to form a bidirectional pattern. The antenna can be made unidirectional with greater gain by including a reflecting curtain. A broadside antenna is large in size and has a medium to high gain. It has a narrow bandwidth, is not practical to tune, and consequently is restricted to a single narrow frequency band of operation. Mechanical steering is impractical, but limited electrical steering (beam slewing) is possible.

An end-fire antenna is formed from a number of coplanar elements that are excited to form a pattern with the main lobe in the plane of the elements. It is medium to large in size. The commonest end-fire array is the Yagi antenna, which consists of a set of parallel dipoles. One or more of the elements are driven while the remainder (usually the majority) are parasitically excited by the fields of the driven elements. The lengths of the dipole elements are tapered to form a unidirectional pattern with medium to high gain. An end-fire antenna has a narrow bandwidth, is not practical to tune, and consequently is restricted to a single narrow frequency band of operation. Electrical steering is impractical, but complete ( $360^\circ$ ) mechanical steering is practical at frequencies above about 10 MHz.

A log-periodic antenna is formed from a set of parallel dipole elements whose center form a line. The electrical size and spacing of

adjacent elements change logarithmically along the line, and all of the elements are driven. A log-periodic antenna is medium to large in size and has a medium to high gain. The bandwidth of a log-periodic antenna is approximately equal to the ratio of the size of the largest element at one end of the array to that of the smallest element at the other end. Its bandwidth typically is large and can be made to cover the entire HF band, thus requiring little or no tuning. A log-periodic antenna is not electrically steerable, but complete (360°) mechanical steering is practical if the antenna is designed for frequencies above about 10 MHz.

In HF aeronautical mobile communication, the entire metal aircraft is used as an antenna. Wire, cap, or notch coupling is used to connect the aircraft with the transmitter or receiver. In slower aircraft, wire coupling is obtained by driving an external wire (mounted or trailing) against the aircraft structure. In faster (jet) aircraft, where the aerodynamic drag of an external wire is undesirable, cap or notch coupling can be used. Cap coupling (Granger, 1950) is obtained by driving an electrically insulated portion of the aircraft structure, such as a wing tip or the vertical fin, against the remainder of the structure. Notch coupling (Tanner, 1958) is obtained by driving the open end of a notch in an edge of the metallic aircraft structure, such as the faring in the leading edge of the fin or the fillet in a trailing-edge wing root. The notch is faired with nonconducting material to maintain aerodynamic efficiency. All three types of coupling, wire, cap, and notch, can be made electrically efficient (low loss). The notch, even though a small fraction of a wavelength in size, is efficient because of its location in a high rf current density portion of the aircraft. Aircraft antenna patterns depend on the size and shape of the aircraft relative to the HF wavelength, and consequently change with frequency. Aircraft antennas have low gain, narrow bandwidth, and require tuning. Steering can be accomplished only by turning the aircraft.

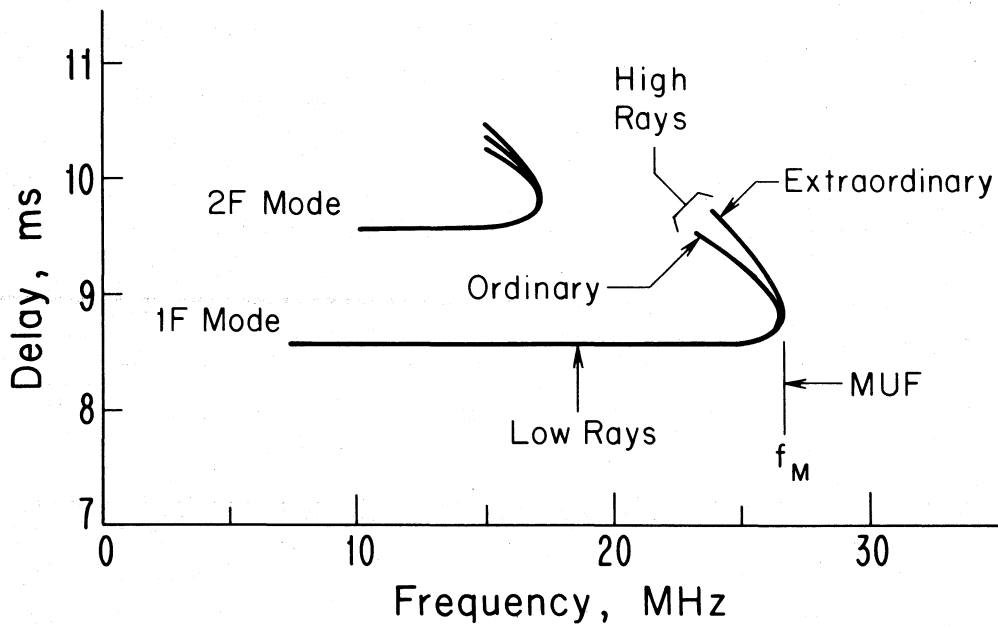
The only equipment distortion that a transmitting antenna introduces is filtering distortion imposed by its generally frequency-selective response.

## 4. HF CHANNEL

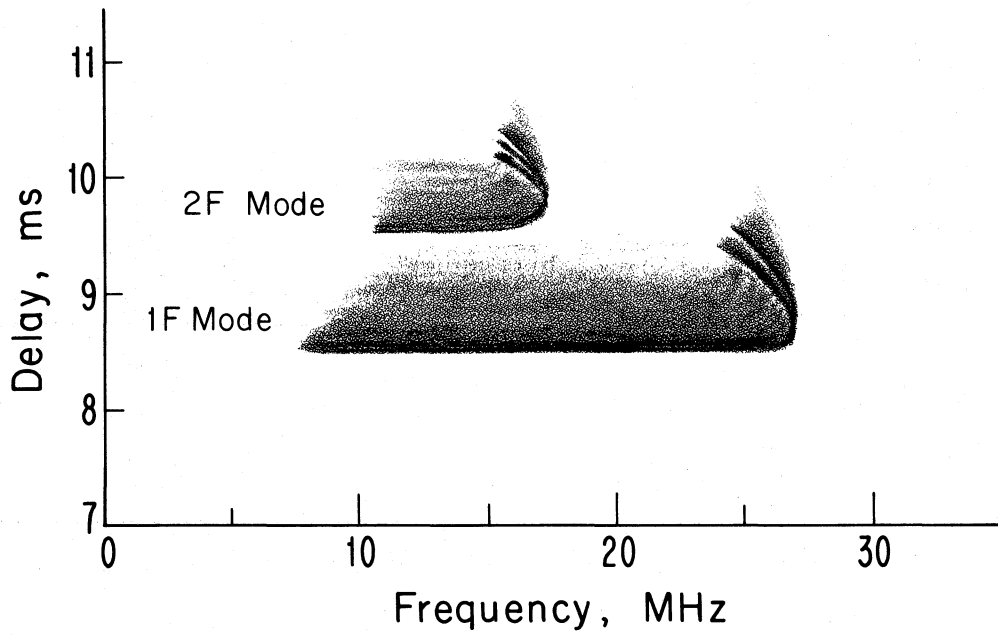
### 4.1 Propagation Characteristics

The ionosphere is a portion of the earth's atmosphere that is ionized by solar radiation. It extends in altitude from about 50 km to several hundred km and higher. The free-electron density as a function of altitude typically has variations called layers: the D, E,  $F_1$ , and  $F_2$  layers. An HF transmitted signal propagates to a receiving antenna by reflection from one or more of the upper layers: E,  $F_1$ , and  $F_2$  (Davies, 1965). The reflections (actually refractions) are produced by the interaction between the signal field and the free electrons. In general, the signal can propagate to the receiver via several major modes: e.g., a single reflection from an F layer (a 1F mode), a double reflection from an F layer with an intermediate reflection from the earth (a 2F mode), a double reflection from an F layer with an intermediate upward reflection from the E layer (an M mode), etc.

Figure 9(a) presents a hypothetical example of the delay (propagation) times for 1F and 2F modes as functions of frequency (an oblique ionogram) for a quiet ionosphere (explained later). In general, each mode contains both low and high rays which merge at the maximum frequency for that mode. The largest of these is usually called the MUF (maximum usable frequency). Both high and low rays contain ordinary and extraordinary components produced by the earth's magnetic field. The propagation times of the ordinary and extraordinary components are essentially identical for the low rays, but may be significantly different in the high rays. For each of the magnetoionic components, dispersion can be defined as the negative of the derivative of the propagation delay with respect to frequency; i.e., the negative of the slope of each curve in Figure 9(a). It can be seen then that the low rays have no significant dispersion, except near the maximum frequency of the mode, while the high rays exhibit significant dispersion. However, over the bandwidths



(a) QUIET IONOSPHERE



(b) SPREAD - F

Figure 9. Hypothetical ionograms.

of typical HF digital systems (<12 kHz), the high-ray differential delay from the low to the high end of the signal band is quite small compared to the differential delays between the low and high rays and between different major modes. Consequently, the high-ray dispersion is not important practically.

The propagation modes that exist for any HF radio system depend on the time (state of the ionosphere), the transmitter-receiver distance, and the operating frequency. The differential delay between the shortest and longest propagation paths depends on both transmitter-receiver distance and operating frequency. This dependence, which was determined experimentally from a number of oblique ionograms (Bailey, 1959; Salaman, 1962), is illustrated in Figure 10. For each transmitter-receiver distance,  $d$ , the maximum differential delay,  $\Delta\tau_m$ , increases monotonically as the operating frequency,  $f_o$ , decreases below the maximum usable frequency,  $f_M$ . Each curve itself has a maximum, with the maxima of the various curves forming the loci of the dashed curve,  $\Delta\tau'_m$ . The maximum differential delay,  $\Delta\tau'_m$ , varies with transmitter-receiver distance,  $d$ , as shown in Figure 11.

The ionosphere always has a turbulent structure that affects the signal on each propagation mode or path in two ways: it modulates the signal in both amplitude and phase in a random fashion, thus generating sidebands that scatter or spread the signal in frequency; and it scatters or spreads the signal in time. When the turbulence is relatively mild (the usual case), the ionosphere is said to be quiet, and the major effect of the turbulence is to scatter the signal in frequency (produce fading<sup>1</sup>) on each mode while producing no significant scattering in time. Each propagation mode then is essentially discrete in time, as illustrated by the curves in Figure 9(a). When the turbulence is more severe, a spread-F condition exists. The more severe turbulence still scatters the signal in

---

<sup>1</sup> The radio signal fading produced by ionospheric turbulence is similar to the scintillation of star light produced by tropospheric turbulence.

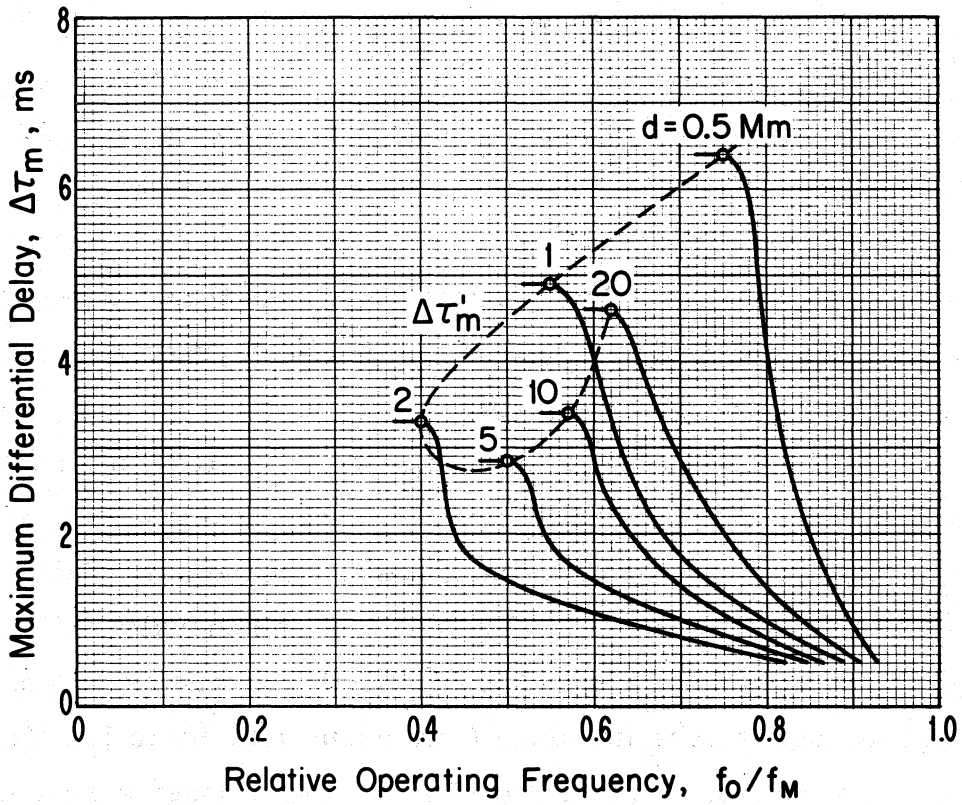


Figure 10. Maximum differential delay versus relative operating frequency for HF channels.

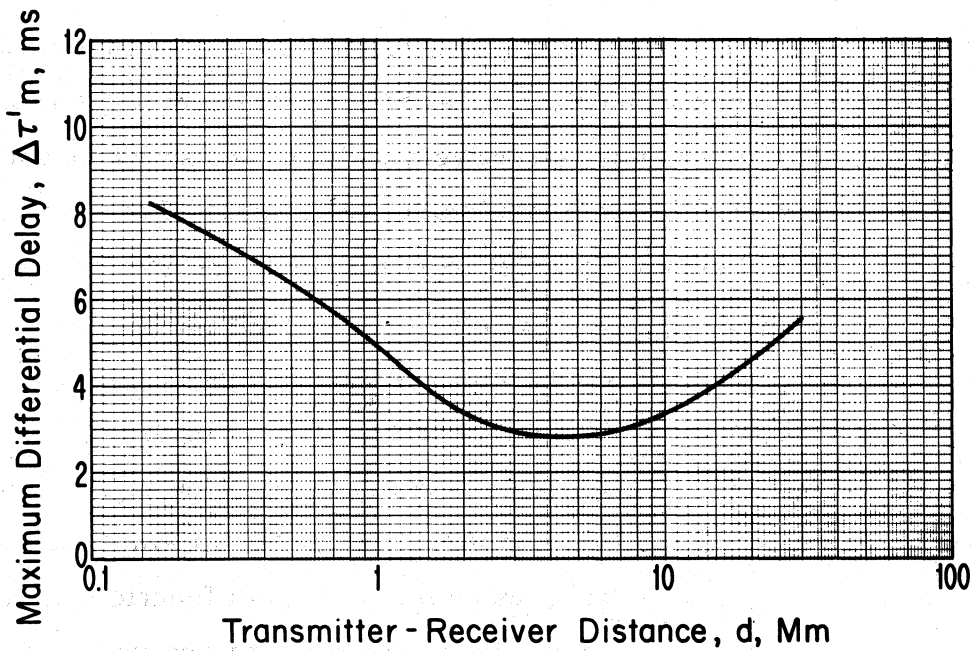


Figure 11. Maximum differential delay versus distance for HF channels.

frequency, usually by a larger amount (a higher fading rate), but also scatters the signal in time by a significant or substantial amount, as illustrated by Figure 9(b). Each propagation mode or path that is essentially discrete in time with a quiet ionosphere in effect is replaced under spread-F conditions by a multiplicity of faster fading paths with different generally larger closely spaced delays (a time continuum of paths). Spread-F conditions exist part of the time predominantly in high-latitude and equatorial regions of the earth.

In addition to the time scattering imposed on a signal by multipath propagation, and frequency scattering imposed by the fading on each path, the generally increasing or decreasing heights of the ionospheric layers (greatest near sunrise and sunset) will introduce generally different mean Doppler shifts on the various multipath signal components. Doppler shifts and frequency spreads range from about 0.01 Hz to 1.0 Hz with a quiet ionosphere, but range up to 10 Hz or more under spread-F conditions.

#### 4.2 Channel Model

The multipath, Doppler, and fading characteristics of the ionosphere affect the performance of an HF digital radio system in ways that can be described and evaluated most effectively in terms of an HF channel model. Figure 12 is a diagram of an experimentally validated HF channel model (Watterson et al., 1970) for a quiet ionosphere. The transmitted signal,  $x(t)$  in complex-envelope notation, feeds an ideal delay line and appears at a selectable number of taps with adjustable delays,  $\{\tau_p\}$ , where  $p=1, 2, 3, \dots, P$  is an integer that numbers the paths. In general, one tap or path is used for each magnetoionic component. The signal at each tap,  $x(t-\tau_p)$  at the  $p$ th tap, is multiplied (modulated in amplitude and phase) by a complex, baseband, random, path-gain function,  $g_p(t)$ . The delayed and modulated multipath signal components are summed in general with noise and interference,  $n(t)$  and  $i(t)$  respectively, to form

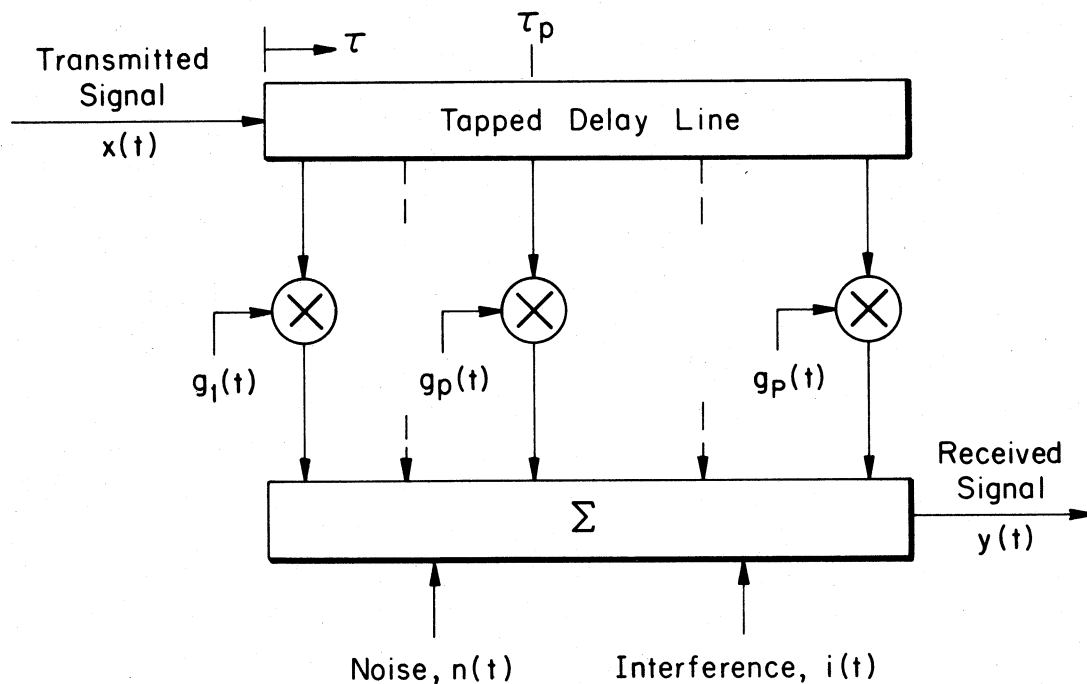


Figure 12. HF channel model.

the received aggregate,  $y(t)$ . The functions  $n(t)$ ,  $i(t)$ , and  $y(t)$ , like  $x(t)$ , are complex envelope functions that are defined with respect to the same rf reference frequency,  $f_r$ .

The channel model in Figure 12 excludes dispersion because it is **not** significant over bandwidths typical of HF digital systems (<12 kHz). If dispersion were significant, it could be included in the model by incorporating all-pass dispersion filters in each path immediately preceding the path-gain multiplier.

From Figure 12 it can be seen that

$$y(t) = \sum_{p=1}^P g_p(t)x(t-\tau_p) + n(t) + i(t) \quad (32)$$

The complex, time-varying, impulse response of the channel,  $x(t)$  to  $y(t)$ ,

is

$$h(\tau, t) = \sum_{p=1}^P g_p(t) \delta(\tau - \tau_p) \quad , \quad (33)$$

where  $\delta(\tau)$  is the Dirac delta function. The Fourier transform of  $h(\tau, t)$  on  $\tau$  is the complex time-varying frequency response of the channel,

$$H(f, t) = \sum_{p=1}^P g_p(t) \exp(-j2\pi\tau_p f) \quad . \quad (34)$$

Because each path-gain function,  $g_p(t)$ , is a random process, it must be described in terms of its statistical parameters. In the experimental validation of the HF channel model, it was shown that the path-gain functions are independent Gaussian-scattering (Rayleigh-fading) processes with generally different mean Doppler shifts. Specifically, it was shown that each complex path-gain function is accurately described by

$$g_p(t) = g_{p0}(t) \exp(j2\pi\nu_p t) \quad , \quad (35)$$

where  $g_{p0}(t)$  is a stationary, zero-mean, circular, complex-Gaussian process<sup>2</sup>, and  $\nu_p$  is the mean Doppler shift on the path. If

$$C_p(\Delta t) = E[g_p^*(t) g_p(t + \Delta t)] \quad (36)$$

is the autocorrelation of the path-gain function, then it was shown that its Fourier transform, the power spectrum of  $g_p(t)$ , is

$$\nu_p(\nu) = \frac{C_p(0)}{\sqrt{2\pi} \sigma_p} \exp \left[ \frac{-(\nu - \nu_p)^2}{2\sigma_p^2} \right] \quad , \quad (37)$$

---

<sup>2</sup> A stationary, zero-mean, circular, complex-Gaussian random process has real and imaginary components that are independent, stationary, zero-mean Gaussian processes with identical even power spectrums.

where  $2\sigma_p$  is defined as the frequency spread (approximately the fading rate) on the path. Equation (37) is illustrated in Figure 13. It can be seen that the statistical characteristics of the path-gain function,  $g_p(t)$ , are completely specified by three parameters: the path power gain,  $C_p(0)$  {or the path attenuation in decibels,  $A_p = -10 \log[C_p(0)]$ }; the path Doppler shift,  $\nu_p$ ; and the path frequency spread,  $2\sigma_p$ .

Each path as described above represents one magnetoionic component when the two magnetoionic components in a high ray or low ray have significantly different delays, Doppler shifts, or frequency spreads; i.e., when their differential delay is a significant fraction of the reciprocal of the bandwidth of the channel being modeled, when their differential Doppler shift is a significant fraction of their frequency spreads, or when their frequency spreads are significantly different. When the delays, Doppler shifts, and frequency spreads of the two magnetoionic components are nearly the same, as they typically are on daytime F-layer low-ray modes, then a single path can represent both magnetoionic components.

The channel can be described in a similar way. The channel correlation function is defined by

$$R(\Delta f, \Delta t) = E[H^*(f, t) H(f + \Delta f, t + \Delta t)] \quad . \quad (38)$$

The channel scatter function is defined as the double Fourier transform on  $\Delta f$  and  $\Delta t$  of  $R(\Delta f, \Delta t)$ , which for the model of Figure 12 is

$$s(\tau, \nu) = \sum_{p=1}^P \delta(\tau - \tau_p) \nu_p(\nu) \quad . \quad (39)$$

Equation (39) is illustrated in Figure 14 for a hypothetical channel with 1F and 2F low-ray modes where the two magnetoionic components in each mode have essentially identical delays, Doppler shifts, and frequency spreads.

Because  $g_p(t)$  and  $H(f, t)$  are dimensionless, their autocorrelations,  $C_p(\Delta t)$  and  $R(\Delta f, \Delta t)$ , are also dimensionless.  $C_p(0)$  is the power gain on

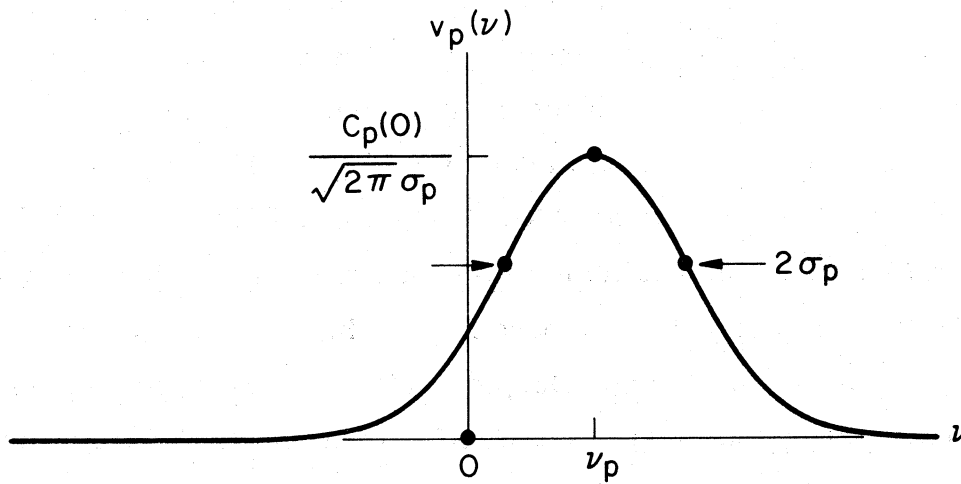


Figure 13. Path-gain spectrum.

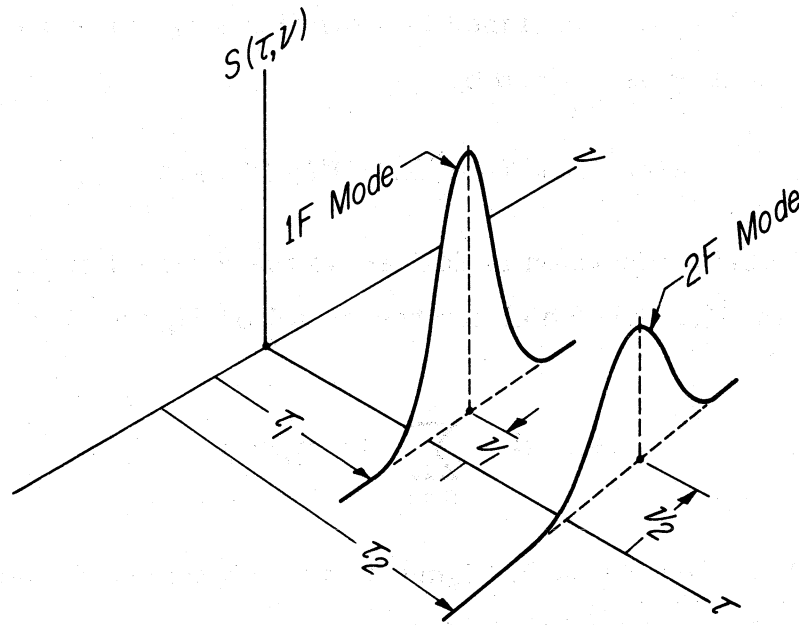


Figure 14. Hypothetical channel scatter function.

the  $p$ th path, while  $R(0, 0)$  is the channel power gain. Therefore,  $v_p(\nu)$  and  $s(\tau, \nu)$  are power-gain density functions:  $v_p(\nu)$  is the ratio of the output signal power per unit frequency interval received over the  $p$ th path to the channel signal input power, and  $s(\tau, \nu)$  is the ratio of the output signal power per unit frequency interval and per unit time interval over all paths to the channel signal input power. Each path can be viewed as a continuum of infinitesimal specular (nonfading) paths with a common delay, different frequency shifts with equal adjacent infinitesimal spacings, and random phases, where the magnitudes of the infinitesimal specular components are proportional to  $\sqrt{s(\tau, \nu)}$ , the square root of the channel scatter function in (39). Because each fading path is a Gaussian-scattering process, the channel is a Gaussian-scattering process; i.e., the signal carried by each path and the total signal carried by the channel exhibit Rayleigh fading (the magnitude of the received signal envelope has a Rayleigh density function).

The preceding validated channel model applies only to a quiet ionosphere (the usual case) where the propagation modes are essentially discrete in time. Under spread-F conditions, the model presumably could be modified by replacing the time-discrete  $\delta(\tau - \tau_p)$  in the channel scatter function, (39), with a suitable nondiscrete time-scatter function, possibly the exponential function

$$u_p(\tau) = \begin{cases} \frac{1}{\rho_p} \exp[-(\tau - \tau_p)/\rho_p] & , \quad \tau \geq \tau_p \\ 0 & , \quad \tau < \tau_p \end{cases} \quad (40)$$

where  $\rho_p$  is the time spread on the "path" (analogous to the frequency spread,  $2\sigma_p$ ). Such a model has not been validated, however.

From the preceding descriptions of the propagation characteristics of the HF channel and the HF channel model, it can be seen that the types of distortion that an HF channel can impose on a signal can be classified as follows:

## Types of Channel Distortion

- (1) Additive
  - (a) Noise
    - (i) Thermal (Gaussian)
    - (ii) Impulsive (atmospheric, man-made)
  - (b) Interference (unwanted signals)
- (2) Multiplicative
  - (a) Time scatter (frequency selective)
    - (i) Differential delay (multipath)
    - (ii) Dispersion (assumed negligible)
  - (b) Frequency scatter (time selective)
    - (i) Differential Doppler (multipath)
    - (ii) Fading

When a channel has a single propagation path with a delay,  $\tau_1$ , and a Doppler shift,  $\nu_1$ , the channel does not impose any delay distortion because it is assumed the demodulator can compensate for the delay by suitably synchronizing to the single-path signal. However, with two or more propagation paths with different delays, the multipath propagation introduces a differential-delay distortion (2ai above) even with optimum receiver synchronization.

In an analogous way, when a channel has a single propagation path with a delay,  $\tau_1$ , and a Doppler shift,  $\nu_1$ , the channel does not impose any Doppler distortion because it is assumed the demodulator can compensate for the Doppler shift with a suitable Doppler-correction circuit (as it is assumed to do for equipment frequency errors). However, with two or more propagation paths with different Doppler shifts, the multipath propagation introduces a differential-Doppler distortion (2bi above) even with optimum Doppler correction.

## 5. RECEIVER

### 5.1 Receiving Antenna

It is common practice in HF communications to use either the same antenna or antennas of similar design for both transmitting and receiving. The classifications and descriptions of HF transmitting antennas that were presented in Section 3.4 therefore also apply to HF receiving antennas, and do not need to be repeated. However, HF antennas sometimes are designed and used for receiving only because of three advantages:

#### Advantages of Receiving Antennas

- (1) Lower power
- (2) Smaller size
- (3) Adaptibility

The rf powers handled by receiving antennas are many orders of magnitude lower than those handled by transmitting antennas. Consequently, the high-voltage insulation and corona problems that must be considered in transmitting antenna designs are not present in receiving antenna designs, which usually simplifies the physical design.

In general, an HF antenna with a given pattern can be made physically smaller for receiving applications, because the decreased efficiency (greater fractional power loss) that usually accompanies the smaller size can be tolerated in HF receiving applications. A more lossy antenna can be tolerated because the ambient atmospheric noise level is usually substantially greater than the thermal noise level in a receiver with a low noise figure (CCIR, 1964); i.e., the power loss in the receiving antenna reduces both the signal and atmospheric noise levels at the HF receiver input, but does not significantly change the signal-to-atmospheric -and-receiver-noise ratio, provided the loss is not excessive. An example of a smaller size, single-element receiving antenna is an untuned loop that is a small fraction of a wavelength in diameter. Arrays of such

elements can be used to provide gain and directivity.

Antenna adaptability can be defined as the ability to change electrically the pattern or steering of an antenna. While adaptive transmitting antennas can be and are used, adaptability is generally easier to obtain in a receiver-only antenna: the outputs of the several antenna elements can be electrically controlled over a large range of amplitude and  $360^\circ$  of phase shift by suitable low-level active circuits to provide greater versatility in both pattern shape and steering.

Receiving antennas, like transmitting antennas, introduce filtering distortion imposed by their generally frequency-selective responses. Adaptive receiving antennas with active circuits may also introduce other types of equipment distortion (p. 8), such as thermal noise and interference, that depend on their design.

## 5.2 HF Receiver

A typical HF receiver is illustrated in Figure 15. It consists of a tunable band-pass HF amplifier followed by a first frequency converter, a fixed-tuned band-pass first-IF amplifier, a second frequency converter, and a fixed-tuned band-pass lower frequency second-IF amplifier that delivers the receiver output aggregate (signal and distortion) to the demodulator. Some receivers use three frequency converters, each followed by a fixed-tuned band-pass IF amplifier. The first local-oscillator frequency is adjusted with the HF amplifier tuning to tune the HF receiver to the desired HF signal frequency. The frequency translations in the HF receiver nominally restore the signal pulse trains to the frequencies at which they were generated in the modulator, usually in the ELF range.

The HF amplifier, which is tuned to the signal frequency, provides image rejection for the first converter and suppresses out-of-signal-band interference which otherwise, if sufficiently strong, might overload the receiver. The HF amplifier is usually designed to have a low noise

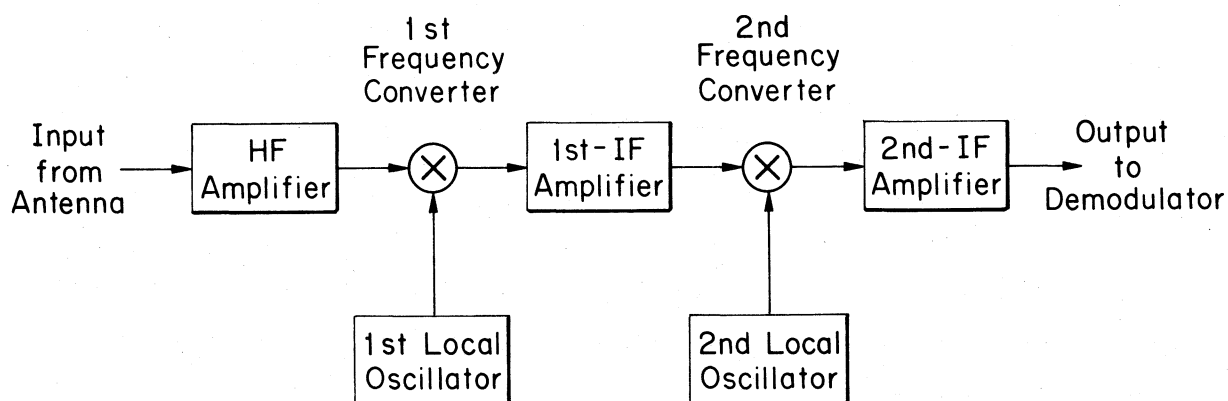


Figure 15. Typical HF receiver.

figure and sufficient amplification to make the atmospheric noise delivered by the antenna predominate over the thermal noise generated in the HF amplifier and subsequent converters and IF amplifiers.

The two or more fixed-tuned band-pass IF amplifiers provide additional amplification and filtering. The filtering suppresses the unwanted sideband generated by each frequency converter, suppresses the local-oscillator components if the balancing of the frequency converters is inadequate, and also suppresses any undesired out-of-signal-band higher order intermodulation products generated by converters that are not good approximations of true multipliers. The IF filtering also provides suppression of out-of-signal-band noise and interference, particularly at frequencies near the signal band that are not adequately filtered by the usually wider band HF-amplifier filtering.

The aggregate delivered at the HF receiver output, and sometimes the aggregate at an earlier point in the receiver, are maintained at nominally constant power levels by a suitable AGC circuit that controls the gains of the amplifiers. The response time of the AGC is sometimes selectable.

It can be seen that the HF receiver performs three interleaved primary functions:

## HF Receiver Functions

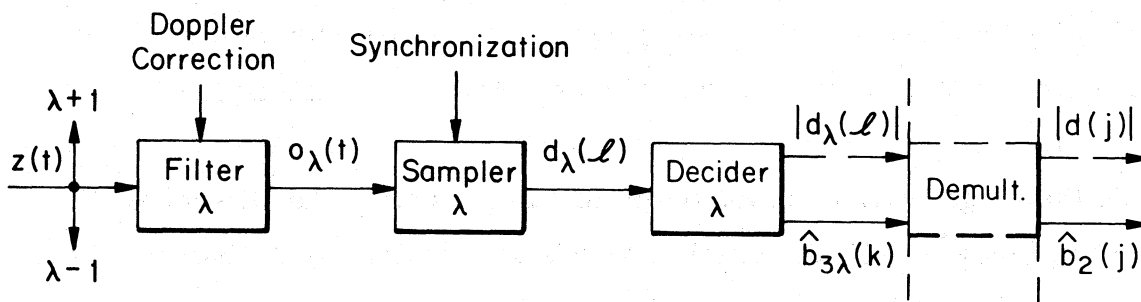
- (1) Frequency translation
- (2) Filtering
- (3) Amplification

In performing these functions, the HF receiver, like the HF transmitter, can introduce all of the types of equipment distortion listed on p. 8 except quantizing noise (provided all-analog circuits are used), synchronization distortion, and Doppler-correction distortion (because it is assumed that any frequency error introduced by the local oscillators in Figure 15 can be compensated or corrected by the Doppler-correction circuit in the demodulator). While the distortions in the HF receiver may be no greater than those in the HF transmitter, their effects on system performance can be much greater under some channel conditions.

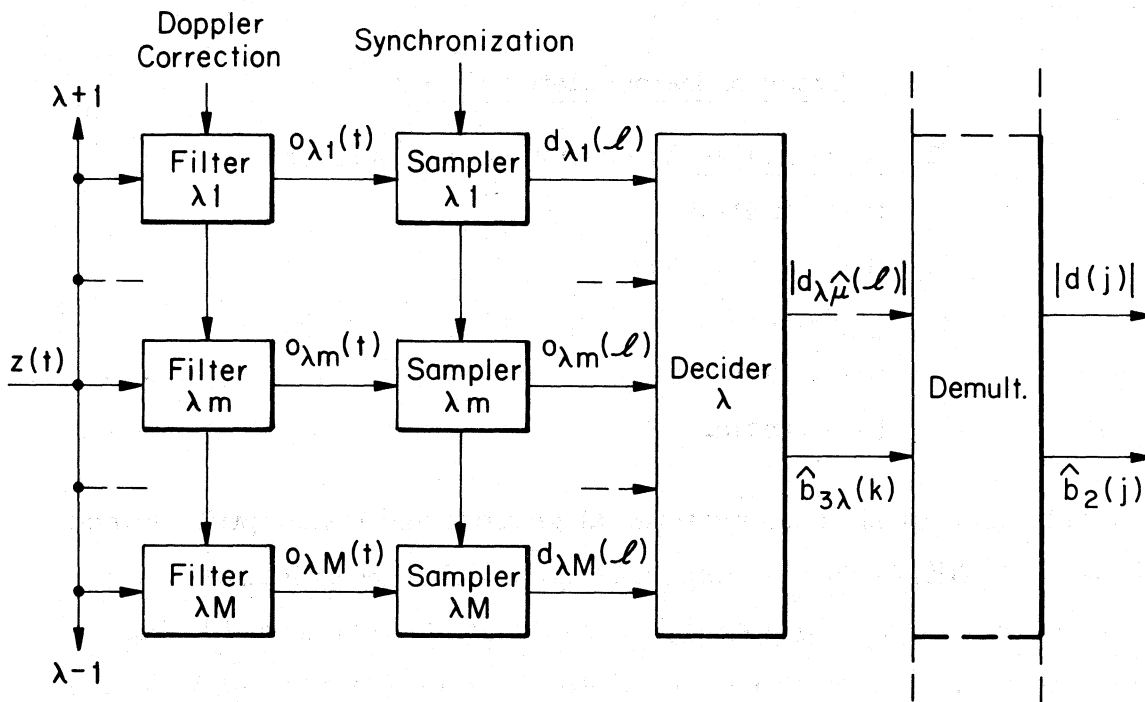
### 5.3 Demodulator

The aggregate delivered by the HF receiver to the demodulator generally contains several trains of frequency-multiplexed or concentrically multiplexed signal pulses with distortion components introduced by the equipment and the HF channel. The demodulator separates the several trains of pulses by suitable filtering and samples each filtered train of pulses to obtain an estimate of the amplitude, the phase, or the amplitude and phase of each pulse. Each pulse sample is delivered to a decider, which for each data bit carried by the pulse, decides whether a zero or one bit was transmitted.

Because the processing that a demodulator performs on each pulse train is basically the same, demodulator operation can be described in more detail by describing the processing for one train, the  $\lambda$ th. The processing depends on whether a single-filter or a multiple-filter keying method (p. 15) is used in the modulator. Figure 16(a) illustrates the processing for the  $\lambda$ th pulse train in a single-filter demodulator, while



(a) Single-Filter Demodulator



(b) Multiple-Filter Demodulator

Figure 16. Portions of demodulators for pulse train  $\lambda$ .

Figure 16(b) illustrates the processing for the  $\lambda$ th pulse train in a multiple-filter demodulator. Both show what actual demodulators do in effect, regardless of the specific instrumentation techniques that are used. A description of the operation of the single-filter demodulator will be presented first, and then a description of the multiple-filter demodulator.

In the single-filter demodulator of Figure 16(a), the HF-receiver output aggregate,  $z(t)$  in complex-envelope notation, is delivered to a single  $\lambda$ th filter whose purpose ideally is to maximize the signal-to-distortion power ratio in its output,  $o_\lambda(t)$ . The types of demodulator filters that can be used in both single-filter and multiple-filter demodulators are:

#### Types of Demodulator Filters

- (1) Nonadaptive (time-invariant response)
  - (a) Matched
  - (b) Nonmatched
- (2) Adaptive
  - (a) Quasi-static
  - (b) Dynamic

Nearly all digital radio systems at present use nonadaptive demodulator filters, filters whose responses do not change with time. Nonadaptive demodulator filters may be matched or nonmatched to the signal pulses generated in the modulator. To define a matched filter, let the fundamental pulse waveform,  $p(t)$  in (12), p. 15, after multiplexing for the  $\lambda$ th pulse train,  $w_\lambda(t)$  in (21), p. 19, be

$$p_\lambda(t) = \mathcal{M}_\lambda [p(t)] \quad . \quad (41)$$

Then in the single-filter demodulator of Figure 16(a), a matched filter is one whose generally complex impulse response is

$$h_\lambda(t) = g_\lambda p_\lambda^*(\tau_\lambda - t) \quad , \quad (42)$$

where  $g_\lambda$  is an arbitrary complex gain, and  $\tau_\lambda$  is a semi-arbitrary fixed time delay required for physical filter realizability. The frequency response of the matched demodulator filter, the Fourier transform of  $h_\lambda(t)$ , therefore is

$$H_\lambda(f) = g_\lambda P_\lambda^*(f) \exp(-j2\pi\tau_\lambda f) \quad , \quad (43)$$

where  $P_\lambda(f)$  is the Fourier transform of  $p_\lambda(t)$ . The frequency response of the matched demodulator filter is the complex conjugate of  $P_\lambda(f)$ , the amplitude spectrum of the multiplexed fundamental pulse waveform, except for an arbitrary complex gain,  $g_\lambda$ , and a semi-arbitrary fixed time delay,  $\tau_\lambda$ . In the single-filter demodulator, when the single nonadaptive filter for the  $\lambda$ th pulse train is matched to the multiplexed fundamental pulse waveform,  $p_\lambda(t)$  in (41), then it is matched to all of the keyed pulses in the  $\lambda$ th pulse train,  $w_\lambda(t)$  in (21).

To illustrate the characteristics of matched-filter operation, consider the operation of a frequency-multiplexed system [(22), p. 20] that uses binary PSK on adjoining unit-magnitude rectangular pulses. Assume operation under the ideal conditions of no equipment distortions and no channel distortions, which means the frequency response from the modulator output to the demodulator input is constant in amplitude and delay over the significant signal band. Then Figure 17 illustrates the operation for the  $\lambda$ th pulse train with a matched demodulator filter. The first waveform shows an example of  $b_{3\lambda}(k)$ , the binary data sequence that determines the keying sequence,  $K_\lambda(t)$ , on the  $\lambda$ th pulse train in the modulator. The second waveform is the generally complex envelope of the  $\lambda$ th basic pulse train,  $\bar{w}_\lambda(t)$  in (18), p. 18, which is real in the binary PSK example. Because  $M=2$ , the phase-keying values,  $K_\lambda(t)$ , are +1 or -1 [Figure 3(b),  $N=1$ , p. 17], and  $\bar{w}_\lambda(t)$  is real with +1 or -1 values. The value of each rectangular pulse in  $\bar{w}_\lambda(t)$  is determined by the value of  $b_{3\lambda}(k)$  at the start of the pulse.

Under the ideal conditions of no equipment or channel distortions, the  $\lambda$ th frequency-multiplexed pulse train,  $w_\lambda(t)$  in (22), p. 20, produces a

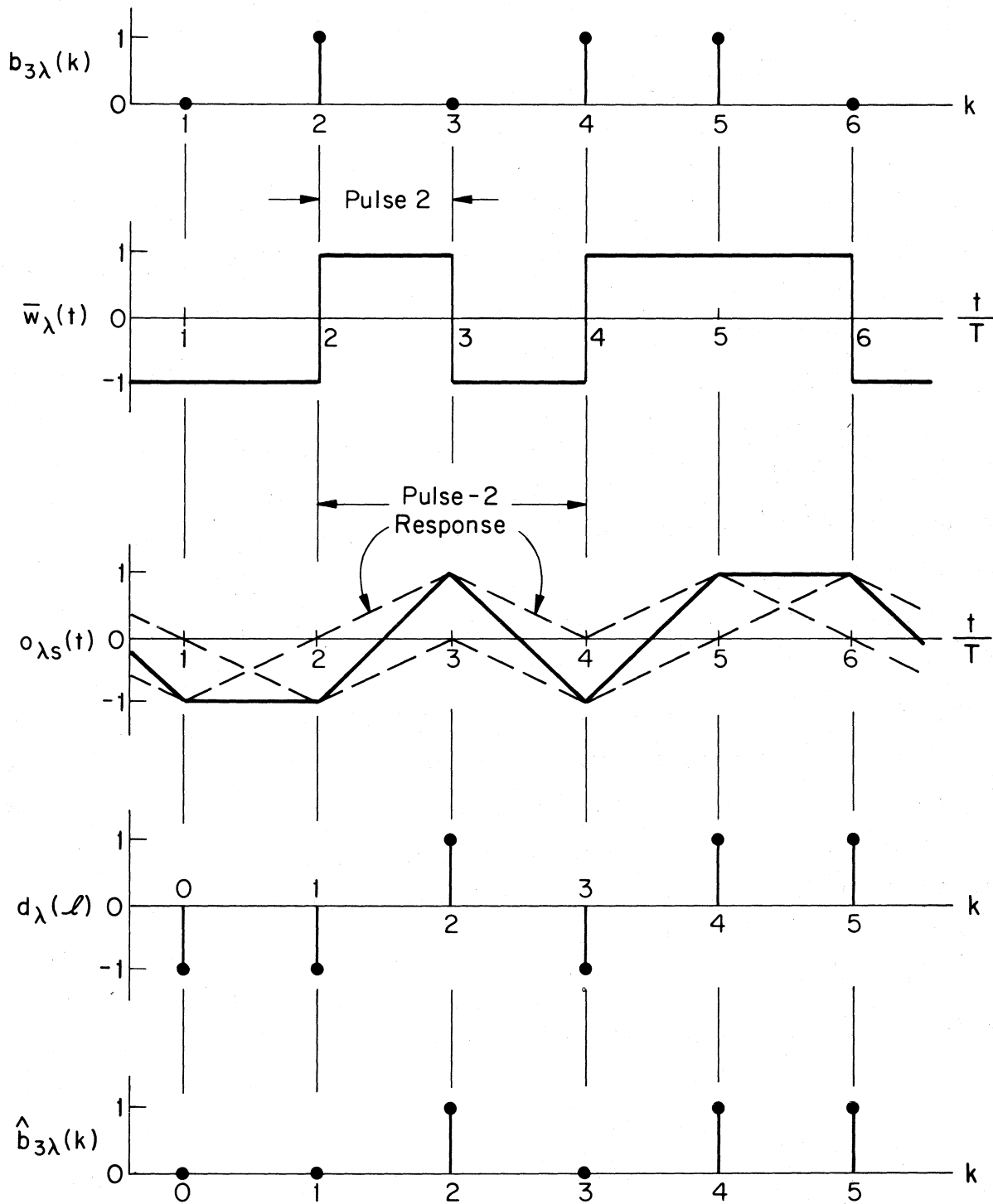


Figure 17. Characteristics of matched-filter system with binary PSK under ideal conditions.

signal response,  $o_{\lambda s}(t)$ , at the output of the single  $\lambda$ th matched demodulator filter in Figure 16(a). The response is illustrated by the solid line segments in the third waveform in Figure 17, where it is assumed the receiver gain is set to give peak responses of  $\pm 1$ . The illustration ignores the signal delay introduced by the equipment and channel between the modulator output,  $w(t)$ , and the demodulator input,  $z(t)$ , but includes the delay in the demodulator filter. In the example of  $o_{\lambda s}(t)$ , the positive and negative dashed-line equilateral triangles, each of duration  $2T$ , are the demodulator filter responses to the individual rectangular pulses of duration  $T$  in  $w_{\lambda}(t)$ . The sum of the dashed-line triangular responses form the total response,  $o_{\lambda s}(t)$ , shown by the solid line segments. For the illustrated response, the arbitrary matched-filter gain coefficient,  $g_{\lambda}$  in (42) and (43), is such that  $o_{\lambda s}(t)$  is real. If the phase of  $g_{\lambda}$  were changed by  $\Delta\angle g_{\lambda}$ , then the real  $o_{\lambda s}(t)$  in Figure 17 would be multiplied by a constant phase factor,  $\exp(j\Delta\angle g_{\lambda})$ , to become complex, but Figure 17 would still illustrate the amplitude component of the complex  $o_{\lambda s}(t)$ .

Under nonideal conditions, when channel and equipment distortions are present, the demodulator filter output becomes

$$o_{\lambda}(t) = o_{\lambda s}(t) + o_{\lambda d}(t) \quad , \quad (44)$$

where  $o_{\lambda d}(t)$  is the total distortion component. When only white noise distortion is present, a matched demodulator filter maximizes the signal-to-noise ratio in  $o_{\lambda}(t)$  at integer values of relative times  $t/\ell T$ ; i.e., no other filter can provide a larger signal-to-noise ratio in its output. However, when other types of distortion are present, a matched demodulator filter generally does not maximize the signal-to-distortion ratio at its output.

For all distortions other than white noise, there is generally for each distortion condition a nonmatched filter that maximizes the signal-to-distortion ratio in the filter output,  $o_{\lambda}(t)$ . However, such a filter would not maximize the signal-to-distortion ratio under other distortion

conditions. Therefore, nearly all HF digital receivers with single-filter demodulators use nonadaptive filters that are nominally matched, so as to obtain maximum signal-to-noise ratio in  $o_\lambda(t)$ .

Because channel distortions other than white noise predominate a large part of the time, overall receiver performance can be improved with an adaptive demodulator filter, one whose response is automatically adjusted to maximize the signal-to-distortion ratio in its output,  $o_\lambda(t)$ , according to the distortion conditions. If  $h_\lambda(\tau, t)$  is the generally complex time-varying impulse response of an adaptive demodulator filter, then

$$o_\lambda(t) = \int_0^{\infty} z(t-\tau) h_\lambda(\tau, t) d\tau \quad , \quad (45)$$

where  $z(t)$  is the input to the filter. The adaptive filter has a time-varying frequency response,  $H_\lambda(f, t)$ , that is the Fourier transform of  $h_\lambda(\tau, t)$  on  $\tau$ .

An adaptive demodulator filter must incorporate a circuit which measures or analyzes the aggregate on a continuing basis. The data obtained from the analysis, possibly coupled with a-priori knowledge of the multiplexed fundamental pulse waveform,  $p_\lambda(t)$  in (41), is then used in a suitable algorithm to adjust or control the parameters of the adaptive filter to maximize the signal-to-distortion ratio in its output,  $o_\lambda(t)$ . A quasi-static adaptive filter is one whose parameters and response change slowly with time to maximize the long-term signal-to-distortion ratio in  $o_\lambda(t)$ . A dynamic filter is one whose parameters and response change rapidly with time, up to rates comparable to the signal bandwidth, to maximize the short-term signal-to-distortion ratio in  $o_\lambda(t)$  [Watterson, C. C. (1979), An adaptive receiver filter for interference suppression in digital spread-spectrum radio systems (U), NTIA Tech. Memo. 79-9C, pp. 1-122, Feb. (Secret) (U.S. Dept. of Commerce, Boulder, CO 80303)]. Quasi-static adaptive filters, like nonadaptive filters, are normally linear, unless a nonlinear transfer characteristic

such as clipping is incorporated. Dynamic adaptive filters are inherently nonlinear, however, because the control function that rapidly adapts the filter response is dependent on the filter input aggregate; consequently, the superposition theorem does not apply and the filter is nonlinear. At the present time adaptive receiver filters have received only a very limited theoretical and experimental consideration (Di Toro et al., 1964; Brown, 1977; Milstein et al., 1978).

In the single-filter demodulator of Figure 16(a), the demodulator filter output,  $o_\lambda(t)$ , is delivered to a sampler. The sampler samples  $o_\lambda(t)$  at the pulse rate of the train,  $1/T$ , to obtain an estimate of the complex value of each pulse in the train. The pulse-sampling times are determined by a clock whose timing (phase) is controlled by a synchronization circuit that is not shown in Figure 16(a). Because  $o_\lambda(t)$  is a complex envelope function, the successive samples of  $o_\lambda(t)$  for a complex demodulator pulse-sample sequence,

$$d_\lambda(\ell) = d_{\lambda s}(\ell) + d_{\lambda d}(\ell) \quad , \quad (46)$$

where  $d_{\lambda s}(\ell)$  and  $d_{\lambda d}(\ell)$  are the signal and distortion components respectively. Under ideal conditions (no equipment or channel distortions),  $d_{\lambda d}(\ell) = 0$ , and  $d_\lambda(\ell) = d_{\lambda s}(\ell)$  may have any one of  $M$  discrete complex values corresponding to the  $M$  different waveforms that may be transmitted;  $+1$  or  $-1$  for the ideal binary PSK system in Figure 17. For the single-filter (ASK, PSK, and APSK) modulator keying values illustrated in Figure 3, p. 17, the  $M$  discrete values of  $d_\lambda(\ell) = d_{\lambda s}(\ell)$  under ideal conditions would be identical to the keying values except for an arbitrary constant complex scaling.

Under nonideal conditions, distortion components are present in  $o_\lambda(t)$ , and the demodulator pulse-sample sequence,  $d_\lambda(\ell)$ , is consequently non-discrete; i.e., it has a continuous distribution in the complex  $d$ -plane, even when the signal component,  $d_{\lambda s}(\ell)$ , is real. When equipment or channel distortions are present in  $o_\lambda(t)$ , optimum synchronization exists when the pulse samples are taken at times when the expected signal-to-

distortion ratio in  $o_{\lambda}(t)$  is a maximum. With white noise distortion present in the matched-filter binary-PSK example of Figure 17, the illustrated sampling times constitute optimum synchronization because the expected signal-to-noise ratio is greatest at these times. With a nonmatched filter, optimum synchronization would be different. In general, optimum synchronization depends not only on the filter response, but on the types and characteristics of the distortions that are present. Regardless of the types of distortion present, the loss or degradation in receiver performance introduced by nonoptimum synchronization can be viewed as being produced by synchronization distortion (equipment distortion 2ai in the list on p. 8).

In the single-filter demodulator of Figure 16(a), each pulse sample in  $d_{\lambda}(t)$  is delivered in turn to a decider which, for each of the N data bits carried by that pulse, decides whether a zero or one bit was transmitted. The bit-decision methods that may be used in both single-filter and multiple-filter demodulators are:

#### Bit-Decision Methods

- (1) Coherent
- (2) Partially coherent
- (3) Differentially coherent
- (4) Noncoherent

Table 2 relates the four bit-decision methods to the single-filter and multiple-filter keying methods described earlier. Each combination is rated theoretical only (T), practical (P), or impossible (I). The most widely used practical combinations are circled. The reasons for the ratings will be given in the descriptions of the bit-decision methods. At this point, we will consider the four bit-decision methods in turn as they apply to the single-filter (ASK, PSK, and APSK) demodulator in Figure 16(a).

Coherent, partially coherent, and differentially coherent bit decisions

Table 2. Keying methods for various bit-decision methods

Bit-Decision Method	Keying Method				
	Single Filter			Multiple Filter	
	ASK	PSK	APSK	FSK	CPK
Coherent	T	T	T	T	T
Partially coherent	P	P	P	P	P
Differentially coherent	I	Ⓟ	P	I	I
Noncoherent	P	I	I	Ⓟ	P

T= theoretical only, P= practical, and I= impossible.  
 Circled practical combinations are the most widely used.

are basically the same but differ in that coherent bit decisions are only theoretically possible, while partially coherent and differentially coherent bit decisions are practical approximations of coherent bit decisions. When coherent, partially coherent, or differentially coherent bit decisions are made in a single-filter demodulator, Figure 16(a), the decider in effect divides the complex value of each pulse sample,  $d_\lambda(t)$ , by the corresponding value in a complex reference sequence,  $r_\lambda(t)$ , to obtain an approximate keying value,

$$\tilde{K}_\lambda(t) = \frac{d_\lambda(t)}{r_\lambda(t)} \quad (47)$$

$\tilde{K}_\lambda(t)$  is a nondiscrete (continuously distributed) approximation of the discrete (M-ary) true keying value,  $K_\lambda(t)$ . In general,  $\tilde{K}_\lambda(t)$  differs from  $K_\lambda(t)$  for two reasons: because  $d_\lambda(t)$  contains distortion components, and  $r_\lambda(t)$  is not optimum.

The decider then in effect compares each approximate keying value,  $\tilde{K}_\lambda(t)$ , with stored values of the M possible true keying values,  $\{K_m\}$ , such as those illustrated in Figure 3, p. 17. The purpose of the comparison is to determine which of the M true keying values is closest to  $\tilde{K}_\lambda(t)$ ,

and to decide the closest true keying value was the particular one of  $M$  possible values that was transmitted. Specifically, the decider in effect computes

$$\Delta\tilde{K}_{\lambda m}(\ell) = |\tilde{K}_{\lambda}(\ell) - K_m| \quad , \quad m = 0, 1, 2, \dots, M-1 \quad . \quad (48)$$

Then if

$$\Delta\tilde{K}_{\lambda\hat{\mu}}(\ell) = \min\{\Delta\tilde{K}_{\lambda m}(\ell)\} \quad , \quad m = 0, 1, 2, \dots, M-1 \quad , \quad (49)$$

the decision is made that the  $\hat{\mu}$ th pulse waveform was transmitted, where  $\hat{\mu}$  is a discrete ( $M$ -ary) estimate of  $\mu$ , the number of the pulse waveform that actually was transmitted; i.e.,  $\hat{\mu}$  may be in error because  $\tilde{K}_{\lambda}(\ell)$  in (47) is an approximation of the true keying value,  $K_{\lambda}(\ell)$ .

In partially coherent, differentially coherent, and noncoherent single-filter systems, each selected pulse-waveform number,  $\hat{\mu}$ , in effect is used in a stored table of pulse waveform number,  $m$ , versus keying values,  $K_m$ , to determine  $\hat{K}_{\lambda}(\ell)$ , a discrete estimate of the true keying value,  $K_{\lambda}(\ell)$ .  $\hat{K}_{\lambda}(\ell)$  is then used to generate the reference sequence,  $r_{\lambda}(\ell)$ , in a manner to be described.

In all single-filter demodulators, each selected pulse-waveform number,  $\hat{\mu}$ , in effect is used in a stored table of assigned bit permutations, such as Table 1, p. 11, to determine and deliver the corresponding bit permutation. For successive values of  $\ell$ , the corresponding successive bit permutations form  $\hat{b}_{3\lambda}(k)$ , a discrete estimate of the binary data sequence,  $b_{3\lambda}(k)$ , that is delivered to the  $\lambda$ th pulse-train generator in the modulator. The set of sequences,  $\{\hat{b}_{3\lambda}(k)\}$ , delivered by the  $\Lambda$  deciders (one sequence for each pulse train) are combined in the demultiplexer in Figure 16(a) to form  $\hat{b}_2(j)$ , a discrete estimate of the binary data sequence,  $b_2(j)$ , that is delivered to the modulator. The estimated binary data sequence,  $\hat{b}_2(j)$ , is an output of the demodulator, as shown in Figure 1, p. 4.

In some single-filter systems with error coding, the magnitude of the demodulator pulse-sample sequence in the  $\lambda$ th train,  $|d_{\lambda}(\ell)|$ , is also

delivered to the demultiplexer, as illustrated in Figure 16(a). The set of sequences,  $\{|d_\lambda(\ell)|\}$ , delivered by the  $\Lambda$  deciders are paired with the proper data bits in  $\hat{b}_2(j)$  (each value of  $|d_\lambda(\ell)|$  is used  $N$  times) to form  $|d(j)|$ , a continuously distributed sequence which, for each value of  $j$ , specifies the magnitude of the demodulator pulse sample from which the data bit,  $\hat{b}_2(j)$ , was obtained. The sequence  $|d(j)|$  is delivered as a demodulator output to the error decoder, as shown in Figure 1.

Now consider coherent, partially coherent, and differentially coherent bit decisions in turn, for which (47)-(49) apply. For any combination of basic pulse waveform, keying method, and multiplexing method, coherent bit decisions by definition provide the theoretically best bit-error-probability performance that is possible under some specified channel conditions. Coherent bit decisions are usually defined under very restricted channel conditions by four specifications:

#### Restricted Definition of Coherent Bit Decisions

- (1) The channel contains only a single nonfading or arbitrarily slow Rayleigh-fading path with white thermal noise the only channel distortion.
- (2) There are no equipment distortions.
- (3) The demodulator uses a matched nonadaptive filter.
- (4) The reference sequence,  $r_\lambda(\ell)$ , is identical to  $d_{\lambda c}(\ell;1)$ , the demodulator pulse-sample sequence for  $K_\lambda(\ell)=1$  when thermal noise is absent.

Specification (3) maximizes the signal-to-noise ratio in  $d_\lambda(\ell)$  and causes the noise component in  $d_\lambda(\ell)$  to have an autocorrelation sequence that is zero for all integer displacements,  $\Delta\ell$ , except  $\Delta\ell=0$ ; i.e., it insures that the noise component in  $d_\lambda(\ell)$  has no predictable component. Consequently, the receiver bit-error-probability performance is the best that is theoretically possible.

It is desirable to extend the restricted definition of coherent bit

decisions to a general definition of coherent bit decisions that provides the theoretically best possible performance with any type of additive and multiplicative channel distortions:

General Definition of Coherent Bit Decisions

- (1) Any type of channel distortion may be present.
- (2) There are no equipment distortions.
- (3) The demodulator in general uses a dynamic adaptive filter.
- (4) The demodulator processes the pulse samples,  $\{d_\lambda(\ell)\}$ , for all  $\lambda$  and all past values of  $\ell$  to generate a reference sequence,  $r_\lambda(\ell)$ , for each pulse train.
- (5) For any specified channel conditions, the adaptive filtering and the processing used to generate the reference sequences are chosen to maximize the signal-to-distortion ratio in the approximate keying values,  $\tilde{K}_\lambda(\ell)$ .

Unfortunately, such a general definition has limited practical value because the optimum combination of filtering and reference generation are difficult or impractical to specify except under some restricted channel conditions. However, to the extent that it is practical, coherent bit decisions will be considered with partially coherent, differentially coherent, and noncoherent bit decisions throughout the report.

With partially coherent bit decisions, the reference sequence,  $r_\lambda(\ell)$ , is generated by processing a finite number of preceding pulse samples in the  $\lambda$ th pulse train. In PSK and APSK systems, where the keying value  $K_m \neq 0$  for all  $m$ ,  $r_\lambda(\ell)$  might be determined from

$$r_\lambda(\ell) = \mathcal{O} \left\{ \frac{d_\lambda(\xi)}{\hat{K}_\lambda(\xi)} \right\}, \quad \ell - \Xi \leq \xi \leq \ell - 1 \quad . \quad (50)$$

Equation (50) means that for each value of  $\ell$ , some operation or processing,  $\mathcal{O}$ , such as linear predictive filtering, is performed on the set of  $\Xi$  values of  $d_\lambda(\xi)/\hat{K}_\lambda(\xi)$  for  $\ell - \Xi \leq \xi \leq \ell - 1$ . For each  $\xi$ ,  $d_\lambda(\xi)$  is

divided by  $\hat{K}_\lambda(\xi)$  to remove the keying from  $d_{\lambda s}(\xi)$ , the signal component in  $d_\lambda(\xi)$ . When  $\hat{K}_\lambda(\xi)$  is in error, the keying on  $d_{\lambda s}(\xi)$  is not correctly removed, of course. The operation in (50) therefore is performed on a set of estimates of the values the pulse-sample sequence,  $d_\lambda(\xi)$ , would have if the keying values on all of the pulses in the set were  $K_m = 1$ . The method of obtaining  $r_\lambda(t)$  specified by (50) for PSK and APSK systems might be modified for ASK systems (where  $K_m = 0$  is one of the  $M$  keying values) by using values of  $d_\lambda(\xi)/\hat{K}_\lambda(\xi)$  only when  $\hat{K}_\lambda(\xi) \neq 0$ .

When differentially coherent bit decisions are made in PSK and APSK systems, the usual direct-keying sequence in the modulator,  $K_\lambda(t)$ , is replaced by a phase-differential keying sequence,  $K_{\lambda\Delta}(t)$ , as specified by (19) for time-differential keying and by (20) for frequency-differential and concentric-differential keying. When time-differential keying is used in PSK systems, the differentially coherent reference sequence in (47) becomes

$$r_\lambda(t) = d_\lambda(t-1) \quad ; \quad (51)$$

i.e., the preceding pulse sample is used as a reference. When frequency-differential or concentric-differential keying is used in PSK systems, the differentially coherent reference sequence in (47) becomes

$$r_\lambda(t) = d_{(\lambda-1)}(t) \quad ; \quad (52)$$

i.e., the concurrent pulse sample in the adjacent  $(\lambda-1)$ th train of pulses is used as a reference.

When time-differential keying is used in APSK systems, the differentially coherent reference sequence becomes

$$r_\lambda(t) = \frac{d_\lambda(t-1)}{|\hat{K}_\lambda(t-1)|} \quad . \quad (53)$$

In APSK systems, unlike PSK systems, the keying values,  $\{K_m\}$ , have more than one magnitude, as illustrated by Figure 3(c), p. 17.

Consequently,  $d_\lambda(\ell-1)$  in (53) must be scaled by  $1/|\hat{K}_\lambda(\ell-1)|$  to change its magnitude to the nominal value it would have if the pulse had been keyed by one of the lowest-magnitude keying values, 1,  $j1$ ,  $-1$ , or  $-j1$  in Figure 3(c). The use of (53) in (47) then yields the desired approximate APSK keying value,  $\tilde{K}_\lambda(\ell)$ . Similarly, when frequency-differential or concentric-differential keying is used in APSK systems, the differentially coherent reference sequence in (47) becomes

$$r_\lambda(\ell) = \frac{d_{(\lambda-1)}(\ell)}{|\hat{K}_{(\lambda-1)}(\ell)|} \quad (54)$$

Now consider the ratings in Table 2, p. 58, for single-filter systems with coherent, partially coherent, and differentially coherent bit decisions. Coherent, partially coherent, and differentially coherent bit decisions make use of both the amplitude and phase information in the demodulator pulse samples,  $d_\lambda(\ell)$ , as specified by (47)-(49). With PSK and APSK, the keying values,  $\{K_m\}$ , carry phase information, as shown by Figures 3(b) and 3(c), p. 17. Consequently, as shown by Table 2, with PSK and APSK, coherent bit decisions are theoretically possible and most useful, and partially coherent and differentially coherent bit decisions are practical and most useful. With ASK, coherent bit decisions are theoretically possible and partially coherent bit decisions are practically possible. However, if coherent or partially coherent bit decisions are made, better performance can be obtained with PSK or APSK; consequently, coherent or partially coherent bit decisions with ASK while theoretically possible and practical, are not the most useful. With ASK, differentially coherent bit decisions are impossible because the ASK pulse train does not contain phase keying.

When noncoherent bit decisions are made in the single-filter demodulator of Figure 16(a), the phase information in the demodulator pulse-sample sequence,  $d_\lambda(\ell)$ , is discarded; i.e.,  $|d_\lambda(\ell)|$  is used to make the noncoherent bit decisions. Because PSK and APSK systems depend on

phase information in  $d_\lambda(\ell)$ , noncoherent bit decisions are impossible in PSK and APSK systems, as shown by Table 2, p. 58. Noncoherent bit decisions in ASK systems are made in the manner specified by (47)-(49) for coherent, partially coherent, and differentially coherent bit decisions except for minor modifications: the positive real  $|d_\lambda(\ell)|$  replaces  $d_\lambda(\ell)$ ; the reference sequence,  $r_\lambda(\ell)$ , is positive real; a zero or positive real approximate keying value,  $\tilde{k}_\lambda(\ell)$ , is obtained in place of the generally complex  $\tilde{K}_\lambda(\ell)$ ; and  $\Delta\tilde{k}_m(\ell)$  replaces  $\Delta\tilde{K}_m(\ell)$ . With noncoherent bit decisions in ASK systems, the reference sequence might be obtained from a modification of (50) by using values of  $|d_\lambda(\xi)|/\hat{k}_\lambda(\xi)$  only when  $\hat{k}_\lambda(\xi) \neq 0$ .

Now consider the operation of the multiple-filter demodulator illustrated in Figure 16(b) for the  $\lambda$ th pulse train. Unlike the single-filter demodulator in Figure 16(a), which uses a single filter for each ASK, PSK, or APSK pulse train, the multiple-filter demodulator in Figure 16(b) use  $M$  filters for each of the FSK or CPK pulse trains. As explained in the descriptions of the multiple-filter keying methods, pp. 23-28, each train of FSK or CPK pulses can be viewed as  $M$  dependent trains of binary ASK pulses in which, for each pulse number,  $\ell$ , only one of the  $M$  binary ASK pulses is on. The  $M$  filters in Figure 16(b) correspond to and separate the  $M$  trains of binary ASK pulses. The  $M$  filters may be nonadaptive or adaptive, as specified on p. 51.

The outputs of the  $M$  filters for the  $\lambda$ th pulse train,  $\{o_{\lambda m}(t)\}$ , are delivered to  $M$  corresponding samplers. The  $M$  samplers simultaneously sample the filter outputs at the pulse rate of the FSK or CPK pulse train,  $1/T$ , and deliver  $M$  corresponding generally complex continuously distributed demodulator pulse-sample sequences,  $\{d_{\lambda m}(\ell)\}$ . The sampling times are determined by a clock whose timing (phase) is controlled by a synchronization circuit that is not shown in Figure 16(b). For each pulse in the  $\lambda$ th train, only one of the  $M$  samples will contain a signal component, while all  $M$  samples will contain distortion components. If the  $\mu$ th binary ASK pulse in the  $\lambda$ th FSK or CPK pulse train is on for the  $\ell$ th pulse, so

that only the sample of the  $\mu$ th filter output contains a signal component, then

$$d_{\lambda m}(\ell) = \begin{cases} d_{\lambda ms}(\ell) + d_{\lambda md}(\ell) & , \quad m = \mu \\ d_{\lambda md}(\ell) & , \quad m \neq \mu \end{cases} \quad (55)$$

where  $d_{\lambda ms}(\ell)$  and  $d_{\lambda md}(\ell)$  are the signal and distortion components respectively.

The  $M$  pulse-sample sequences for the  $\lambda$ th FSK or CPK pulse train,  $\{d_{\lambda m}(\ell)\}$ , are delivered by the  $M$  samplers to a single decider for the  $\lambda$ th pulse train, as shown in Figure 16(b). With coherent or partially coherent bit decisions, an approximate keying value,

$$\tilde{K}_{\lambda m}(\ell) = \frac{d_{\lambda m}(\ell)}{r_{\lambda m}(\ell)} \quad , \quad m = 0, 1, 2, \dots, M-1 \quad , \quad (56)$$

is obtained for each of the  $M$  binary ASK pulse trains that compose the  $\lambda$ th FSK or CPK pulse train, as specified by (47). However, the decision process specified by (48) and (49) is not used, as it is in single-filter systems. Rather, for each pulse,  $\ell$ , the decider determines which of the  $M$  approximate keying values,  $\{\tilde{K}_{\lambda m}(\ell)\}$ , has the greatest real component to decide which of the  $M$  binary ASK pulses was on, thereby deciding which of the  $M$  possible waveforms was transmitted. Specifically, if

$$\text{Re}[\tilde{K}_{\lambda \hat{\mu}}(\ell)] = \max\{\text{Re}[\tilde{K}_{\lambda m}(\ell)]\} \quad , \quad m = 0, 1, 2, \dots, M-1 \quad , \quad (57)$$

then the decision is made that the  $\hat{\mu}$ th pulse waveform was transmitted, where  $\hat{\mu}$  is a discrete ( $M$ -ary) estimate of  $\mu$ , the number of the pulse waveform that actually was transmitted; i.e.,  $\hat{\mu}$  may be in error because all  $M$  of the demodulator pulse-sample sequences,  $\{d_{\lambda m}(\ell)\}$ , generally contain a distortion component.

While coherent and partially coherent bit decisions are theoretically and practically possible with FSK and CPK, as shown in Table 2, p. 58,

they are not the most useful decision methods for the same reason they are not the most useful decision methods with ASK: if coherent and partially coherent bit decisions are made, better performance can be obtained with PSK or APSK.

As shown in Table 2, differentially coherent bit decisions are impossible with FSK or CPK because the  $M$  binary-ASK pulse trains that compose the  $\lambda$ th FSK or CPK pulse train do not contain phase keying.

With noncoherent bit decisions in FSK and CPK systems, for each pulse,  $\ell$ , the decider determines which of the  $M$  pulse samples,  $\{d_{\lambda m}(\ell)\}$ , has the greatest magnitude to decide which of the  $M$  possible waveforms was transmitted; i.e., if

$$|d_{\lambda \hat{\mu}}(\ell)| = \max\{|d_{\lambda m}(\ell)|\} \quad , \quad m=0, 1, 2, \dots, M-1 \quad , \quad (58)$$

the decision is made that the  $\hat{\mu}$ th pulse waveform was transmitted, where  $\hat{\mu}$  is a discrete ( $M$ -ary) estimate of  $\mu$ , the number of the pulse waveform that actually was transmitted. As shown by Table 2, noncoherent bit decisions are most useful with FSK and CPK, as they are with ASK, and for the same reasons.

In multiple-filter (FSK and CPK) demodulators, as in single-filter (ASK, PSK, and APSK) demodulators, each selected pulse-waveform number,  $\hat{\mu}$ , in effect is used in a table of assigned bit permutations to determine and deliver the corresponding bit permutation. For successive values of  $\ell$ , the corresponding successive bit permutations form  $\hat{b}_{3\lambda}(k)$ , a discrete estimate of the binary data sequence,  $b_{3\lambda}(k)$ , that is delivered to the  $\lambda$ th pulse-train generator in the modulator. The set of sequences,  $\{\hat{b}_{3\lambda}(k)\}$ , delivered by the  $\Lambda$  deciders are combined in the demultiplexer in Figure 16(b) to form  $\hat{b}_2(j)$ , a discrete estimate of the binary data sequence,  $b_2(j)$ , that is delivered to the modulator. The estimated binary data sequence,  $\hat{b}_2(j)$ , is an output of the demodulator, as shown in Figure 3, p. 17.

In some multiple-filter systems with error coding, successive values of the magnitude of the  $\hat{\mu}$ th pulse estimate in the  $\lambda$ th train,  $|d_{\lambda \hat{\mu}}(\ell)|$  in (58),

are also delivered to the demultiplexer, as illustrated in Figure 16(b). The set of sequences,  $\{|d_{\lambda\hat{u}}(\ell)|\}$ , from the  $\Lambda$  decoders are paired with the proper data bits in  $\hat{b}_2(j)$  (each value of  $|d_{\lambda\hat{u}}(\ell)|$  is used  $N$  times) to form  $|d(j)|$ , a continuously-distributed sequence which, for each value of  $j$ , specifies the magnitude of the  $\hat{u}$ th demodulator pulse sample from which the data bit,  $\hat{b}_2(j)$ , was obtained. The sequence  $|d(j)|$  is delivered as a demodulator output to the error decoder, as shown in Figure 1, p. 4.

In both single-filter and multiple-filter demodulators (Figure 16), a synchronization circuit is required to control the timing (phase) of the sampler clock. Ideally, each pulse sample should be taken at that time during the pulse period when the expected signal-to-distortion ratio in the demodulator filter output is a maximum. The synchronization circuit operates from the one or more pulse trains that carry the digital data in a manner that depends on the fundamental pulse waveform and the keying method that is used. In frequency-multiplexed quaternary PSK systems using adjoining rectangular pulses, slot synchronization is commonly used. With slot synchronization and  $\Lambda$  pulse trains, one of  $\Lambda+1$  frequency-multiplexed subchannels carries no pulse train (is vacant). In the demodulator, the filter tuned to the vacant subchannel responds to all of the frequency-offset pulse trains at nonoptimum sampling times. The output of the vacant filter is sampled twice for each pulse number,  $\ell$ , at times earlier and later than the single sampling time for the  $\Lambda$  pulse trains. The early and late samples are combined and filtered to control the phase of the sampler clock. In binary FSK systems using adjoining rectangular pulses with noncoherent bit decisions, the magnitude of one or more of the demodulator filter outputs can be processed to control the phase of the sampler clock.

Most single-filter and multiple-filter demodulators also incorporate a Doppler-correction circuit whose function in the frequency domain is analagous to that of the synchronization (delay-correction) circuit in the time domain. A single Doppler-correction circuit is used to shift the frequencies of all  $\Lambda$  pulse trains by a common amount to compensate for

the mean Doppler shift imposed by the channel and equipment. Ideally, the Doppler correction should be that frequency shift required to maximize the expected signal-to-distortion ratio in the demodulator filter outputs. The Doppler-correction circuit may operate from one or more of the pulse trains that carry the digital data, or it may operate from a CW Doppler-correction signal just outside the signal band. A CW Doppler-correction signal is commonly used in frequency-multiplexed quaternary PSK systems using adjoining rectangular pulses. The techniques used by Doppler-correction circuits in the frequency domain are analagous to those used by synchronization circuits in the time domain.

For most applications, where a transmission continues for a relatively long time, the response times of the synchronization and Doppler-correction circuits can be and usually are relatively long (tens or hundreds of pulse periods). In burst communication systems, where a transmission may be short (tens or hundreds of pulse periods), short response times are required.

The demodulator in general introduces all of the types of equipment distortions listed on p. 8.

#### 5.4 Error Decoder

As illustrated in Figure 1, p. 4, the error decoder processes  $\hat{b}_2(j)$ , a discrete estimate of the binary data sequence,  $b_2(j)$ , that is generated by the error coder in the transmitter. Some error decoders also process  $|d(j)|$ , the continuously distributed magnitude of the pulse-sample sequence which, for each value of  $j$ , specifies the magnitude of the demodulator pulse sample from which the corresponding data bit,  $\hat{b}_2(j)$ , was obtained. The purpose of an error decoder is to detect, and in general, to correct as many errors in  $\hat{b}_2(j)$  as practical. In general, fewer errors can be corrected than detected, and not all errors can be detected.

For both block and convolutional codes (p. 9), there are two major

types of decoding:

### Types of Decoding

- (1) Hard
- (2) Soft

With hard decoding, only  $\hat{b}_2(j)$ , the estimate of the binary data sequence, is processed. The decoding is called hard because it makes use of the discrete (hard) decisions made by the decider in the demodulator that constitute  $\hat{b}_2(j)$ . Using a decoding algorithm suited to the specific code that is used, the decoder in effect uses the redundancy provided by the check bits to detect and correct errors.

With soft decoding, both  $\hat{b}_2(j)$ , the estimate of the binary data sequence, and  $|d(j)|$ , the magnitude of the pulse-sample sequence, are processed. The decoding is called soft because it makes use of the continuously distributed (soft) magnitude of the pulse-sample sequence, as well as the discrete estimate of the binary data sequence. In effect, the soft decoding algorithm first uses  $\hat{b}_2(j)$  to detect and correct those errors which the hard decoding permits, and then uses  $|d(j)|$  to correct additional errors. Substantial additional error correction is possible when the errors are highly correlated with  $|d(j)|$ . This is the case in any channel with substantial fading, such as HF channels. With such channels, the short-term bit error probability on each pulse train is inversely related to the magnitude of the pulse; i.e., errors occur when fading reduces the magnitude of the pulse, without affecting the distortion level, to decrease temporarily the signal (pulse)-to-distortion ratio in the demodulator filter output to a level low enough to produce errors in the bit-decision process.

Soft decoding is illustrated in Figure 18 for a (25,16) block code with  $n_1 = 16$  information bits and  $n_c = 9$  check bits (Chase, 1973). In the error coder in the transmitter, successive sets of 16 information bits in the input information bit sequence,  $b_1(i)$ , are each combined with 9 check bits to form a  $5 \times 5$  matrix. This is illustrated in Figure 18(a), where

$$\begin{bmatrix} I_{11} & I_{12} & I_{13} & I_{14} & P_{15} \\ I_{21} & I_{22} & I_{23} & I_{24} & P_{25} \\ I_{31} & I_{32} & I_{33} & I_{34} & P_{35} \\ I_{41} & I_{42} & I_{43} & I_{44} & P_{45} \\ P_{51} & P_{52} & P_{53} & P_{54} & P_{55} \end{bmatrix}$$

(a) Data-bit matrix

$$\begin{bmatrix} D_{11} & D_{12} & D_{13} & D_{14} & D_{15} \\ D_{21} & D_{22} & D_{23} & D_{24} & D_{25} \\ D_{31} & D_{32} & D_{33} & D_{34} & D_{35} \\ D_{41} & D_{42} & D_{43} & D_{44} & D_{45} \\ D_{51} & D_{52} & D_{53} & D_{54} & D_{55} \end{bmatrix}$$

(b) Pulse-sample matrix

Figure 18. Matrices for soft decoding of a (25,16) block code.

the I elements are information bits and the P elements are parity check bits. Given the 16 information bits, the parity check bits are chosen to make the modulo-two sum in each of the five rows and five columns equal to zero. The 25 bits in each block are distributed among the pulse trains,  $\lambda$ , and in time,  $\ell$ , to reduce the probability of large bursts of errors in any code block.

In the receiver decoder, the corresponding bit matrix, formed from  $\hat{b}_2(j)$ , is identical to Figure 18(a) except for those information and parity check bits that are in error. The decoding algorithm initially checks the parity of each row and column. If a single error occurs, its position is unambiguously determined by the one row and one column that violate the parity checks, and a hard correction of the error can be effected. For example, if  $I_{23}$  only is in error, the second row and third column violate the parity check, thus permitting the hard correction of  $I_{23}$ . If two or more errors occur, the parity checks cannot unambiguously determine the locations of the bit errors, and soft error correction is utilized. For example, if  $I_{23}$  and  $P_{35}$  are in error, the parity checks in rows two and three and columns three and five are violated, indicating  $I_{23}$  and  $P_{35}$  may be in error or, with equal probability, that  $I_{33}$  and  $P_{25}$  may be in error.

To resolve the ambiguity, the error decoder examines a corresponding  $5 \times 5$  matrix of values of  $|d(j)|$ , as illustrated in Figure 18(b). Each subscripted D element in Figure 18(b) is the magnitude of the pulse sample from which the bit value in the same row and column in Figure 18(a) was obtained. To determine which pair of bits is in error,  $I_{23}$  and  $P_{35}$  or  $I_{33}$  and  $P_{25}$ , each pair of corresponding generally weighted D values is summed. The pair with the smallest sum (the weakest pulses) then specifies with a low probability of error which pair of bits is in error, thus permitting their soft correction.

The soft decoding algorithm can easily be made to handle two errors in the same row or column, and can quite practically be made to handle as many as five or six errors in the illustrated example. The example shows that soft decoding can provide substantially better error correction than hard decoding because it makes use of additional valuable information: that the magnitude of the pulse samples and the bit errors are highly correlated in HF digital radio systems because of the fading characteristic of HF channels.

There are three ways in which error coding can be utilized in HF digital radio systems:

#### Error Coding Methods

- (1) Error detection and correction (one way)
- (2) Error detection and repeat transmission (two ways)
- (3) Error detection, correction, and repeat transmission (two ways)

In the first method, which is used in simplex (one-way) HF digital communication systems, the error decoding is used to detect and correct as many of the digital errors as practical. The second and third methods can be used only in duplex (simultaneous two-way) systems. In the second method, the error decoder at each end of the two-way link only detects errors and, when an error is detected in some pre-arranged block of data, requests via the return link that the transmitter repeat

that block of data. In the third method, each error detector detects errors and corrects them if they are few enough in number to be reliably corrected; otherwise, it requests a repeat transmission. The second and third methods can provide a reduction in error probability comparable to the first method with simpler error coding, because error detection is simpler than error correction. However, it requires a duplex system and suitable buffering at each end to handle the random changes in overall data rate that results from the repeat transmissions.

Following the detection and correction of errors in the estimate of the binary data sequence,  $\hat{b}_2(j)$ , the error decoder separates the information bits to form the receiver output,  $\hat{b}_1(i)$ , an estimate of the binary information sequence,  $b_1(i)$ , that was delivered to the transmitter.

Because error decoders typically are digital equipments, they introduce no distortion components.

## 5.5 Diversity Operation

With diversity operation, the digital data are received two or more times, the number of times being the order of the diversity,  $D$ . The redundant data from the  $D$  diversity channels are combined in a diversity demodulator to improve the performance of the system. Substantial performance improvement is obtained when the correlation of the fading in the  $D$  diversity channels is reasonably small or negative. Diversity operation can be classified as follows:

### Types of Diversity

- (1) Single transmission (space, antenna)
  - (a) Polarization
  - (b) Separation
- (2) Multiple transmission
  - (a) Frequency
  - (b) Time

With single-transmission diversity, also called space diversity and antenna diversity, each keyed pulse is transmitted only once, but is received over D antennas that feed D HF receivers whose outputs are delivered to a single demodulator that is designed for diversity reception. With polarization diversity, two concentric perpendicularly polarized antennas provide dual (D= 2) diversity. With separation diversity, two or more antennas with a common polarization are separated by from one to several wavelengths. Separated antennas with different polarizations provide polarization and separation diversity.

With multiple-transmission diversity, each keyed pulse is transmitted D times to a single receiving antenna. With frequency diversity, the redundant pulses are transmitted simultaneously in D frequency-multiplexed pulse trains. With time diversity, the redundant pulses are transmitted at different times in the same pulse train. With frequency and time diversity, the redundant pulses are distributed in both frequency and time. Concentric multiplexing of the redundant pulses is not effective.

Single-transmission separation diversity (1b) and multiple-transmission frequency diversity (2a) are commonly used in HF digital radio systems.

With all types of diversity operation, the diversity demodulator in effect combines the redundant data in the deciders (Figure 16). In systems using coherent, partially coherent, or differentially coherent bit decisions, each generally complex approximate keying value,  $\tilde{K}_\lambda(t)$  in (47), p. 58, in single-filter systems or  $\tilde{K}_{\lambda m}(t)$  in (56), p. 65, in multiple-filter systems, is weighted and summed with the other D-1 redundant approximate keying values to form a single combined approximate keying value. With noncoherent bit decisions, each real approximate keying value,  $\tilde{k}_\lambda(t)$  in single-filter systems or  $\tilde{k}_{\lambda m}(t)$  in multiple-filter systems, is weighted and summed with the other D-1 redundant real approximate keying values to form a single combined real approximate keying value. In both cases, the combined approximate keying value is then processed as described earlier for a system without diversity.

The weighting imposed on the D redundant approximate keying values is usually one of three types. With selection combining, the magnitude of the reference value,  $|r_\lambda(t)|$  in single-filter systems and  $|r_{\lambda m}(t)|$  in multiple-filter systems, is examined for each diversity channel. The approximate keying value in the diversity channel with the largest reference magnitude receives a weighting of one (is selected), while the other D-1 keying values all receive weights of zero (are discarded). With equal-gain combining, the D approximate keying values receive equal weights of  $1/D$ . With maximal-ratio combining, each approximate keying value is weighted in proportion to the magnitude of the corresponding reference value,  $|r_\lambda(t)|$  in single-filter systems and  $|r_{\lambda m}(t)|$  in multiple-filter systems, and in inverse proportion to the noise power in that diversity channel (which are usually the same).

## 5.6 Performance Monitoring and Prediction

The performance of any HF digital radio system changes both with HF operating frequency and time, because both the additive and multiplicative channel distortions (p. 45) change with frequency and time. For this reason, most systems have a number of available operating frequencies or channels so that ideally at any time the channel that provides the best system performance can be chosen and used. However, this requires a knowledge of the system performance for the channel that is being used and a prediction of the system performance on the other available channels.

Monitoring of the system performance is possible in a number of ways. Visual monitoring of the received information printout is commonly used to obtain a rough estimate of the error probability. In the demodulator, the total distortion;  $\Delta \tilde{K}_{\lambda \hat{u}}(t)$  in (49), p. 59;  $\tilde{K}_{\lambda m}(t)$  for  $m \neq \hat{u}$  in (57), p. 65; or  $d_{\lambda m}(t)$  for  $m \neq \hat{u}$  in (58), p. 66; can have its magnitudes squared and averaged for all  $\Lambda$  pulse trains to determine the signal-to-total-distortion ratio, which indirectly specifies the system performance. In systems with error coding, the error decoder can monitor detected

and corrected bit errors to provide an automatic and accurate method of monitoring system performance.

The prediction of system performance on available channels that are not being used can be done in the following ways:

#### Performance Prediction Methods

##### (1) Simplex (one-way) systems

- (a) Experience
- (b) Propagation predictions

##### (2) Duplex (two-way) systems

- (a) Passive monitoring
- (b) Oblique pulse sounding
- (c) System sounding

In simplex systems, performance prediction is limited to experience and propagation predictions. The experience gained in operating an HF digital radio system between two geographical locations provides useful knowledge about the system performance that can be expected on the available channels at various times. Propagation predictions can augment this knowledge by providing useful information about expected multipath differential-delay and attenuation conditions as functions of frequency and time. Both prediction methods have limited accuracy and cannot predict unusual propagation, interference, or noise conditions. In broadcast transmissions, where the same messages are directed to a number of receivers at different locations, either a commonly acceptable channel is used or the messages are transmitted simultaneously on several channels.

In duplex systems, three additional prediction methods are available. With passive monitoring, real-time information on noise and interference conditions on the available channels is obtained with an auxiliary receiver that measures the noise and interference levels on the available channels. With oblique pulse sounding, an auxiliary sounding transmitter repeatedly

sends spaced pulses with successively different frequencies that scan the HF spectrum. An auxiliary sounding receiver at the other end of the link operates in synchronism to present visually an oblique ionogram, as illustrated in Figure 9, p. 36. Such ionograms are useful in predicting the differential-delay distortions in the available channels. With system sounding, the HF digital radio system itself is used to predict system performance on each of the available channels. Periodically, when the traffic permits or the receiving site so requests, the transmitter and receiver are sequentially switched to the other available channels for brief periods ( $\sim 1$  minute each). For each available channel, the signal-to-distortion ratio is determined by the demodulator as described above to determine indirectly the bit error probability. (A direct counting of bit errors to obtain an error-probability estimate takes too long at lower error probabilities.) Automatic transmitter, antennas, and receiver tuning is necessary. A pre-arranged message is used to coordinate the transmitter and receiver channel scanning.

With all three duplex methods of performance prediction, the receiving site requests the transmitting site to change the channel when this is advantageous.

## 6. SYSTEM PERFORMANCES

Two criteria will be used to specify system performance:

### System Performance Criteria

- (1) Information bit error probability
- (2) Spectral efficiency (information rate / signal bandwidth)

The bit-error-probability performance of a system with respect to the various types of channel and equipment distortions is determined by nine system design features that were described earlier:

## System Design Features

- \* (1) Fundamental pulse waveform (p. 12)
- \* (2) Keying method (p. 15)
- \* (3) Multiplexing method (p. 19)
- \* (4) Demodulator filter type (p. 51)
  - (5) Bit-decision method (p. 57)
  - (6) Transmitter power (p. 29)
  - (7) Antennas (pp. 31, 46)
- \* (8) Diversity (p. 72)
- \* (9) Error coding (pp. 9, 68)

The spectral efficiency of a system, which is independent of channel and equipment distortions, is determined primarily by the six system design features above that are preceded by asterisks. Multiple-transmission diversity affects spectral efficiency, but single-transmission diversity does not. Spectral efficiency is also affected by an auxiliary tone or signal that is transmitted for synchronization or Doppler-correction purposes.

The effects of the system design features on bit-error-probability performances will be evaluated in the following three sections, first with respect to additive channel and equipment distortions, second with respect to multiplicative channel and equipment distortions, and third with respect to nonlinear equipment distortions. Spectral efficiencies will be evaluated in conjunction with the evaluation of bit-error-probability performances. To help in the evaluation of bit-error-probability performances, the channel and equipment distortions that were listed earlier separately (pp. 8, 45) are presented together in Table 3.

### 6.1 Additive Distortions

Unless otherwise stated, it will be assumed throughout this section that the fundamental pulse waveform and multiplexing method are arbitrary,

Table 3. Channel and equipment distortions

Types of Distortion		Specific Distortions	
		Channel	Equipment
Additive	Noise	Thermal Impulsive	Thermal Quantizing
	Interference	Unwanted signals	Internal
Multi- plicative	Time scatter	Differential delay Dispersion	Synchronization Filtering
	Frequency scatter	Differential Doppler Fading	Doppler correction AGC
Nonlinear		---	Nonlinear

the demodulator filters are matched, the antennas are arbitrary but non-adaptive, there is single-diversity operation, there is no error coding, there are no transmitter distortions, and the channel and receiver may introduce only additive distortions. When a channel introduces only additive distortions, it must contain only a single propagation path,  $P=1$ , with no Doppler shift,  $v_1 = 0$ , and arbitrarily slow Rayleigh fading,  $2\sigma_1 \rightarrow 0$ , the last to eliminate significant fading distortion. Such a channel has a time-varying frequency response,  $H(f,t)$  in (34), p. 41, whose magnitude is constant (flat) in frequency and has arbitrarily slow Rayleigh fading in time. When the receiver introduces only additive distortions, the synchronization is perfect, there is no filtering distortion, there is no Doppler-correction error, and the receiver gain is constant (no AGC fluctuations).

First consider the case where there are no receiver distortions and white thermal noise is the only channel distortion. Let the signal-to-noise power ratio at the receiver input be specified by

$$\rho = \frac{S}{N_1} = \frac{S/f_1}{N_1/f_1} = \frac{E_b}{N_d} ; \quad (59)$$

where  $S$  is the average total signal power;  $N_1$  is the white noise power in a bandwidth equal to the information bit rate,  $f_1$  (p. 3);  $E_b = S/f_1$  is the energy per information bit; and  $N_d = N_1/f_1$  is the white noise power spectral density; all at the receiver input<sup>3</sup>. Then with a slow frequency-flat Rayleigh-fading channel, the theoretical bit error probability as a function of the signal-to-noise ratio at the receiver input is specified by the following five equations for various combinations of keying and bit-decision methods:

$$P_e(\rho) = \frac{1}{2} \left( 1 - \sqrt{\frac{\rho}{1+\rho}} \right) \approx \frac{1}{4\rho}, \quad \rho \rightarrow \infty; \text{ coherent PSK, } M=2,4. \quad (60)$$

$$P_e(\rho) = \frac{1}{2} \left( 1 - \sqrt{\frac{\rho}{2+\rho}} \right) \approx \frac{1}{2\rho}, \quad \rho \rightarrow \infty; \text{ coherent FSK, CPK, } M=2. \quad (61)$$

$$P_e(\rho) = \frac{1}{2} \left( 1 - \sqrt{\frac{\rho}{4+\rho}} \right) \approx \frac{1}{\rho}, \quad \rho \rightarrow \infty; \text{ coherent ASK, } M=2. \quad (62)$$

$$P_e(\rho) = \frac{1}{2} \left( \frac{1}{1+\rho} \right) \approx \frac{1}{2\rho}, \quad \rho \rightarrow \infty; \text{ diff-coherent PSK, } M=2. \quad (63)$$

$$P_e(\rho) = \frac{1}{2} \left( \frac{2}{2+\rho} \right) \approx \frac{1}{\rho}, \quad \rho \rightarrow \infty; \text{ noncoherent FSK, CPK, } M=2. \quad (64)$$

The five functions are illustrated in Figure 19. Also included is an approximate performance curve for noncoherent ASK (Schwartz et al., 1966). The differentially coherent PSK equation, (63), and its plot in Figure 19, apply to all three types of phase-differential keying: time-differential, frequency-differential, and concentric-differential keying.

<sup>3</sup> When any type of white noise is the only distortion and bit-error-probability is determined as a function of  $E_b/N_d$  for two or more systems with generally different information rates and system design features, such bit-error-probability performances can be fairly compared because they include the transmitter power used for check bits with error coding, Doppler-correction tones, and other auxiliary components.

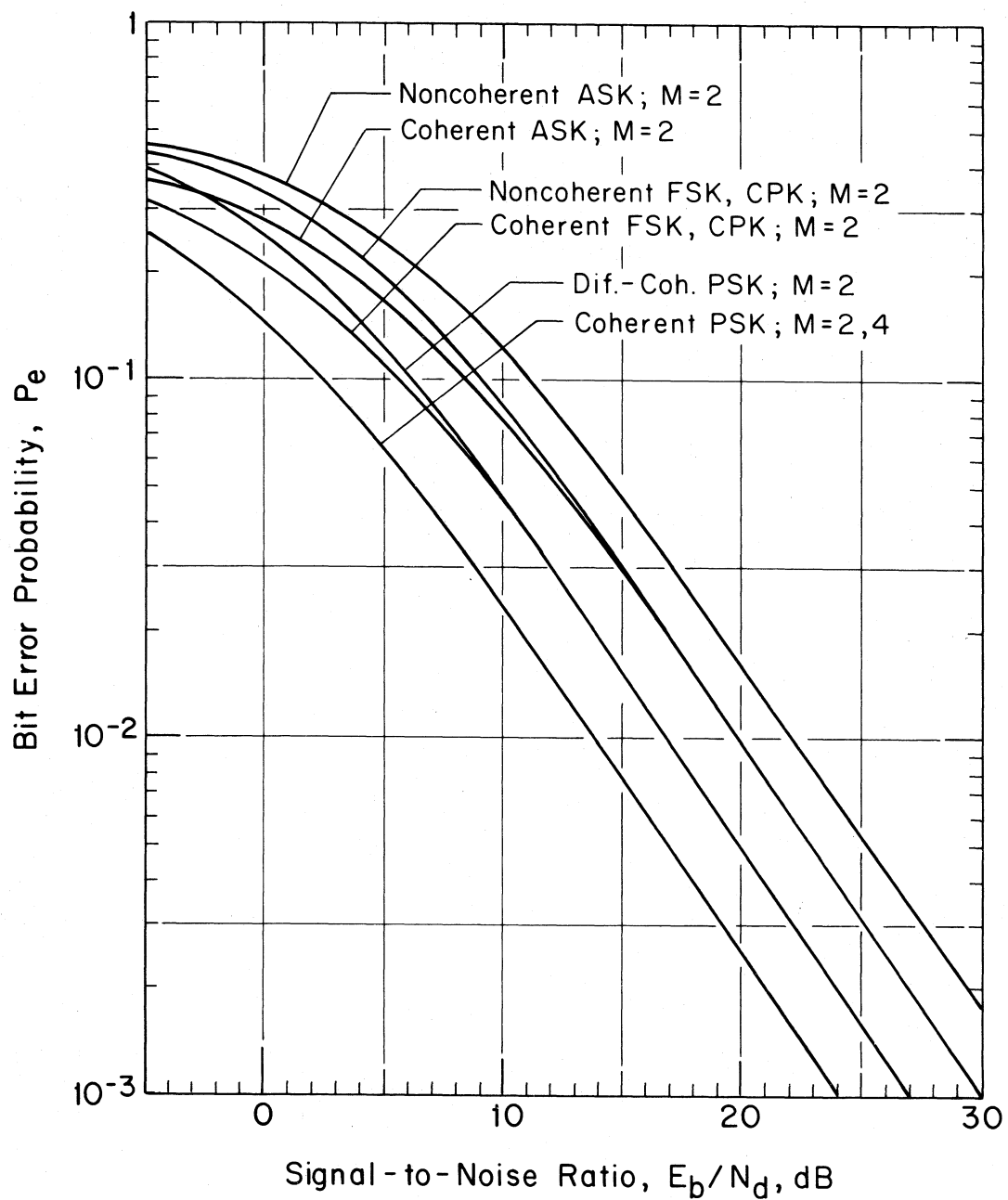


Figure 19. Bit-error-probability performances of matched-filter ASK, PSK, FSK, and CPK systems over a slow, frequency-flat, Rayleigh-fading channel with white thermal noise.

Channel:  $P=1$ ,  $\nu_1=0$ ,  $2\sigma_1 \rightarrow 0$ ,  $S/I \rightarrow \infty$ .

Equipment: No distortions.

In the event the receiver introduces significant thermal noise, the curves of Figure 19 apply if the receiver thermal noise is referred to the receiver input and included with the channel noise in  $N_d$  in (59). The same can be done for any receiver quantizing noise provided the demodulator filtering converts it to near-thermal (near-Gaussian) noise.

An examination of Figure 19 shows that with coherent bit decisions, PSK provides the best bit-error-probability performance, FSK and CPK provide the second-best performance, and ASK provides the poorest performance. As shown by (60)-(62), as  $\rho \rightarrow \infty$ , coherent PSK is 3.0 dB better than coherent FSK and coherent CPK, which in turn are 3.0 dB better than coherent ASK. Practical systems with partially coherent bit decisions can closely approach the performances shown for coherent systems. Differentially coherent PSK and noncoherent FSK and CPK are 3.0 dB poorer than the corresponding coherent systems, while noncoherent ASK is 2.2 dB poorer than coherent ASK.

It is important to note that all of the performance curves in Figure 19 apply only to binary ( $M=2$ ) systems except for the coherent PSK curve, which also applies to quaternary ( $M=4$ ) systems. The differentially coherent PSK curve for  $M=2$  also is accurate for  $M=4$  at the lower bit-error probabilities. Because the bandwidth of a PSK signal does not change when  $M$  is changed from 2 to 4 (when the number of bits/pulse,  $N$ , changes from 1 to 2), the spectral efficiency of PSK can be doubled by increasing  $M$  from 2 to 4 without changing the bit-error-probability performance of the system. Therefore, quaternary PSK not only has a better thermal-noise bit-error-probability performance than binary FSK (by 3.0 dB) and binary ASK (by 6.0 dB), but also has greater spectral efficiency: about four times greater than binary FSK and two times greater than binary ASK when the same fundamental pulse waveform, scaled for the same data rate, is used by all three systems.

As  $M$  is increased above 4 in PSK systems and above 2 in ASK systems, the signal bandwidths remain the same, but the performances with respect to thermal noise become poorer. The poorer performances

can be viewed as the prices paid for the increased spectral efficiency that results. FSK and CPK systems are different, however; as  $M$  is increased above 2, the performance with respect to thermal noise improves, but the spectral efficiency decreases. The poorer spectral efficiency can be viewed as the price paid for the improved thermal-noise performance.

APSK is normally used rather than PSK for  $M \geq 8$ , because its performance is better. When the same fundamental pulse waveforms are used, the bandwidth of an APSK signal is identical to that of a PSK signal. For  $M \geq 8$ , the thermal-noise performance of APSK is poorer than that of PSK for  $M = 2$  or 4 that is illustrated in Figure 19. However, the spectral efficiency is higher. The poorer thermal-noise performance can be viewed as the price that is paid for the higher spectral efficiency.

The performance of any system with respect to white thermal noise is best with matched demodulator filters because such filters maximize the signal-to-noise ratios at their outputs at the optimum pulse-sampling times. However, the bit-error-probability curves of Figure 19 also apply to nonmatched demodulator filters if the curves are translated to the right by the ratio in decibels of the nonmatched-to-matched filter-output signal-to-noise ratios, provided the nonmatched filters, like the matched filters, introduce no filtering distortion.

When white atmospheric or man-made impulsive noise replaces white thermal noise, the relative performances of ASK, PSK, APSK, FSK, and CPK systems remain approximately the same, but their absolute performances may be better or poorer than with white thermal noise of the same spectral power density,  $N_d$ , at the receiver input. In a linear receiver (no pulse clipping), the performances are poorer at suitably low error probabilities (less than about  $10^{-1}$ ), because the impulses generally project well above the rms noise level to cause errors when thermal noise would not [because the probability density function for the magnitude of the complex impulsive noise envelope has a much longer high-magnitude tail than the Rayleigh probability density function for the magnitude of the complex envelope of thermal (Gaussian) noise]. When clipping is

incorporated in a receiver prior to the demodulator input in Figure 16, p. 50, the clipping of the larger noise pulses reduces the rms power of the impulsive noise, improving the system performance relative to that of a linear receiver. If the clipping occurs in a relatively wide-bandwidth portion of the receiver (the wider, the better), the subsequent narrow-bandwidth demodulator filters convert the clipped impulsive noise to near thermal (near-Gaussian) noise. If the clipping level is near optimum and the ratio of the wide to narrow bandwidths is large enough, the performances of the systems with white impulsive noise can be better than with white thermal noise of the same spectral power density at the receiver input. Again, matched demodulator filters provide the best performance.

When channel or receiver interference replaces white thermal noise, the relative performances of ASK, PSK, APSK, FSK, and CPK systems remain approximately the same. However, their absolute performances will depend greatly on the character of the interference and the types of demodulator filters. When the interference is noise-like in character, has a bandwidth that is equal to or larger than the signal bandwidth, and has a spectral power density over the signal band that is compared to white thermal noise of the same spectral power density, the performances of the systems with respect to interference will be comparable to their thermal-noise performances.

When the bandwidth of the interference is smaller than the bandwidth of any pulse train, the bit-error-probability performance for that pulse train will be comparable to the performance with white thermal noise of the same power in the output of the matched or nonmatched nonadaptive demodulator filter. However, with an adaptive filter, the performance with narrow-band interference can be substantially better. This can be illustrated with CW interference and a quasi-static adaptive demodulator filter with an adjustable narrow suppression band incorporated in its otherwise matched or approximately matched frequency response. When the narrow suppression band is automatically centered on the CW

interference, it can effectively remove the interference while introducing only a very small amount of multiplicative filtering distortion. With CW interference, a quasi-static adaptive filter can provide a very substantial improvement in performance (tens of decibels) relative to matched-filter performance. If the bandwidth of the interference is increased, the adaptive filter automatically increases the suppression bandwidth. However, the multiplicative filtering distortion increases, and the performance improvement is therefore less than with CW interference. With a quasi-static adaptive filter, the performance improvement disappears when the interference bandwidth becomes a substantial fraction of the bandwidth of the pulse train. However, with a dynamic filter, substantial performance improvement can still be obtained if the bandwidth of the modulation on the interference (rather than the bandwidth of the interference itself) is suitably smaller than the bandwidth of the pulse train, because the suppression characteristics of the adaptive filter are dynamically adjusted according to the modulation on the interference. Ideally, the quasi-static or dynamic adaptive filter adjusts its response to maximize the signal-to-total-distortion ratio at its output at an optimum sampling time, where in the present case the total distortion is additive interference and multiplicative filtering distortions combined.

The preceding descriptions of system bit-error-probability performances with additive channel and equipment distortions are generally affected by a change in transmitter power. If  $X$  is the average transmitter power, an increase of  $\Delta X$  in transmitter power will improve the system performance by  $10 \log(1 + \Delta X/X)$  dB with respect to channel and equipment thermal noise (assuming the change in signal level does not change the noise figure of the HF receiver via its AGC), but by a generally smaller amount [ $< 10 \log(1 + \Delta X/X)$  dB] with respect to channel and receiver impulsive noise and interference.

If the gain of the transmitting antenna is increased, an equivalent change in transmitter power,  $\Delta X$ , results, and the effects on system performances are those described for a change in transmitter power. If the

gain of the nonadaptive receiving antenna is increased, the performances will generally improve with respect to additive receiver distortions by an amount up to the increased gain. The narrower beamwidth of the higher gain receiving antenna can provide improved performances with respect to additive channel distortions that are suitably directional. Noise typically is only mildly directional, so little if any improvement would result, but interference is highly directional, and the narrower beamwidth can provide substantial performance improvements if the direction of the interference is suitably different from that of the signal.

If the nonadaptive receiving antenna is replaced by an adaptive receiving antenna of the same gain, then the system performances with respect to additive receiver distortions are unchanged. However, the nulls of the adaptive antenna pattern can automatically be adjusted (within limits) to provide greater suppression of the directional additive channel distortions, particularly interference, thereby improving the performances over those with a nonadaptive receiving antenna.

The performances of the single-diversity systems described above are substantially improved by using second-order or higher order diversity. With single-transmission (polarization and separation) diversity, the spectral efficiency does not change as the order of the diversity,  $D$ , increases. With multiple-transmission (frequency and time) diversity, the spectral efficiency decreases inversely with  $D$ , and an increase in transmitter power of  $10 \log(D)$  dB is required to retain the same signal-to-noise ratio in each diversity channel. At the same time, the performance improvements that single-transmission and multiple-transmission diversity can provide are identical, provided the degree of independence of the fading on the diversity channels is the same for both types of diversity. Therefore, multiple-transmission diversity requires  $D$  times more transmitter power and  $D$  times more bandwidth for the same data rate than single-transmission diversity to achieve the same performance improvement.

Of three types of diversity combining, selection combining, equal-gain

combining, and maximal-ratio combining, the last provides the theoretically greatest performance improvement. With maximal-ratio diversity combining, the theoretical bit error probability for matched-filter coherent PSK systems with  $M=2$  or  $4$  is

$$P_e(\rho;D) = \frac{1}{2} \left\{ 1 - \sqrt{\frac{\rho}{1+\rho}} \sum_{k=0}^{D-1} \binom{2k}{k} \left[ \frac{1}{4(1+\rho)} \right]^k \right\}, \quad (65)$$

coherent PSK,  $M=2, 4$ ,

when the arbitrarily slow fading of the signal in the diversity channels is independent, when thermal channel or receiver noise is the only distortion in each diversity channel, and when these noises in the diversity channels are independent (Proakis, 1968).

Equation (65) is illustrated in Figure 20. It can be seen that the performance improvements provided by increasing the order of diversity,  $D$ , are substantial, but the improvement increases less rapidly as  $D$  becomes larger. The diversity performances for coherent FSK with  $M=2$  and coherent ASK with  $M=2$  are 3.0 dB and 6.0 dB poorer respectively than the diversity performances shown in Figure 20 for coherent PSK with  $M=2$  or  $4$ . The performances with selection combining and equal-gain combining are poorer than those illustrated for maximal-ratio combining, but not by very much. The performance improvements are less when the fading on the diversity channels is positively correlated, but the improvements are greater with negatively correlated fading, which can occur with polarization diversity and frequency diversity. The matched-filter curves of Figure 20 also apply for nonmatched filters when the curves are translated to the right by the ratio in decibels of the non-matched-to-matched filter-output signal-to-noise ratios, provided the nonmatched filters, like the matched filters, introduce no filtering distortion.

The performances of the systems described above can also be substantially improved when error coding is incorporated. As previously

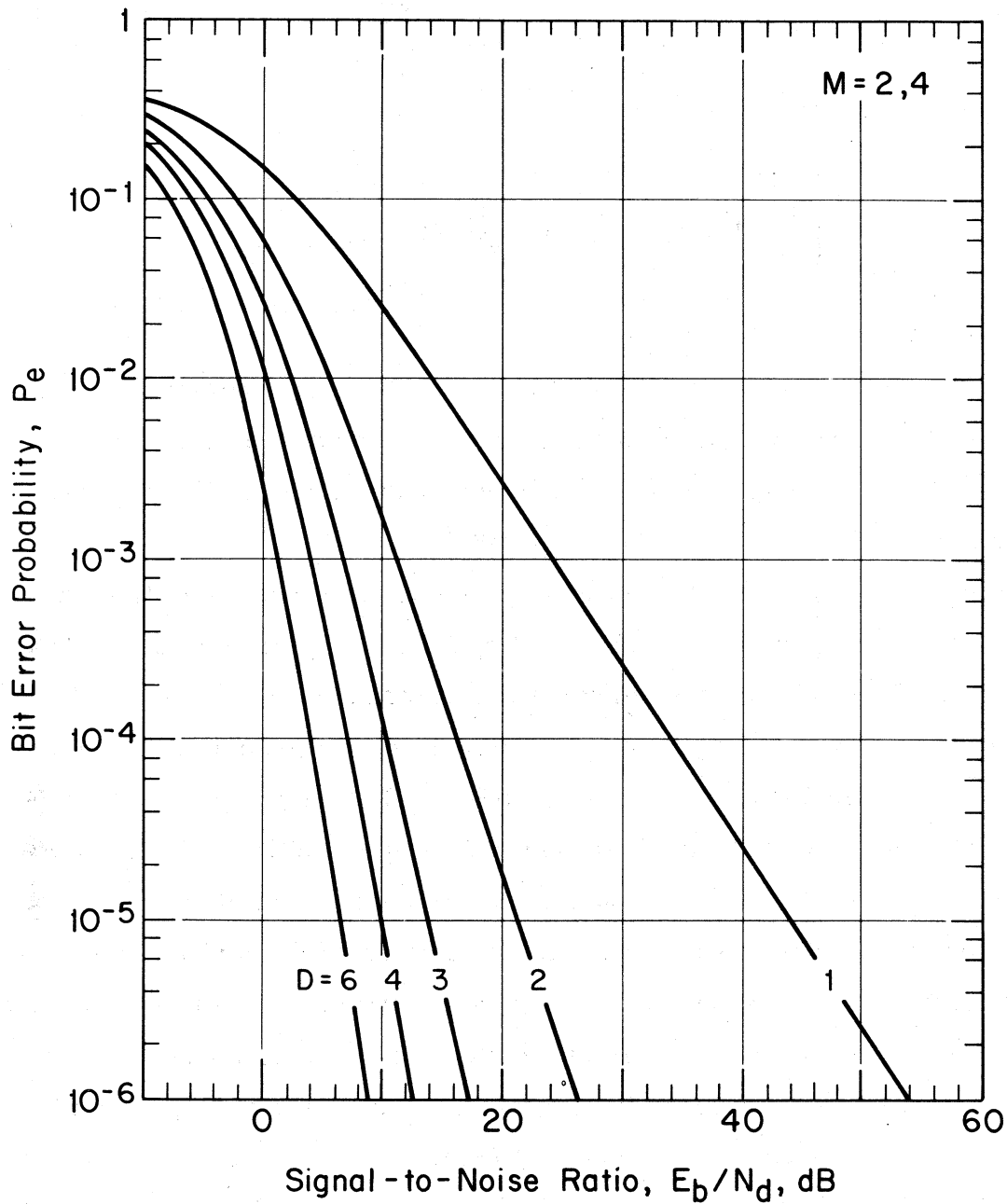


Figure 20. Bit-error-probability performances of matched-filter coherent binary and quaternary PSK systems over slow, frequency-flat, independently Rayleigh-fading diversity channels with independent white thermal noise and maximal-ratio combining.

Channel:  $P=1$ ,  $\nu_1=0$ ,  $2\sigma_1 \rightarrow 0$ ,  $S/I \rightarrow \infty$ .

Equipment: No distortions.

described, soft decoding can provide substantially better error correction than hard decoding because it makes use of additional valuable information: that the magnitude of the demodulator pulse samples and the bit errors are highly correlated in HF digital radio systems because of the Rayleigh-fading characteristic of HF channels. The improvement in system performance provided by soft decoding can be illustrated by comparing the performances of two systems using time-differentially coherent quaternary ( $M=4$ ) PSK with similar but slightly different nonmatched demodulator filters, one system without error coding and the other with the (25,16) block code with soft decoding that is shown in Figure 18, p. 70, and described on pp. 69-71. When the bits in each code block in the system with error coding are assigned to different pulses separated in time sufficiently to suffer independent fading (so the bit errors in each block are independent), then the bit-error-probability performances of the two systems, obtained by computer simulation (Chase, 1973) are as illustrated in Figure 21.

It can be seen that the coding provides a substantial improvement in bit-error-probability performance, particularly at low error probabilities where the curve for the system with coding is much steeper. The system with the (25,16) soft error-correcting coding has a spectral efficiency that is  $16/25=0.64$  times that of the system without coding (neglecting Doppler-correction tones). The moderately poorer spectral efficiency can be viewed as a modest price to pay for the substantial improvement in bit-error-probability performance. In their linear portions, the no-coding curve in Figure 21 is 2.0 dB poorer than the differentially-coherent PSK curve in Figure 19 (which applies for  $M=4$  in its linear portion) because a Doppler-correction tone is incorporated (1.0 dB loss) and a nonmatched filter rather than a matched filter is used (1.0 dB loss).

Now consider the effects of additive transmitter distortions. In all of the preceding discussions of the effects of additive channel and receiver distortions on system performance, it was assumed the additive

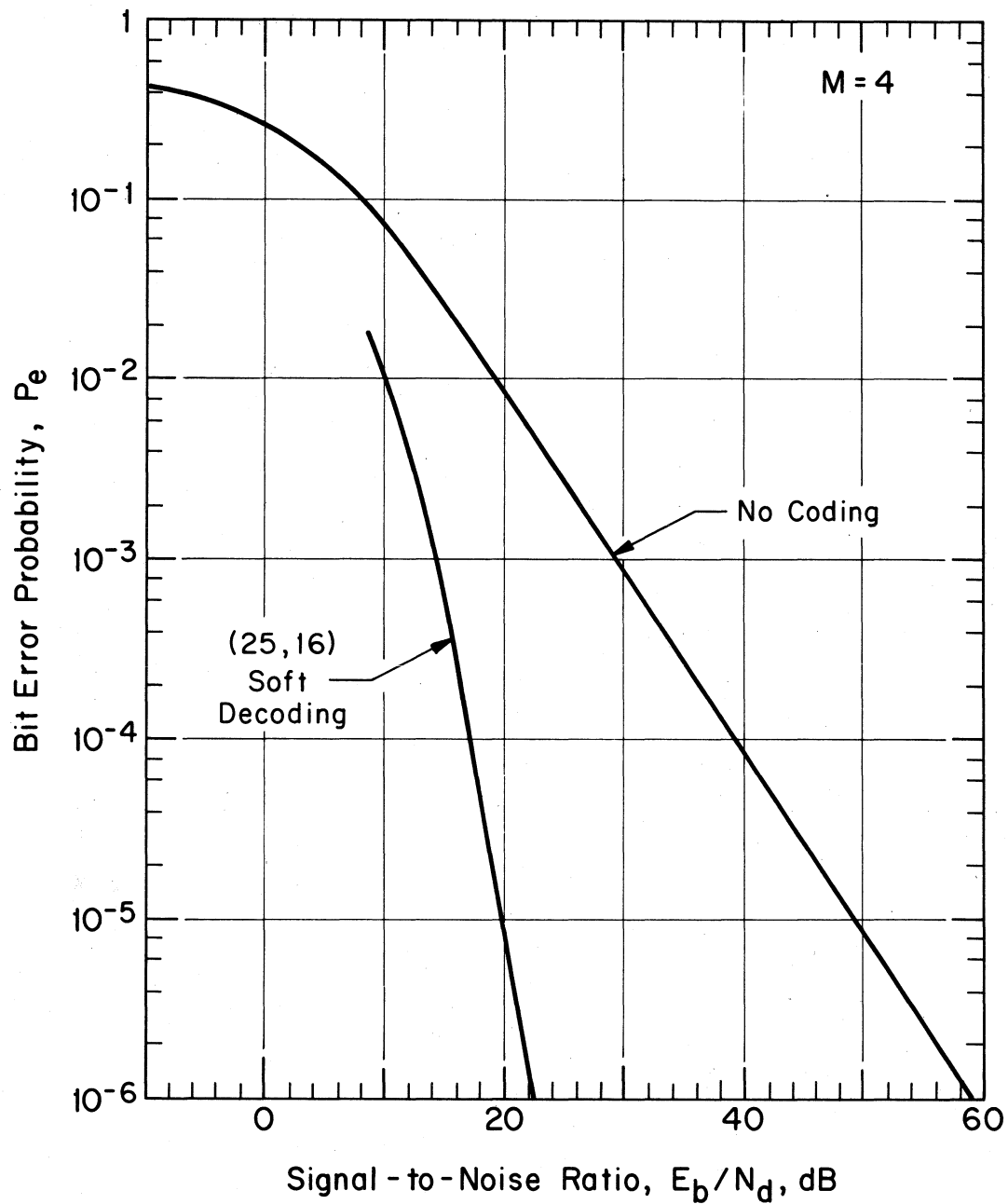


Figure 21. Bit-error-probability performances of nonmatched-filter, frequency-multiplexed, time-differentially coherent, quaternary PSK systems with and without (25,16) soft error-correcting coding over a slow, frequency-flat, Rayleigh-fading channel with white thermal noise.

Channel:  $P=1$ ,  $\nu_1=0$ ,  $2\sigma_1 \rightarrow 0$ ,  $S/I \rightarrow \infty$ .

Equipment: No distortions.

distortions were independent of the signal, which is generally true. However, this is not true for transmitter additive distortions which, when passing through a fading channel, suffer the same fading as the signal. Consequently, the signal never fades into the transmitter additive distortions, as it does with the channel and receiver additive distortions, to produce bit errors. If the transmitter additive distortions are generated at a suitably low level relative to the signal (say  $< -30$  dB), which is usually the case, they affect the system performance very little and can be ignored.

## 6.2 Multiplicative Distortions

Unless otherwise stated, it will be assumed throughout this section that the fundamental pulse waveform, the keying method, and the multiplexing method are arbitrary; the demodulator uses matched or non-matched nonadaptive filters; the bit-decision method is arbitrary; the antennas are arbitrary but nonadaptive; there is single-diversity operation; there is no error coding; and the channel and equipment (transmitter and receiver) may introduce only multiplicative distortions. When a channel introduces only multiplicative distortions, it will generally contain several propagation paths,  $P \geq 1$ , with arbitrary delays,  $\{\tau_p\}$ , arbitrary Doppler shifts,  $\{\nu_p\}$ , and arbitrary frequency spreads,  $\{2\sigma_p\}$ . Such a channel has a time-varying frequency response,  $H(f,t)$ , whose magnitude fluctuates in frequency and time at rates proportional to the amounts of time scatter and frequency scatter respectively. When equipment introduces only multiplicative distortions, it of course introduces no noise or internal interference.

All of the multiplicative channel and equipment distortions affect the bit-error-probability performances of digital systems by appearing in the demodulator in two forms:

## Forms of Multiplicative Distortions

- (1) Crosstalk distortions
- (2) Coherence distortions

When multiplicative channel or equipment distortions are present, they introduce interpulse interference that constitutes crosstalk distortions. Crosstalk distortions affect the bit-error-probability performances of systems with all combinations of bit-decision and keying methods (Table 2, p. 58). When multiplicative channel or equipment distortions are present, the resulting fluctuations in the time-varying frequency response of the system (channel and equipment) introduce a degree of incoherence in the amplitude and phase of the signal that constitutes coherence distortions. Coherence distortions affect the bit-error-probability performances of systems with all combinations of bit-decision and keying methods except noncoherent FSK and CPK. Crosstalk and coherence multiplicative distortions will be considered in turn.

The appearance of multiplicative channel and equipment distortions in the form of crosstalk distortions can be illustrated with a specific system. Consider a frequency-multiplexed single-filter (ASK, PSK, or APSK) system that uses adjoining rectangular pulses of duration  $T$ . Assume the demodulator filters are nonmatched and have rectangular impulse responses of duration  $T_r < T$  that provide a guard time,  $T_g = T - T_r$ , whose purpose is to suppress channel and equipment time-scatter distortions. First consider the reception of a single pulse, the  $\ell$ th in the  $\lambda$ th pulse train, over a single specular (nonfading) path. Assume the pulse sampling time (synchronization) is fixed, there is no filtering distortion, no Doppler correction, and no AGC distortion (constant equipment gain). Let  $d_\lambda(\tau, \nu; \ell)$  be the  $\lambda$ th detector (sampler) response in the  $\ell$ th pulse sample to the  $\ell$ th pulse in the  $\lambda$ th train as a function of the single path delay,  $\tau$  (measured relative to the demodulator time), and the path Doppler shift,  $\nu$ . Under the specified channel and equipment conditions,  $d_\lambda(\tau, \nu; \ell)$ , is the same for all pulse numbers,  $\ell$ . In

frequency-multiplexed systems, it is also the same for all pulse trains,  $\lambda$ , but differs from one pulse train to another in concentrically multiplexed pulse trains because the basic pulse waveforms differ from train to train. Figure 22 illustrates  $|d_\lambda(\tau, \nu; \ell)|$  for the single-filter system using adjoining rectangular pulses with a guard time. The response is shown as a function of the normalized path delay,  $\bar{\tau} = \tau/T_r$ , and the normalized path Doppler shift,  $\bar{\nu} = T_r \nu$  (Watterson and Minister, 1975). In the illustration,  $T_r/T = 9/13$ .

The detector response,  $d_\lambda(\tau, \nu; \ell)$ , also specifies the response of the  $\lambda$ th detector at the  $\ell$ th sampling time to all of the pulses that are transmitted in the frequency-multiplexed pulse trains. Assume for the moment that the single specular path has an arbitrary delay and an arbitrary Doppler shift (no channel distortions). Then in the absence of equipment distortions, the demodulator synchronization and Doppler-correction circuits exactly compensate the arbitrary delay and Doppler shift on the single specular path. The Dirac delta functions (vertical arrows) in Figure 22 then illustrate the time and frequency locations of three time-adjacent pulses, the  $(\ell-1)$ th, the  $\ell$ th, and the  $(\ell+1)$ th, in seven adjacent frequency-multiplexed pulse trains, the  $(\lambda-3)$ th through  $(\lambda+3)$ th, in the  $\lambda$ th detector response in the  $\ell$ th sample. The product of each delta function with  $|d_\lambda(\tau, \nu; \ell)|$  when integrated on  $\tau$  and  $\nu$  specifies the magnitude of the response of the  $\lambda$ th detector at the  $\ell$ th sampling time to that undistorted pulse. For this ideal case (no channel or equipment distortions), it can be seen that at the  $\ell$ th sampling time, the  $\lambda$ th detector responds only to the desired  $\ell$ th pulse in the  $\lambda$ th train at  $(\tau, \nu; \ell) = (0, 0; \ell)$ , because all of the other pulses are located at zeros of the detector response. Consequently, there are no channel or equipment crosstalk distortions.

The preceding description for an ideal channel can be extended to the more realistic Gaussian-scatter HF channel described in Section 4.2 by viewing the Gaussian-scatter channel as the sum of  $P$  fading paths, each of which is viewed as a continuum of infinitesimal specular paths with a common delay, different Doppler shifts with equal infinitesimal adjacent

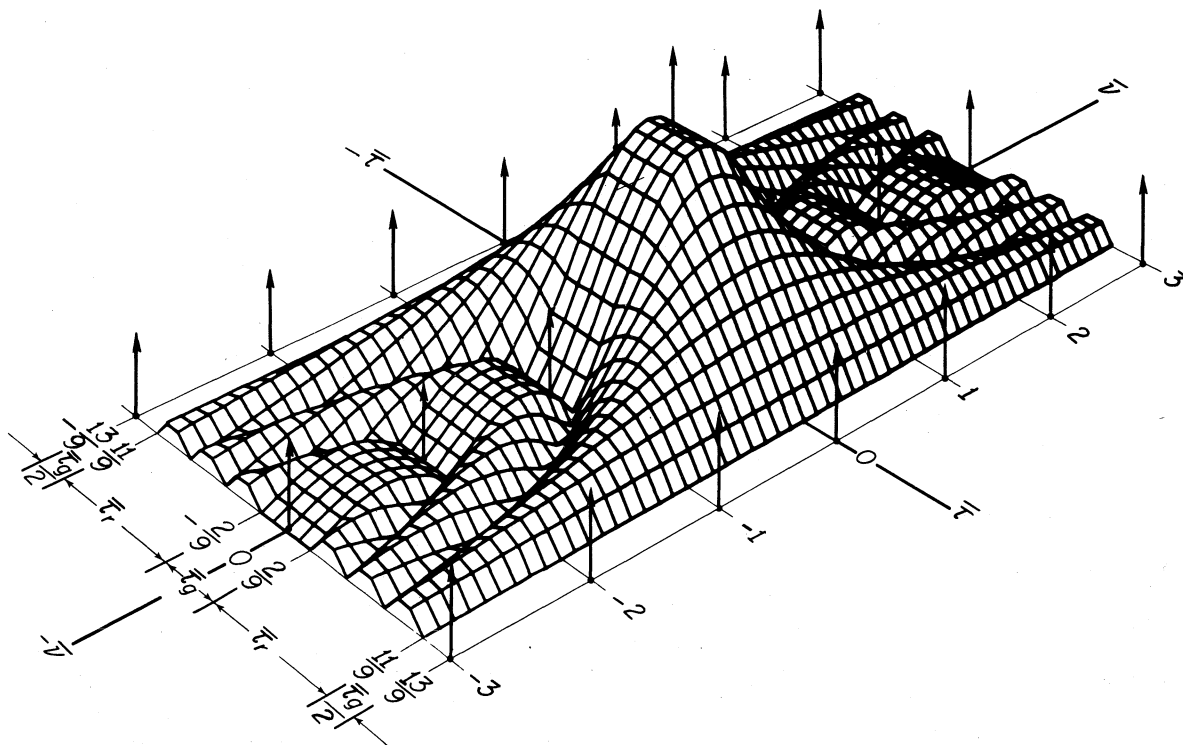


Figure 22. Perspective plot of the magnitude of the response of a detector with guard time to a rectangular pulse. The delta functions illustrate the responses to pulses in frequency multiplexed pulse trains over an ideal channel.

frequency spacings, and random phases, where the magnitudes of the infinitesimal specular components are proportional to  $\sqrt{s(\tau, \nu)}$ , the square root of the channel scatter function in (39), p. 42. The square root of the channel scatter function, suitably displaced in  $\tau$  and  $\nu$ , then replaces each of the delta functions in Figure 22 that represent a single specular path. When this is done with the hypothetical channel scatter function of Figure 14, p. 43, and there are no equipment distortions, the result is illustrated in Figure 23. Each curve is a contour plot of  $|d_\lambda(\tau, \nu; l)|$ , and each pair of arrows represents a top view of the square root of the two-path channel scatter function (displaced and normalized). The figure illustrates the responses in the  $l$ th sample in the  $\lambda$ th detector

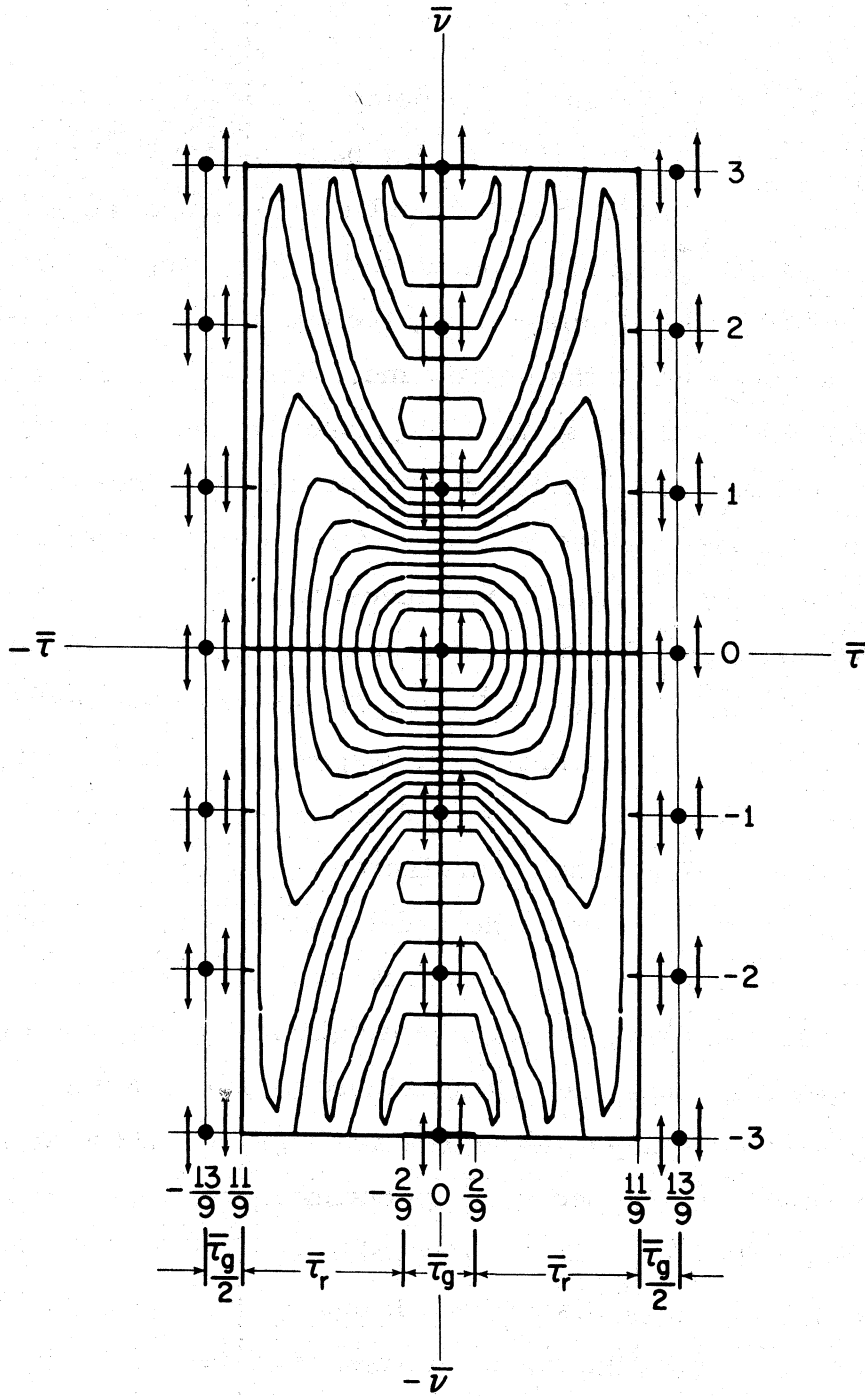


Figure 23. Contour plot of the magnitude of the response of a detector with guard time to a rectangular pulse. The pairs of arrows illustrate the responses to pulses in frequency-multiplexed pulse trains over a realistic two-path Rayleigh-fading channel.

to 21 pulses: the  $(\ell-1)$ th,  $\ell$ th, and  $(\ell+1)$ th pulses in the seven  $(\lambda-3)$ th through  $(\lambda+3)$ th pulse trains.

In Figure 23, the differential path delay,  $\tau_2 - \tau_1$ , is less than the guard time,  $T_g$ . Consequently, the  $\lambda$ th detector has zero responses to the  $(\ell-1)$ th and  $(\ell+1)$ th pulses in all of the pulse trains, and there is no channel differential-delay distortion, despite the presence of two paths with a nonzero differential delay; i.e., the channel differential-delay distortion is suppressed by the guard time. However, because of the nonzero differential Doppler shift,  $\nu_2 - \nu_1$ , and the nonzero frequency spreads,  $2\sigma_1$  and  $2\sigma_2$ , the detector does have undesired responses to the  $\ell$ th pulses in the non- $\lambda$ th pulse trains, as well as the desired response to the  $\ell$ th pulse in the  $\lambda$ th train. The undesired crosstalk constitutes channel differential-Doppler and fading distortions. If the differential path delay,  $\tau_2 - \tau_1$ , is increased in Figure 23 to exceed the guard time,  $T_g$ , the detector sample contains undesired responses to the  $(\ell-1)$ th pulses and the  $(\ell+1)$ th pulses in all trains, and the undesired responses to the  $\ell$ th pulses in the non- $\lambda$ th pulse trains increase. The increase in the total crosstalk constitutes differential-delay distortion. If channel dispersion (not included in the model of Section 4.2) is introduced, it spreads the signal in time, the total crosstalk increases, and the additional crosstalk constitutes channel dispersion distortion.

Multiplicative equipment distortions are similar. If the synchronization is advanced or retarded from its optimum (minimum-crosstalk) value, the crosstalk increases, and the additional crosstalk constitutes equipment synchronization distortion. If equipment filtering distortion is introduced, it spreads the signal in time, the total crosstalk increases, and the additional crosstalk constitutes equipment filtering distortion. Similarly, if the Doppler correction is offset from its optimum (minimum-crosstalk) value, the crosstalk increases, and the additional crosstalk constitutes equipment Doppler-correction distortion. If fluctuations are introduced in any equipment AGC circuit, the resulting modulation of the signal spreads its spectrum to introduce additional

crosstalk that constitutes equipment AGC distortion.

In the example of Figures 22 and 23, it can be seen that the guard time provides protection against channel and equipment time-scatter distortions. The price paid for this protection is a reduction in the spectral efficiency of the system by a factor  $T_r/T$ , and a reduction in the bit-error-probability performance with respect to white noise additive distortions by the same factor  $[10 \log(T_r/T) \text{ dB}]$ . In the absence of a guard time (when  $T_r = T$ ) and with no equipment distortions, the rms channel differential-delay distortion increases approximately linearly from zero as the channel differential delay,  $\tau_2 - \tau_1$ , increases from zero, rather than increasing approximately linearly from zero as the channel differential delay increases above the guard time,  $T_g = T - T_r$ . The rms synchronization distortion similarly increases approximately linearly with synchronization error. With or without the guard time, the rms channel differential-Doppler and frequency-spread distortions increase approximately linearly from zero as the differential Doppler shift,  $\nu_2 - \nu_1$ , and the frequency spreads,  $2\sigma_1$  and  $2\sigma_2$ , together increase linearly from zero.

It is possible by using  $\sin(\pi t/T_r)/(\pi t/T_r)$  as a fundamental pulse waveform and nonmatched filters with impulse responses  $\sin(\pi t/T)/(\pi t/T)$  to rotate the detector response in Figures 22 and 23 by  $90^\circ$ , thereby obtaining a guard time in frequency,  $\nu$ , rather than in time,  $\tau$ . It is not possible to obtain guard times simultaneously in frequency and time, however.

Detector responses can be obtained for any fundamental pulse waveform that may be used in single-filter or multiple-filter systems. Such detector responses are generally easy to obtain and are not only useful in visualizing crosstalk multiplicative distortions, but are required for any calculations of such distortions needed to determine theoretical bit-error-probability performance with respect to these distortions.

Rectangular fundamental pulse waveforms do not provide the best bit-error-probability performances with respect to crosstalk distortions. It

is possible to design fundamental pulse waveforms which, with matched or nonmatched demodulator filters, have a detector response of the form illustrated in Figure 24. This hypothetical response is similar to the response of Figure 22 in having zeros at the locations of all of the undesired pulses (no filtering distortion). However, it is better than the detector response of Figure 22 in also having a zero total derivative, rather than a nonzero total derivative, at these points. Consequently, the rms crosstalk distortion is approximately a parabolic function, rather than a linear function, of the channel and equipment time-scatter-distortion and frequency-scatter-distortion parameters. Systems with such parabolic detector responses consequently have substantially better bit-error-probability performances with respect to multiplicative channel and equipment crosstalk distortions.

Crosstalk multiplicative distortions appear in the demodulator pulse samples,  $d_\lambda(\ell)$  or  $d_{\lambda m}(\ell)$ , and affect the system bit-error-probability performance in the same way that channel and equipment additive distortions do. Therefore, the relative performances of ASK, PSK, APSK, FSK, and CPK systems described in the preceding section for additive distortions also hold for crosstalk multiplicative distortions.

The appearance of multiplicative channel and equipment distortions in the form of coherence distortions can also be illustrated with a frequency-multiplexed single-filter (ASK, PSK, or APSK) system. Assume initially the channel has a single specular path (no channel distortions), and there are no equipment distortions. Then if  $d_\lambda(\ell;1)$  is the value of the  $\ell$ th sample in the  $\lambda$ th detector when the keying is excluded from the pulse sample [i.e., the value of the pulse sample when  $K_\lambda(\ell)=1$ ], then  $d_\lambda(\ell;1)$  has the same value for all pulses,  $\ell$ , in all pulse trains,  $\lambda$ , and contains no distortions.

Now assume the ideal channel is replaced by a Gaussian-scatter channel with both time-scatter and frequency-scatter distortions. Further assume the detector response,  $d_\lambda(\tau, \nu; \ell)$ , is ideal in that it suppresses all crosstalk distortions introduced by the channel and

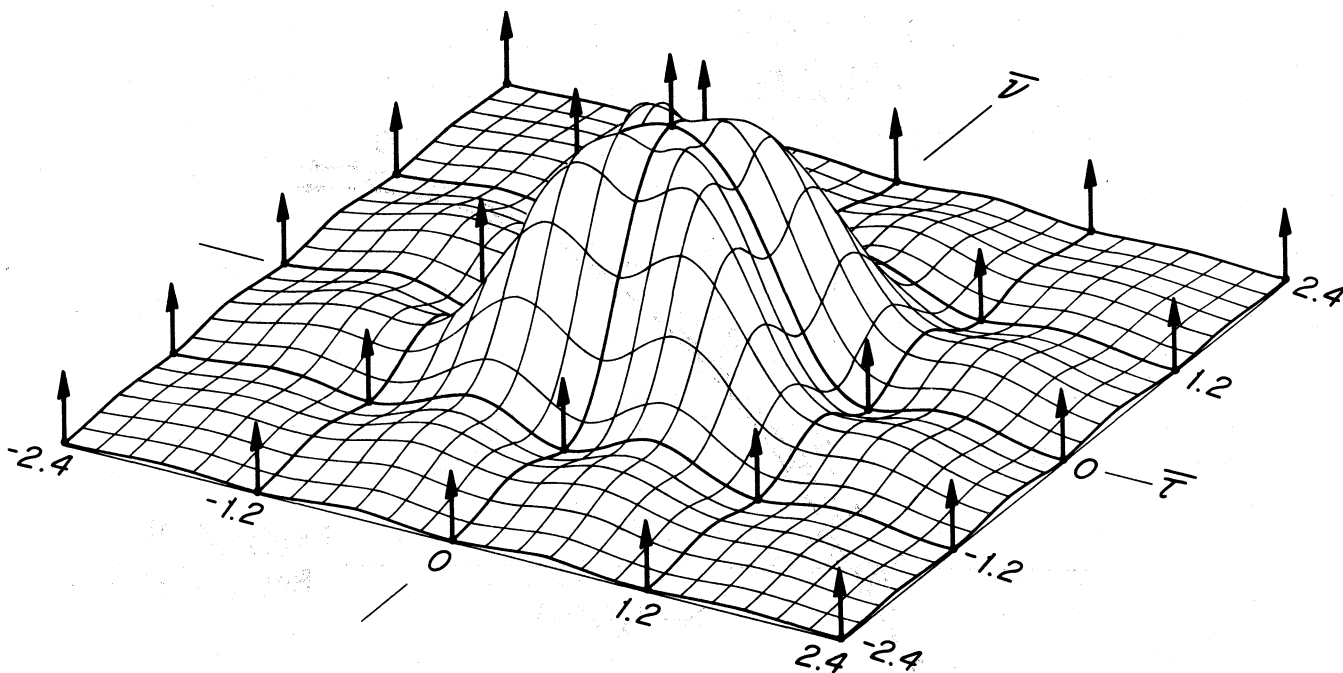


Figure 24. Perspective plot of the magnitude of a hypothetical detector response with zero total derivatives as well as zeros at the locations of undesired pulses in a system with frequency-multiplexed pulse trains.

equipment multiplicative distortions. (This is not possible, of course, but can be assumed possible for present purposes.) Then, because the channel time-varying frequency response,  $H(f, t)$ , fluctuates in both frequency and time, the values of the pulse samples with keying excluded,  $d_\lambda(\ell; 1)$ , fluctuate in amplitude and phase from pulse to pulse in both "frequency",  $\lambda$ , and "time",  $\ell$ . If multiplicative equipment distortions are also introduced, they impose additional fluctuations on the pulse samples. Such amplitude and phase fluctuations in the pulse samples imposed by channel and equipment multiplicative distortions constitute coherence multiplicative distortions.

Coherence multiplicative distortions are illustrated in Figure 25 by a hypothetical example for a single-filter system. The circles on the solid curve illustrate  $d_\lambda(\ell; 1)$ , the complex values of succeeding pulse

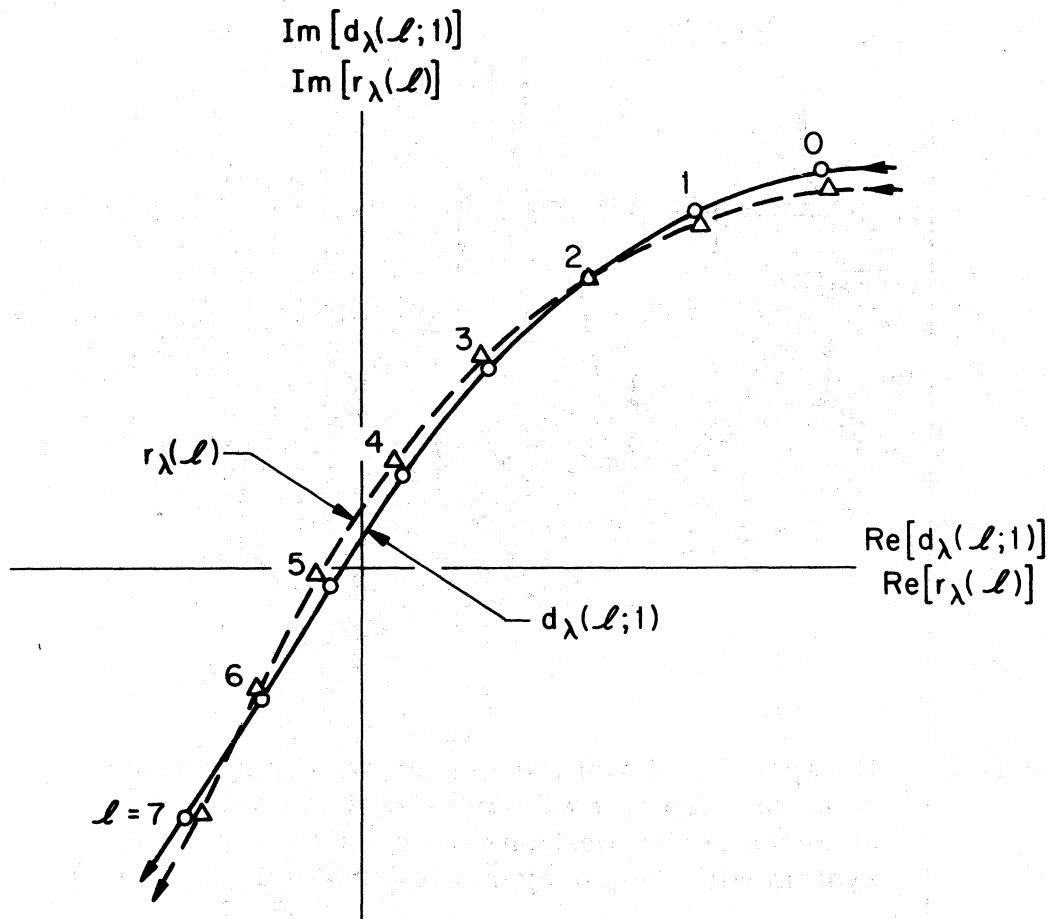


Figure 25. Example of coherence multiplicative distortions in the succeeding demodulator pulse samples in a single-filter ASK, PSK, or APSK system with  $K_{\lambda}(\ell) = 1$  in the absence of additive and crosstalk multiplicative distortions.

samples excluding keying in the  $\lambda$ th detector for  $0 \leq \ell \leq 7$ . Successive pulse samples in this example differ because of the fluctuations in time in the response of the systems (channel and equipment) that are imposed by channel and equipment frequency-scatter distortions. If  $\lambda$  and  $\ell$  are interchanged in Figure 25, the example can illustrate the values of the  $\ell$ th pulse samples excluding keying in pulse trains  $0 \leq \lambda \leq 7$ , in which case the values differ because of the fluctuations in frequency in the system response that are imposed by channel and equipment time-scatter

distortions.

In all types of systems except noncoherent multiple-filter (FSK and CPK) systems (Table 2, p. 58), a complex approximate keying value,  $\tilde{K}_\lambda(\ell)$  in (47), p. 58, or  $\tilde{K}_{\lambda m}(\ell)$  in (56), p. 65, is obtained in effect by dividing the pulse sample,  $d_\lambda(\ell)$  or  $d_{\lambda m}(\ell)$ , by a reference value,  $r_\lambda(\ell)$  or  $r_{\lambda m}(\ell)$  respectively. For all bit-decision methods (including coherent), the approximate keying values,  $\tilde{K}_\lambda(\ell)$  or  $\tilde{K}_{\lambda m}(\ell)$ , contain coherence multiplicative distortions (are approximate) because the reference sequence,  $r_\lambda(\ell)$  or  $r_{\lambda m}(\ell)$ , does not exactly follow the fluctuations in  $d_\lambda(\ell;1)$  or  $d_{\lambda m}(\ell;1)$  imposed by coherence multiplicative distortions.

In coherent (ASK, PSK, APSK, FSK, and CPK) systems,  $r_\lambda(\ell)$  or  $r_{\lambda m}(\ell)$ , is obtained for each pulse in the theoretically best manner possible. Even so, each reference value,  $r_\lambda(\ell)$  or  $r_{\lambda m}(\ell)$ , differs from  $d_\lambda(\ell;1)$  or  $d_{\lambda m}(\ell;1)$ , its corresponding pulse sample excluding keying, by a small amount, and the approximate keying value,  $\tilde{K}_\lambda(\ell)$  or  $\tilde{K}_{\lambda m}(\ell)$ , contains a small amount of coherence multiplicative distortion. The imperfect reference values are illustrated for the single-filter system in Figure 25 by the triangles that fall on the dashed curve.

In partially coherent (ASK, PSK, APSK, FSK, and CPK) systems,  $r_\lambda(\ell)$  or  $r_{\lambda m}(\ell)$  is obtained for each pulse in the manner specified for single-filter systems by (50), p. 61; i.e., in each pulse train in single-filter systems, and in each of the  $M$  binary ASK trains in each pulse train in multiple-filter systems,  $\Xi$  of the preceding pulse samples are processed to obtain  $r_\lambda(\ell)$  or  $r_{\lambda m}(\ell)$ . Such reference values differ from the corresponding pulse samples excluding keying by a generally somewhat larger amount than with the theoretically best coherent bit decisions. The resulting coherence multiplicative distortions in the approximate keying values,  $\tilde{K}_\lambda(\ell)$  or  $\tilde{K}_{\lambda m}(\ell)$ , are produced by the channel and equipment frequency-scatter distortions. The bit-error-probability performances of practical partially coherent systems with respect to coherence multiplicative distortions can presumably approach the corresponding performances of ideal coherent systems.

In time-differentially coherent (PSK and APSK) systems, where the preceding pulse sample,  $d_\lambda(\ell-1)$ , is used as a reference for pulse sample  $d_\lambda(\ell)$ , the full amount of the frequency-scatter coherence distortions between time-adjacent pulse samples appears in the approximate keying value,  $\tilde{K}_\lambda(\ell)$ . In frequency-differentially coherent systems, where the concurrent pulse sample in the adjacent frequency-multiplexed pulse train,  $d_{(\lambda-1)}(\ell)$ , is used as a reference for pulse sample  $d_\lambda(\ell)$ , the full amount of the time-scatter coherence distortions between frequency-adjacent pulse samples appears in the approximate keying value,  $\tilde{K}_\lambda(\ell)$ . Consequently, in both time-differentially coherent and frequency-differentially coherent systems, the bit-error-probability performances with respect to coherence multiplicative distortions are typically much poorer than those of corresponding partially coherent and coherent PSK and APSK systems.

Figure 26 illustrates the bit-error-probability performance of time-differentially coherent binary and quaternary PSK systems with respect to channel fading distortion. The channel has a single Rayleigh-fading path with zero Doppler shift and no additive distortions. The PSK systems use adjoining rectangular pulses of duration  $T = 13.33$  ms and demodulator filters with rectangular impulse responses of duration  $T_r = 9.09$  ms that provide a guard time  $T_g = 4.24$  ms. The detector response,  $d_\lambda(\tau, \nu; \ell)$ , has a magnitude approximately as illustrated in Figure 22, p. 93. It is assumed there are no equipment distortions. The three curves in Figure 26 show the bit error probabilities for the crosstalk fading distortion, the coherence fading distortion, and the total (crosstalk and coherence) fading distortion as functions of the single-path frequency spread,  $2\sigma_1$ . It can be seen that the coherence distortion is considerably greater than the crosstalk distortion, and predominates in determining the performance of the systems with respect to frequency-scatter distortions. The coherence distortion predominates over the crosstalk distortion despite the fact the detector response,  $d_\lambda(\tau, \nu; \ell)$ , has a nonzero derivative with respect to  $\nu$  at its zeros on the  $\nu$  axis,

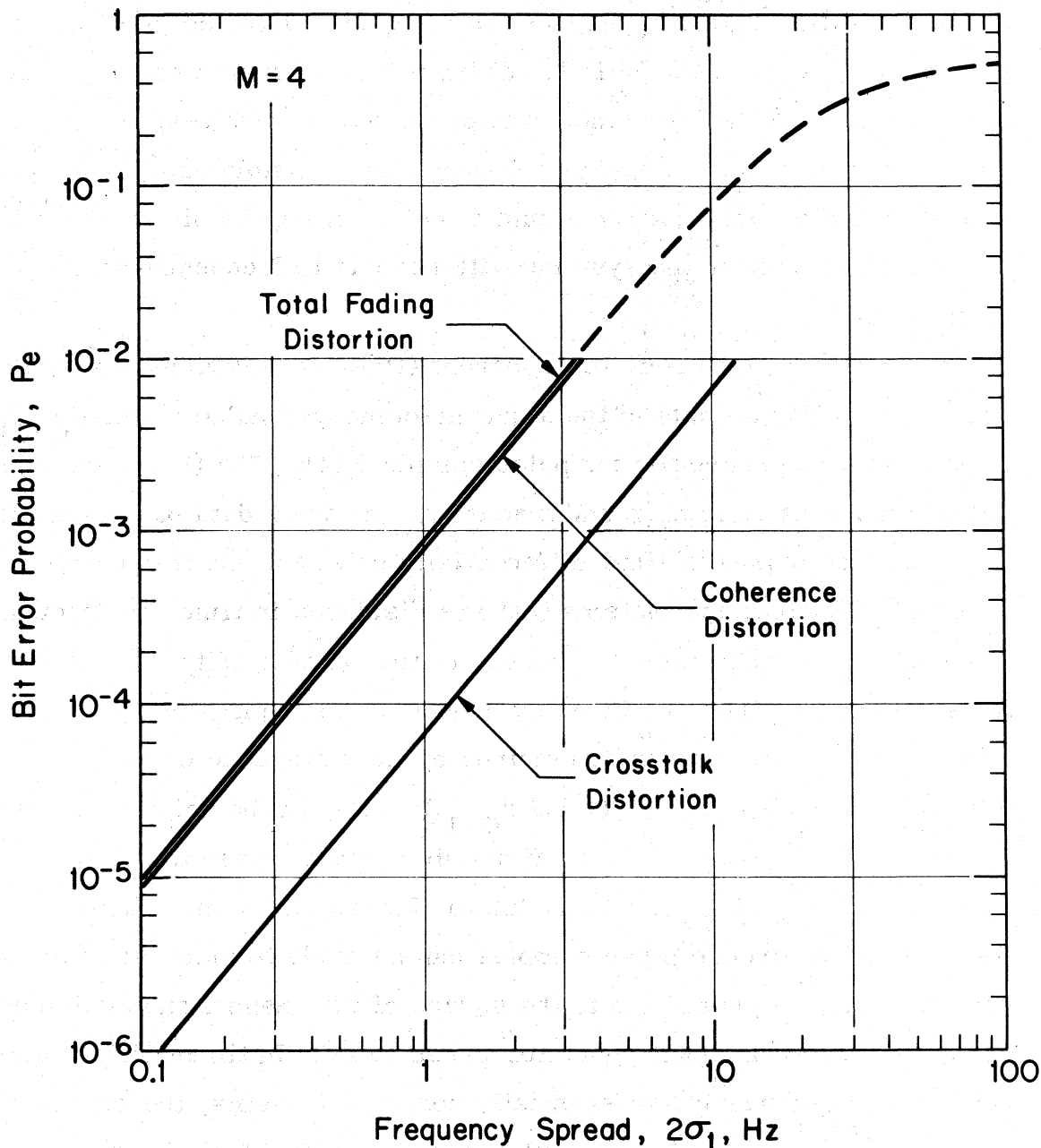


Figure 26. Bit-error-probability performances of nonmatched-filter, frequency-multiplexed, time-differentially coherent, quaternary PSK systems over a frequency-flat, Rayleigh-fading channel.

Channel:  $P = 1$ ,  $\nu_1 = 0$ ,  $E_b/N_d \rightarrow \infty$ ,  $S/I \rightarrow \infty$ .

Equipment: Adjoining rectangular pulses,  $T = 13.33$  ms;  
 demodulator guard time,  $T_g = 4.24$  ms;  
 no equipment distortions.

and consequently is more susceptible to frequency-scatter crosstalk distortion than a detector response of the type illustrated in Figure 24, p. 98. If the time-differentially coherent bit decisions were replaced by partially coherent bit decisions, the performance with respect to coherence distortions would improve substantially, possibly enough to let the crosstalk distortion be predominant in determining the bit-error-probability performance of the systems with respect to frequency-scatter distortions.

In concentric-differentially coherent (PSK and APSK) systems, the concurrent pulse sample in the adjacent-numbered pulse train,  $d_{(\lambda-1)}(\ell)$ , is used as a reference for the pulse sample  $d_{\lambda}(\ell)$ . The  $(\lambda-1)$  reference pulse is concentric in time and frequency with the  $\lambda$  data pulse, unlike the reference pulses in time-differentially coherent and frequency-differentially coherent systems that are displaced in time and frequency respectively. Consequently, because of the concentricity, the fluctuations imposed on the two pulses by coherence multiplicative distortions differ by an amount that is determined by the difference of the two detector responses,  $d_{\lambda}(\tau, \nu; \ell)$  and  $d_{(\lambda-1)}(\tau, \nu; \ell)$ , in the neighborhoods of their origins,  $(\tau, \nu; \ell) = (0, 0; \ell)$ . If suitable care is given to the designs of the pulse waveforms and demodulator filters, the rms difference of the data and reference pulse samples can be made to increase from zero approximately in proportion to the square of the channel and equipment time-scatter and frequency-scatter parameters. In time-differentially coherent and frequency-differentially coherent systems, the rms difference of the data and reference pulse samples unavoidably increases from from zero approximately linearly with increases in the frequency-scatter and time-scatter parameters respectively. The bit-error-probability performances of concentric-differentially coherent systems with respect to coherence multiplicative distortions are then substantially better than those of time-differentially coherent and frequency-differentially coherent systems and comparable with the performances of partially coherent systems. In Figure 25, the triangles,  $r_{\lambda}(\ell)$ , can represent the reference

pulse samples,  $d_{(\lambda-1)}(\ell)$ , in concentric-differentially coherent systems.

Noncoherent multiple-filter (FSK and CPK) systems are immune to coherence multiplicative distortions because these systems do not use reference sequences,  $r_{\lambda m}(\ell)$ . For each pulse number,  $\ell$ , in each pulse train,  $\lambda$ , noncoherent FSK and CPK systems decide which one of  $M$  binary ASK pulses was on by comparing the magnitudes of  $M$  pulse samples,  $\{|d_{\lambda m}(\ell)|\}$ , as specified by (58), p. 66. Consequently, while channel multiplicative distortions cause the pulse samples to fluctuate in time and frequency, the fluctuations (coherence multiplicative distortions) do not affect the relative magnitudes of the  $M$  pulse samples in  $\{|d_{\lambda m}(\ell)|\}$ ; the single on pulse generally has a magnitude greater than zero while the  $M-1$  off pulses have zero magnitudes regardless of the fluctuations. Consequently, noncoherent FSK and CPK systems are immune to coherence multiplicative distortions.

In any system, if the fundamental pulse waveform is scaled up in time, and the spacing of adjacent pulses in each train,  $T$ , is scaled up by the same amount, the detector response,  $d_{\lambda}(\tau, \nu; \ell)$ , is expanded in time,  $\tau$ , and compressed in frequency,  $\nu$  (Figures 22-24). The system then is less susceptible to time-scatter (crosstalk and coherence) multiplicative distortions, but is more susceptible to frequency-scatter (crosstalk and coherence) multiplicative distortions. If  $T$  is scaled down, the opposite is true. Therefore, in practical systems,  $T$  is usually chosen to minimize the combined (total) multiplicative distortions for typical amounts of frequency-scatter and time-scatter distortions. Typical values of  $T$  range from about 20 down to 6.7 ms, corresponding to single-train pulse rates of 50 to 150 pulses/second. This explains why higher data-rate systems use a number of multiplexed trains to carry the data, rather than a single high-pulse-rate train.

While matched nonadaptive demodulator filters provide the best bit-error-probability performances with respect to white additive channel and equipment noise, non matched nonadaptive filters can provide better performances with respect to channel and equipment time-scatter or

frequency-scatter multiplicative distortions. This is illustrated by the detector response in Figure 22, p. 93, for a single-filter system using adjoining rectangular pulses with a mismatched nonadaptive filter that provides a guard time that improves the system bit-error-probability performance with respect to time-scatter distortions. However, dynamic adaptive demodulator filters can provide even better performance with respect to all types of multiplicative channel and equipment distortions. In the absence of additive and nonlinear distortions, this is accomplished by continuously adjusting the response of each demodulator filter to maximize the signal-to-multiplicative-distortions ratio at its output at the optimum sampling times. In the general (and usual) case, when additive and nonlinear distortions as well as multiplicative distortions are present, the response of each dynamic adaptive demodulator filter is adjusted continuously to maximize the signal-to-total-distortion ratio at its output at the optimum sampling times. In general, dynamic adaptive demodulator filters can provide better (and sometimes substantially better) bit-error-probability performances than nonadaptive filters with respect to all types of distortion except white noise. When white noise distortion predominates, dynamic adaptive filters can ideally become matched, of course, to equal the performances of nonadaptive matched filters.

The bit-error-probability performance of any system with respect to both crosstalk and coherence forms of multiplicative channel and equipment distortions is determined by the character of the distortions and all of the system design features (p. 77) except transmitter power. This means that in the absence of all additive channel and equipment distortions, increasing the transmitter power will not change the bit error probability because the levels of the signal and multiplicative distortions in the demodulator increase by the same fractional amounts. It also means that in the absence of all channel and equipment additive distortions, the transmitter power can be decreased to an arbitrarily small amount without affecting the system performance. In practice this is not possible,

of course, because additive channel and equipment distortions are always present, the performance of the system with respect to the additive distortions is dependent on transmitter power, and sufficient transmitter power must be used to obtain an acceptable signal-to-additive-distortions ratio in the receiver.

If the gain of the transmitting antenna is increased, the equivalent change in transmitter power has no effect on system performance with respect to channel and equipment multiplicative distortions. However, the resulting narrower antenna beamwidth can discriminate against some ionospheric propagation modes that were significant with the wider beamwidth antenna. This reduces the amount of channel differential-delay distortion and improves the system bit-error-probability performance if such distortion is significant. The same argument applies with respect to the receiving antenna. High-gain transmitting and receiving antennas are therefore desirable to minimize channel differential-delay distortion.

Both diversity and error coding can substantially improve the bit-error-probability performance of any HF digital radio system with respect to additive channel and equipment distortions as described in the preceding section. The reason for this is because all types of channel and equipment distortions ultimately appear in the demodulator as distortion components in the approximate keying values,  $\tilde{K}_\lambda(t)$  or  $\tilde{K}_{\lambda m}(t)$  in most systems [or in  $d_{\lambda m}(t)$  in noncoherent FSK and CPK systems] to produce errors in the following bit-decision process. Errors occur when the signal component in  $\tilde{K}_\lambda(t)$  or  $\tilde{K}_{\lambda m}(t)$  fades to a level comparable to the rms level of the total distortion to increase greatly the short-term probability of an error in the bit-decision process. This is illustrated in Figure 25 for coherence multiplicative distortions in single-filter systems. For  $\ell = 0$ , the rms value of the distortion component,  $d_{\lambda}(0;1) - r_{\lambda}(0)$ , is small compared with the magnitude of the reference component,  $r_{\lambda}(0)$ . The rms amplitude and phase error in  $\tilde{K}_{\lambda}(0) = d_{\lambda}(0)/r_{\lambda}(0)$  then is small and very unlikely to produce an error in the bit-decision process. For  $\ell = 5$ , the rms value of the distortion component,  $d_{\lambda}(5;1) - r_{\lambda}(5)$ , remains

unchanged. However, the reference value,  $r_\lambda(5)$ , has a much smaller magnitude because it has followed the fading signal to a lower level. As a result, the rms amplitude and phase error in  $\tilde{K}_\lambda(5)$  is much larger and quite likely to cause an error in the bit-decision process.

The same effect results from additive distortions and crosstalk multiplicative distortions, all of which add to the signal values, illustrated by the circles in Figure 25, to form a different  $d_\lambda(\ell)$  that has a larger rms separation from the reference values. However, while the additional additive and crosstalk multiplicative distortions increase the average bit-error probability, the bit errors still occur when the signal fades to a level comparable to the rms total distortion level.

It can be seen then that the bit errors in any HF digital radio system are highly correlated with the strength of the fading signal for all types of channel and equipment additive and multiplicative distortions. Therefore, diversity can provide substantial improvement in the bit-error-probability performance of any system with respect to all types of channel and equipment additive and multiplicative distortions when the fading in the diversity channels has a reasonable degree of independence or is negatively correlated. Similarly, block error coding with soft decoding can provide substantial improvement in the bit-error-probability performance of any system with respect to all types of channel and equipment additive and multiplicative distortions when the fading on the pulses carrying the bits in each code block has a reasonable degree of independence. To obtain independence, the bits in each block are normally assigned to pulses that are separated as much as is practical in time, and in frequency-multiplexed systems, to pulses that are also separated in frequency. The bit errors in each block are essentially independent, and the maximum performance improvement results, when the channel and equipment frequency scatter are comparable to or greater than the reciprocal of the adjacent time spacing of the pulses carrying the bits in each block. Less but still substantial performance improvement results when the frequency scatter is as small as one-tenth of the reciprocal of

the spacings of the code-block pulses. In the latter case, the loss in performance improvement can be recovered under some but not all multipath channel conditions by the additional distribution of the code-block pulses in frequency in frequency-multiplexed systems.

### 6.3 Nonlinear Distortions

Nonlinear distortions in the transmitter produce intermodulation components, some of which may fall in the frequency band of the signal. Such nonlinear distortion components are similar to additive transmitter distortions in that when passing through a Rayleigh-fading channel, they suffer the same fading as the signal. Consequently, the signal never fades into the transmitter nonlinear distortions, as it does with additive channel and receiver distortions and multiplicative channel and equipment (transmitter and receiver) distortions<sup>4</sup>. If the transmitter nonlinear distortions, like the transmitter additive distortions, are generated at a suitably low level relative to the signal (say  $< -30$  dB), which is usually the case, they affect the system performance very little and can be ignored.

The bit-error-probability performance of a system with respect to receiver nonlinear distortions depends not only on the amount of the non-linearity in the receiver but, in multiple-pulse-train systems, on the type of multiplexing that is used: frequency-multiplexed systems are far more susceptible to receiver nonlinear distortions than single-pulse-train systems or concentrically multiplexed multiple-pulse-train systems. This can be explained with the help of Figure 27, which presents the results of channel-simulator performance measurements on three HF

---

<sup>4</sup>Under frequency-selective fading conditions, the signal in one of several frequency-multiplexed pulse trains can fade into transmitter multiplicative distortions (filtering and AGC distortions) that appear in the demodulator in the form of crosstalk distortions from other pulse trains. Such transmitter multiplicative distortions are usually weak and not significant, however.

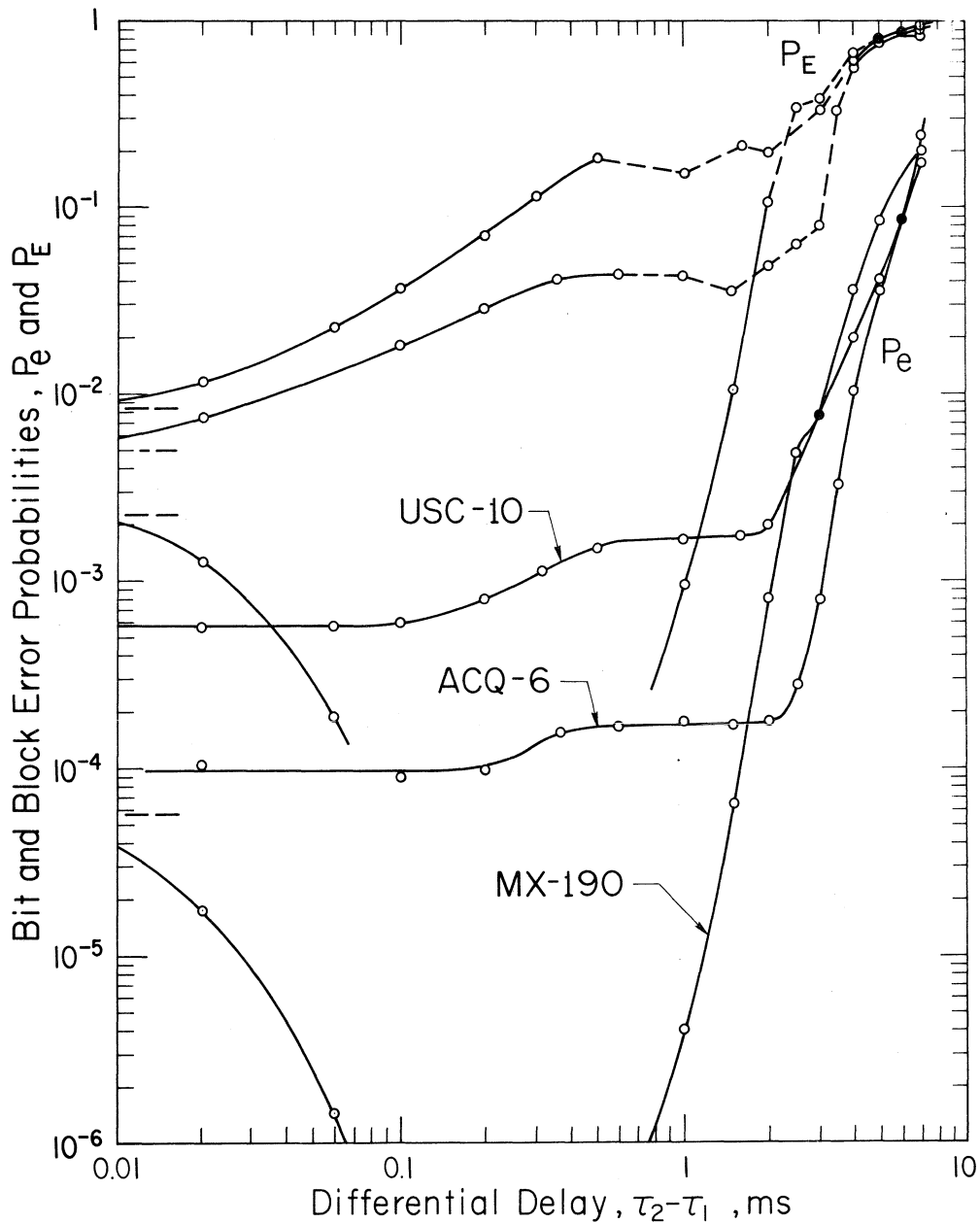


Figure 27. Bit and block error-probability performances of the USC-10, ACQ-6, and MX-190 frequency-multiplexed, time-differentially coherent, quaternary PSK modems over a two-path, frequency-selective, Rayleigh-fading channel.

Channel:  $P = 2$ ,  $A_2 = A_1 = 3.0$  dB,  $\nu_2 = \nu_1 = 0$ ,  $2\sigma_2 = 2\sigma_1 = 0.2$  Hz,  $E_b/N_d \rightarrow \infty$ ,  $S/I \rightarrow \infty$ .

Equipment: Additive, multiplicative, and nonlinear distortions present.

digital modems (modulator-demodulators), the USC-10, ACQ-6, and MX-190 (Watterson and Minister, 1975). All three are frequency-multiplexed, time-differentially coherent, quaternary-PSK systems with information rates of  $f_1 = 2400$  bits/second. The USC-10 and ACQ-6 use 13.33-ms adjoining rectangular pulses with a 4.24-ms demodulator guard time (Figure 22, p. 93) in 16 pulse trains with 110-Hz adjacent frequency spacings without error coding. The experimental MX-190 uses 13.33-ms adjoining rectangular pulses with a 2.67-ms demodulator guard time in 25 pulse trains with 93.75-Hz adjacent frequency spacings with error coding, the (25,16) block code with soft decoding described earlier (pp. 69-71). The 25 bits in each code block are assigned to 25 concurrent pulses in the 25 pulse trains. In Figure 27, bit-error probability,  $P_e$ , and block-error probability,  $P_E$  (the probability of one or more bits in a 672-bit block being in error), are presented as functions of the differential delay,  $\tau_2 - \tau_1$ , in a two-path Gaussian-scatter channel specified by the model in Section 4.2. The signals on the two independently Rayleigh-fading paths had equal relative attenuations (equal rms values),  $A_2 = A_1 = 3.0$  dB; no Doppler shifts,  $\nu_2 = \nu_1 = 0$ ; equal frequency spreads,  $2\sigma_1 = 2\sigma_2 = 0.2$  Hz; no noise,  $E_b/N_d \rightarrow \infty$ ; and no interference,  $S/I \rightarrow \infty$ .

In Figure 27, the USC-10 and ACQ-6 bit-error-probability curves are characterized by five intervals: low, middle, and high plateaus (the last not shown) with two intermediate positive-slope intervals. In the low-plateau interval ( $\tau_2 - \tau_1 < 0.2$  ms), the errors are caused primarily by additive distortions generated in the demodulators: internal interference in the USC-10 and quantizing noise (8 bits/sample) in the ACQ-6. In the absence of these demodulator additive distortions, the channel fading distortion would produce a bit error probability of  $P_e = 4 \times 10^{-5}$  in both systems (see Figure 26 for  $2\sigma_1 = 0.2$  Hz). In the lower-positive-slope and middle-plateau intervals ( $0.2 < \tau_2 - \tau_1 < 2$  ms), additional errors are introduced by nonlinear distortions generated in the demodulators ahead of the filters. In the low-plateau, lower-positive-slope, and middle-plateau intervals, channel differential-delay and receiver-synchronization

distortions are excluded by the 4.24-ms guard time (Figure 22, p. 93). In the upper-positive-slope and high-plateau interval ( $\tau_2 - \tau_1 > 2$  ms), the errors are caused primarily by channel differential-delay and demodulator synchronization distortions that are not excluded by the guard time. In the absence of synchronization distortion, the curves would break and rise from the middle plateau when the channel differential delay exceeded 4.24 ms.

The reason the demodulators' nonlinear distortions are not significant in the low-plateau interval but are significant in the lower-positive-slope and middle-plateau intervals is as follows: When the differential delay is less than about 0.2 ms, the Rayleigh fading is relatively flat in the 1.8-kHz band occupied by the 16 frequency-multiplexed pulse trains. All pulse trains then fade approximately together, and the nonlinear distortion (inter-pulse-train intermodulation products) fades with them. The demodulator nonlinear distortion then has no significant effect on system performance. When the channel differential delay increases above about 0.2 ms, the fading across the 1.8-kHz signal band becomes increasingly frequency selective, and some pulse trains are weak while others are strong. Bit errors are then produced by the weak pulse trains fading into the relatively strong intermodulation products produced by the strong pulse trains. From this description, it can be seen that frequency-multiplexed systems are particularly susceptible to nonlinear receiver distortions when there is enough channel time-scatter distortion. It can also be seen that single pulse trains and concentrically multiplexed pulse trains are presumably less susceptible to receiver nonlinear distortions. If the bit error probability with respect to receiver nonlinear distortions is to be held below  $10^{-6}$ , the nonlinear distortion level in a frequency-multiplexed system would need to be approximately  $< -60$  dB relative to the rms level of the Rayleigh-fading signal. The same bit-error-probability performance with respect to receiver nonlinear distortions in single-pulse-train and concentrically multiplexed multiple-pulse-train systems presumably could be achieved with a receiver nonlinear-

distortion level  $< -30$  dB relative to the rms signal level.

Receiver nonlinear distortions appear in the demodulator pulse samples,  $d_\lambda(\ell)$  or  $d_{\lambda m}(\ell)$ , and affect the system bit-error-probability performance in the same way that channel and equipment additive distortions do. Therefore, the relative performances of ASK, PSK, APSK, FSK, and CPK systems described in Section 6.1 for additive distortions also hold for receiver nonlinear distortions.

Because the bit errors produced by receiver nonlinear distortions are highly correlated with the strength of the fading signal, diversity can provide substantial improvement in the bit-error-probability performance of any system with respect to receiver nonlinear distortions, as it can for channel and equipment additive and multiplicative distortions, provided the fading in the diversity channels has a reasonable degree of independence or is negatively correlated. Similarly, block error coding with soft decoding can provide substantial improvement in the bit-error-probability performance of any system with respect to receiver nonlinear distortions, as well as channel and equipment additive and multiplicative distortions, provided the fading on the pulses carrying the bits in each code block has a reasonable degree of independence. The importance of the independence and the effectiveness of soft error-correcting decoding are illustrated by the MX-190 bit-error-probability curve in Figure 27. The MX-190 curve differs in form from the USC-10 and ACQ-6 curves primarily because of the (25,16) coding the MX-190 incorporates. Recall that the 25 bits in each code block are assigned to 25 concurrent pulses in the 25 pulse trains. In Figure 27, as the channel differential delay,  $\tau_2 - \tau_1$ , approaches zero and the channel fading becomes flat in frequency, bit errors are very likely to occur in all 25 of the concurrent data bits in a code block when all 25 pulse trains simultaneously fade into the demodulator quantizing noise (8 bits/sample). The data bit errors in a code block are then highly correlated, the error-correcting decoding is ineffective, and the information-bit error probability asymptotically approaches  $6 \times 10^{-4}$  (shown by the dashed line). As the channel differential

delay increases, the channel fading becomes increasingly frequency selective, and the data bit errors caused by the demodulator quantizing noise and nonlinear distortion become more randomly distributed in frequency and time. While there may be more errors, because of the nonlinear distortion, they occur with a higher degree of independence, no code block is overwhelmed by too many errors, and the soft error-correcting decoding becomes effective. The curve illustrates the importance of assigning the bits in each code block to pulses that are separated in time. Had this been done in the MX-190, its bit-error-probability performance curve in Figure 27 would remain well below  $P_e = 10^{-6}$  for channel differential path delays  $\tau_2 - \tau_1 < 0.7$  ms. It is important to retain good bit-error-probability performance under frequency-flat (small time-scatter) channel conditions because such channel conditions occur a substantial fraction of the time.

## 7. PERFORMANCE IMPROVEMENTS

The purpose of this section is to use the results of the preceding sections to select the best methods that may be used to improve the performance and reliability of U.S. military HF digital radio communications. There are two general methods that can be used to improve system performance: by using better system designs and by using better operating techniques. These methods will be considered in turn in the following two sections.

### 7.1 System Design

The HF digital radio systems presently used by the various U.S. military services are primarily of the following three types:

## Common Types of Military HF Digital Radio Systems

- (1) Single-pulse-train, noncoherent, binary FSK systems without error coding that operate at information rates from 50 to 150 bits/second with or without single-transmission space diversity (e.g., the TH-22).
- (2) Multiple-pulse-train, frequency-multiplexed, noncoherent, binary FSK systems without error coding that operate at 600 bits/second with dual multiple-transmission in-band frequency diversity or at 1200 bits/second without diversity (e.g., the UCC-1).
- (3) Multiple-pulse-train, frequency-multiplexed, time-differentially coherent, quaternary PSK systems without error coding that operate at 1200 bits/second with dual multiple-transmission in-band frequency diversity or at 2400 bits/second without diversity (e.g., the USC-10).

All of the systems use adjoining rectangular pulses and nonadaptive demodulator filters with various transmitter powers and a large variety of antennas. The frequency-multiplexed systems typically use one standard voice band (3 kHz).

In general, it is not economically or technically practical to modify existing equipments to improve their performances. Therefore, there are only two generally feasible methods that can be used to improve the performance characteristics of military HF digital radio systems: by incorporating additional equipment without replacing or modifying existing equipments and by replacing existing equipments with equipments of better design.

There appears to be only one type of additional equipment that might be incorporated into existing systems to improve their bit-error-probability performances: error-coding equipment. The incorporation of suitable error coders at the inputs of present modulators (Figure 1, p. 4) and compatible hard decoders at the outputs of present demodulators would significantly improve the bit-error-probability performances of

existing systems with respect to all types of channel and equipment distortions (Table 3, p. 78). However, the price of the improved bit-error-probability performances would necessarily be reductions in the systems' information rates by factors equal to the coding ratios [(1), p. 9] and corresponding decreases in the spectral efficiencies of the systems. While decreases in the spectral efficiencies may be acceptable, the reductions in information rates may not be for practical reasons.

Although the incorporation of error-coding equipment into existing military HF digital radio systems can improve their bit-error-probability performances, considerably greater improvements in bit-error-probability performances can be obtained with simultaneous improvements in spectral efficiencies by replacing some of the existing equipment with new equipment that has more efficient designs. Improvement in spectral efficiency as well as bit-error-probability performance is very desirable to minimize any unnecessary waste of the HF spectrum and to minimize the interference with other systems. It is also necessary if the reliable transmission of good quality digital voice signals in a 3-kHz band is to be made practical. To determine the characteristics that new equipment should have to optimize simultaneously bit-error-probability performances and spectral efficiencies, the system design features listed on p. 77 will be considered in turn to determine the best combinations based on the system performance evaluation of Section 6.

All fundamental pulse waveforms provide the same best bit-error-probability performance with respect to channel and equipment white noise when matched demodulator filters are used. The choice of fundamental pulse waveform also has no effect on bit-error-probability performance with respect to coherence multiplicative distortions when the pulse spacings are unchanged. However, this is not true with respect to crosstalk multiplicative distortions, whose levels in the detector response are strongly affected by the choice of fundamental pulse waveform and demodulator filter in combination. As explained earlier (p. 96), the almost universally used adjoining rectangular pulses with matched or

nonmatched filters do not provide the best performance with respect to crosstalk multiplicative distortions. Better fundamental pulse waveform designs are possible and should be developed and used.

The keying and bit-decision methods can best be considered in combination (Table 2, p. 58). Of the available practical combinations, partially coherent PSK and partially coherent APSK are undoubtedly the best for the following reasons: Partially coherent PSK provides the best bit-error-probability performances with respect to all types of channel and equipment distortions, additive, multiplicative, and nonlinear<sup>5</sup>. Also, PSK and APSK provide substantially better spectral efficiencies (M times better) than FSK and CPK.

Frequency multiplexing and concentric multiplexing both provide comparable spectral efficiencies when used with suitably designed fundamental pulse waveforms. However, concentrically multiplexed systems presumably are far less susceptible to receiver nonlinear distortion, and are preferable for this reason.

The best type of demodulator filter is one which maximizes the signal-to-total-distortion ratio at its output at the optimum sampling times. No nonadaptive filter can do this except for a single distortion condition, such as matched filters do when white noise distortion predominates. However, dynamic adaptive filters ideally can maximize the signal-to-total-distortion ratios at their outputs under all distortion conditions. Dynamic adaptive demodulator filters are therefore the best because they can provide significant and sometimes substantially better bit-error-probability performances with respect to nonwhite additive distortions and multiplicative distortions than nonadaptive and even quasi-static adaptive filters. However, little use has been made of them primarily because little is known about their theoretical performance and practical

---

<sup>5</sup> Partially coherent PSK should not be confused with the commonly used time-differentially coherent PSK whose performance with respect to all types of distortion is significantly or substantially poorer.

design. Therefore, the theoretical and experimental development of adaptive demodulator filters should be pursued.

Transmitter power affects the bit-error-probability performance of a system only with respect to additive channel and equipment distortions. In properly designed receivers, additive equipment distortions are not significant (considered below). Of the two types of additive channel distortions (noise and interference), noise is probably predominant in determining the bit-error-probability performances of systems only a small fraction of the time. Therefore, except for systems that may use relatively low transmitter powers, increasing transmitter power will have relatively little effect in improving system performances with respect to noise. Increasing transmitter powers to improve system performances with respect to interference is undesirable because it is self-defeating; if all transmitter powers are raised proportionally, no improvement with respect to interference is achieved. Therefore, except for systems that may be using relatively low powers, increasing transmitter powers is not desirable.

It is not possible to specify one best type of antenna for transmitting or receiving. In general, both transmitting and receiving antennas should have gains as high as are practically consistent with acceptable size, portability, and steerability. Electronically adaptable receiving antennas are highly desirable because of their ability to reject interference. However, little use has been made of them because of their limited availability. Therefore, the theoretical and experimental development of adaptive receiving antennas should be pursued.

Diversity reception in general can substantially improve the bit-error-probability performances of any system with respect to all types of channel and equipment distortions. However, the performance improvement provided by single-transmission diversity (p. 72) without increasing transmitter power or signal bandwidth can be equaled by multiple-transmission diversity only with an increase in transmitter power by a factor of  $D$ , the order of diversity, and by an increase in

signal bandwidth by a factor of  $D$ . At the same time, single-transmission diversity requires  $D$  receiving antennas and  $D$  HF receivers, while multiple-transmission diversity requires only a single receiving antenna and a single HF receiver. However, with dual diversity ( $D=2$ ), a single antenna with dual polarization can provide single-transmission polarization diversity. Therefore, the best dual diversity method is probably polarization diversity because it can be obtained with a single receiving antenna without increasing transmitter power, signal bandwidth, or interference to other systems. Higher order single-transmission separation diversity with  $D$  receiving antennas or  $D/2$  dual-polarized antennas should be used when practical.

Error coding, like diversity, can significantly or substantially improve the bit-error-probability performance of any system with respect to all types of channel and equipment distortions. In general, the performance improvement increases as the complexity of the coding increases; i.e., as the block size in block codes or constraint length in convolutional codes (p. 9) increases. The bit-error-probability performance improvement also generally increases as the coding ratio, and consequently the spectral efficiency, decrease. It is not possible to specify one best code; in general, the performance improvement must be balanced against the complexity (practicality) of the code and the reduction in spectral efficiency to obtain an optimum compromise. However, soft decoding in convolutional or block codes can provide substantially better error correction, and therefore substantially better performance improvement, than hard decoding, because it makes use of additional valuable information: that the magnitude of the demodulator pulse samples and the bit errors are highly correlated in HF digital radio systems because of the Rayleigh-fading characteristics of HF channels. Therefore, soft error-correcting coding should be used with a code that achieves an optimum balance between bit-error-probability performance improvement, coding complexity, and reduction in spectral efficiency.

The preceding evaluation considered the best combinations of system

design features (p. 77) for simultaneously maximizing the bit-error-probability performance and spectral efficiency of an HF digital radio system. While spectral efficiency is independent of the type and amount of channel and equipment distortions, bit-error-probability performance is not. Therefore, it is also possible to improve the bit-error-probability performance of a system by reducing or effectively eliminating equipment distortions.

Because transmitter distortions are generated prior to the HF channel, they suffer the same fading as the signal. The signal therefore does not fade into the transmitter distortions as it does the receiver distortions to produce bit errors. Consequently, greater transmitter distortions can be tolerated than receiver distortions without significantly affecting the bit-error-probability performance of a system. If the rms level of the transmitter distortions is approximately  $< -30$  dB relative to the rms level of the signal, the distortions have no significant effect on the bit-error-probability performance of a system. Most present-day systems meet this criterion, so significant system performance improvements are not possible with further reductions in transmitter distortions.

Because HF channels exhibit multipath propagation that produces frequency-selective fading, the relative level of receiver distortions must be substantially lower than transmitter distortions, approximately  $< -60$  dB, to have little or no significant effect on bit-error-probability performance in frequency-multiplexed systems. Many if not most present-day systems do not meet this criterion, and their bit-error-probability performances are substantially degraded as a result. It is quite practical to eliminate effectively all receiver distortions except synchronization and Doppler-correction distortions. Internal interference can be effectively eliminated by suitable decoupling (filtering and shielding). Demodulator analog-to-digital converters typically use 8 bits/sample which introduces excessive quantizing noise; this can easily be substantially reduced and effectively eliminated by using converters with 12 or more bits/sample. The HF receiver filtering distortion

introduced by analog lumped-element IF filters can be effectively eliminated by using digital filters, which can completely eliminate delay distortion and greatly reduce amplitude distortion. A greater selection of filter responses is also much easier to obtain.

Substantial improvements in demodulator synchronization and Doppler-correction circuits are also possible. For example, the USC-10 and ACQ-6 frequency-multiplexed, time-differentially coherent, quaternary PSK systems that were described earlier (p. 108) incorporate 4.24-ms guard times. With optimum synchronization, both systems would reject channel differential-delay distortion for any number of paths whose maximum differential delay does not exceed the guard time. However, as shown by the USC-10 and ACQ-6 bit-error-probability curves in Figure 27, p. 109, the slot synchronization circuits in these modems permit differential-delay distortion to enter rapidly when the two-path differential delay exceeds about 1.9 ms for the USC-10 and 2.1 ms for the ACQ-6, values that are somewhat less than one-half the 4.24-ms guard time. Better synchronization and Doppler-correction circuits are desirable and practical, and should be developed.

Most HF receivers incorporate a fast AGC circuit for use with digital systems. It can be argued that a fast AGC circuit can partly compensate amplitude changes in a signal imposed by a fading channel, but not the phase changes, thereby partly reducing the amplitude portions of the crosstalk and coherence frequency-scatter distortions. Fast HF receiver AGC circuits are therefore presumably desirable. It is known (Watterson and Minister, 1975) that under frequency-flat channel fading conditions (a single fading path with no Doppler shift), a fast AGC will keep a frequency-multiplexed, time-differentially coherent, quaternary PSK signal from fading into excessive demodulator additive distortions to improve system performance with respect to these distortions, while producing no change in system performance with respect to the channel fading distortions, presumably because the phase portion of the coherence fading distortion is not affected. However, it is also known that under

multipath channel conditions a fast AGC can degrade the bit-error-probability performance of a system. Unequal AGC attack and release times may be a factor. Additional work needs to be done on the effects of various receiver AGC characteristics on the performances of various types of digital systems.

## 7.2 System Operation

The performance of any HF digital radio system changes both with HF operating frequency and time, because both the additive and multiplicative channel distortions change with frequency and time. For this reason, most systems have a number of available operating frequencies or channels so that ideally at any time the channel that provides the best system performance can be chosen and used. However, this requires a knowledge of the system performance for the channel that is being used (performance monitoring) and an estimate of the system performance on the other available channels (performance prediction).

Of the three performance-monitoring methods that are described on p. 74, monitoring of the signal-to-total-distortion ratio in the demodulator should be used because it is simple, effective, and can be used in systems with or without error coding. In systems with error coding, monitoring of the detected and corrected bit errors should also be used because it is most accurate and specifies the system bit-error-probability performance directly.

Five performance-prediction methods are listed on p. 75. In simplex systems, the two methods of predicting system performance on available channels, experience and propagation predictions, should both be used because, while they have limited accuracy, they are the only methods available. In duplex systems, system sounding is the best of the three performance-prediction methods for several reasons: System sounding provides the most accurate predictions because it utilizes the actual communication system, including antennas; i.e., rather than measuring

channel characteristics to predict indirectly how the HF digital radio system will perform, it directly measures the performance of the system. System sounding also requires no auxiliary equipment, and does not introduce additional interference into other systems as oblique sounders do.

## 8. SUMMARY AND CONCLUSIONS

This report has presented a comprehensive survey of HF digital radio communication techniques to determine the best methods of improving the performance and therefore the reliability of HF digital radio communications. HF digital radio systems consist of three major parts: the transmitter, the HF ionospheric channel, and the receiver. The performances of such systems can be specified in terms of bit error probability and spectral efficiency (information rate/signal bandwidth). The bit-error-probability performance of a system is determined by the signal processing techniques that are used in the transmitter and receiver, and by the types and magnitudes of the distortions that are imposed on the signal by the equipment and the HF channel. The spectral efficiency of a system is determined by the signal processing techniques and is independent of channel and equipment distortions.

The transmitter in general contains an error coder, a modulator, an HF transmitter, and an antenna. The characteristics of the transmitter that affect system performance were considered in detail by classifying and describing the types of error codes: block and convolutional; the digital keying methods: ASK, PSK, APSK, FSK, and CPK; the multiplexing techniques: frequency multiplexing and concentric multiplexing; the HF transmitter operation: frequency translation, filtering, and amplification; the size, gain, bandwidth, and steering characteristics of a large variety of transmitting antennas; and the additive, multiplicative, and nonlinear equipment distortions introduced by the various parts of the transmitter.

The HF channel in general consists of a number of propagation modes or paths over which the signal travels from the transmitter to the receiver. Because the paths introduce different propagation delays, the channel introduces time-scatter multiplicative distortion, and because each path introduces Doppler shift and Rayleigh fading on the signal, the channel introduces frequency-scatter multiplicative distortions. A description was presented of a validated HF channel model that was used to characterize the channel.

The receiver in general contains an antenna, an HF receiver, a demodulator, and an error decoder. The characteristics of the receiver that affect system performance were considered in detail by classifying and describing the types of antennas, including adaptive receiver antennas for suppressing interference; the HF receiver operation: frequency translation, filtering, and amplification; the types of demodulator filters: matched and nonmatched nonadaptive filters and quasi-static and dynamic adaptive filters; the bit-decision (detection) methods: coherent, partially coherent, differentially coherent, and noncoherent; the types of error decoding: hard and soft; and the additive, multiplicative, and nonlinear equipment distortions introduced by the various parts of the receiver. Also classified and described were the types of diversity operation: single-transmission polarization and separation diversity and multiple-transmission frequency and time diversity; and performance monitoring and prediction methods.

The bit-error-probability performance of a system with respect to the various types of channel and equipment distortions is affected by nine system design features: the fundamental pulse waveform, the keying method, the multiplexing method, the type of demodulator filter, the bit-decision (detection) method, the transmitter power, the antennas, diversity, and error coding. The spectral efficiency of a system is determined by the first four and last two of the same design features. The effects of the system design features on bit-error-probability performance were evaluated with respect to additive channel and equipment

distortions, multiplicative channel and equipment distortions, and non-linear equipment distortions in turn. The effects of the system design features on spectral efficiency were evaluated in conjunction with the evaluation of the bit-error-probability performance. The results of the evaluation were then used to determine the best methods of improving the performance and reliability of military HF digital radio communications. These methods are summarized in the following conclusions:

(1) In general, it is not economically or technically practical to modify existing equipment to improve its performance. Therefore, there are only two generally feasible methods that can be used to improve the performance characteristics of military HF digital radio systems:

(a) by incorporating additional equipment without replacing or modifying existing equipment, and (b) by replacing existing equipment with equipment of better design.

(2) There appears to be only one type of additional equipment that might be incorporated with existing systems to improve their bit-error-probability performances: error-coding equipment with hard decoding, because most present-day military HF digital radio systems do not use error coding. However, the necessary reduction in information rate (equal to the coding ratio) may not be acceptable for practical reasons.

(3) While the incorporation of error-coding equipment into existing military HF digital radio systems can significantly improve their bit-error-probability performances, substantially greater improvements in bit-error-probability performances can be obtained with simultaneous improvements in spectral efficiencies by replacing some the the existing equipment with new equipment that utilize an optimum combination of design features. The best equipment designs are considered in the conclusions that follow.

(4) The universally used adjoining rectangular fundamental pulse waveform should be replaced by better waveforms that can and should be developed.

(5) The best combination of keying method and bit-decision (detection)

method is partially coherent PSK with  $M=4$  or  $8$ , or partially coherent APSK with  $M \geq 16$ , depending on the spectral efficiency desired, because they simultaneously provide the best spectral efficiency and the best bit-error-probability performances with respect to all types of channel and equipment distortions.

(6) Concentric multiplexing is better than frequency multiplexing because it provides comparable spectral efficiency with presumably much better immunity to receiver nonlinear distortions.

(7) Dynamic adaptive demodulator filters can provide the best bit-error-probability performances with respect to all types of channel and equipment distortions because they ideally maximize the signal-to-total-distortion ratios at their outputs at the optimum sampling (detection) times. Their performances can be substantially better than those of nonadaptive filters, particularly with respect to channel interference and multiplicative distortions. Their theoretical and experimental development should be pursued.

(8) Except for systems that may be using relatively low powers, increasing transmitter powers is not desirable.

(9) Transmitting and receiving antennas should have gains as high as are practically consistent with acceptable size, portability, and steerability. Electronically adaptive receiving antennas, because of their ability to reject interference, are highly desirable, and their theoretical and experimental development should be pursued.

(10) Diversity can provide substantial improvements in system bit-error-probability performance and should be utilized. Single-transmission polarization and separation diversity are much better than multiple-transmission frequency and time diversity because the latter requires  $D$  times more transmitter power and  $D$  times more bandwidth, where  $D$  is the order of diversity, to provide the same improvement in bit-error-probability performance.

(11) Error coding can provide substantial improvements in system bit-error-probability performance and should be utilized. It is not

possible to specify one best code; in general, the performance improvement must be balanced against the complexity (practicality) of the code and the reduction in spectral efficiency to obtain an optimum compromise. However, soft decoding in convolutional or block codes can provide substantially better error correction, and therefore substantially better performance improvement, than hard decoding, because of the Rayleigh-fading characteristic of the HF channel.

(12) Transmitter distortions, because they fade with the signal, have less effect on system bit-error-probability performance than receiver distortions, into which the signal can fade. The rms level of transmitter distortions should be  $< -30$  dB relative to the rms level of the signal. Most present-day transmitters meet this criterion. Receiver distortions should be  $< -60$  dB relative to the rms level of the signal with or without AGC. Most present-day receivers do not meet this criterion, and their bit-error-probability performances are substantially degraded as a result. It is quite practical to reduce substantially or to eliminate effectively all receiver distortions except synchronization and Doppler-correction distortions. Synchronization and Doppler-correction distortions can be substantially reduced with the development of improved synchronization and Doppler-correction circuits.

(13) The relationship between HF receiver AGC characteristics and system bit-error-probability performance needs further investigation.

(14) In all systems, the signal-to-total-distortion ratio in the demodulator can easily and should be continuously determined to monitor system performance. In systems with error coding, the detected and corrected bit errors should also be monitored.

(15) In simplex systems, the two methods of predicting system performance on unused available channels, experience and propagation predictions, should be used because, while they have limited accuracy, they are the only methods available.

(16) In duplex systems, system sounding (p. 76) is the best method of predicting system performance on unused available channels.

## 9. RECOMMENDATIONS

Based on the preceding results, the following recommendations are made:

(1) The U.S. Department of Defense should consider the practicality of incorporating error coding equipment with hard decoding in present military HF digital radio systems that have no coding to improve system performance for an interim period.

(2) The U.S. Department of Defense should strongly support the theoretical and experimental investigation of improved fundamental pulse waveforms, concentric multiplexing, adaptive demodulator filters, partially coherent detection, electronically adaptive receiving antennas, and soft error-correcting coding in the development of new equipment for longer term improvement of military HF digital radio communications.

## 10. ACKNOWLEDGEMENTS

The author gratefully acknowledges the helpful suggestions provided by H. Akima, E. M. Gray, and J. R. Juroshek in their reviews of the report.

## 11. REFERENCES

- Bailey, D.K. (1959), The effect of multipath distortion on the choice of operating frequencies for high frequency communication circuits, IRE Trans. Ant. Prop. AP-7, pp. 397-404, June.
- Brown, G.J. (1977), High-frequency interference suppression, Tech. Rept. NOSC/TR 155, pp. 1-104, August (Naval Ocean Systems Center, San Diego, CA 92152).
- CCIR (1964), Worldwide distribution and characteristics of atmospheric radio noise, Rept. 322, Doc. Xth Plenary Assembly, pp. 1-78 (Access. No. PB-255060, National Technical Information Service, Springfield, VA 22161).

- Chase, D. (1973), A combined coding and modulation approach for communication over dispersive channels, *IEEE Trans. Commun. COM-21*, pp. 159-174, March.
- Davies, K. (1965), *Ionospheric Radio Propagation*, National Bureau of Standards Monograph 80 (U.S. Gov't Printing Office, Washington, DC 20402).
- DiToro, M.J., J. Hanulec, P. Ahrens, and M. Glass (1964), HF anti-multipath device (Adapticom), Final Rept., Contract No. DA-36-AMC-02339(E), pp. 1.1-7.6, June (Ft. Monmouth, NJ 07703).
- Granger, J.F.N. (1950), Wing-cap and tail-cap aircraft antennas, SRI Rept. No. 6, Proj. 188, pp. 1-49, March (Stanford Research Institute, Menlo Park, CA 94025).
- Jahnke, E., F. Emde, and F. Losch (1960), *Tables of Higher Functions*, pp. 100-109 (McGraw-Hill Book Co., New York, NY).
- Jasik, H. (Editor) (1961), *Antenna Engineering Handbook* (McGraw-Hill Book Co., New York, NY).
- Milstein, L.B., P.K. Das, and D.R. Arsenault (1978), Narrowband jammer suppression in spread spectrum systems using SAW devices, NTC 78 Conf. Record, pp. 43.2.1-43.2.5, Dec. (IEEE Service Center, 445 Hoes Lane, Piscataway, NJ 08854).
- Proakis, J.G. (1968), Probabilities of error for adaptive reception of M-phase signals, *IEEE Trans. Commun. Tech. COM-16*, pp. 71-81, February.
- Salaman, R.K. (1962), A new ionospheric multipath reduction factor, *IRE Trans. Commun. Systems CS-10*, pp. 221-222, June.
- Schwartz, M., W.R. Bennett, and S. Stein (1966), *Communication Systems and Techniques*, p. 401 (McGraw-Hill Book Co., New York, NY).
- Tanner, R.L. (1958), Shunt and notch-fed aircraft antennas, *IRE Trans. Ant. Prop. AP-6*, pp. 35-43, January.
- Watterson, C.C., J.R. Juroshek, and W.D. Bensema (1970), Experimental confirmation of an HF channel model, *IEEE Trans. Commun. Technol. COM-18*, pp. 792-803, December.
- Watterson, C.C., and C.M. Minister (1975), HF channel-simulator measurements and performance analyses on the USC-10, ACQ-6, and MX-190 PSK modems, OT Rept. 75-56, pp. 1-265, July (Access. No. COM75-11206, National Technical Information Service, Springfield, VA 22161).

**BIBLIOGRAPHIC DATA SHEET**

1. PUBLICATION OR REPORT NO. NTIA Report 79-29		2. Gov't Accession No.	3. Recipient's Accession No.
4. TITLE AND SUBTITLE Methods of Improving the Performances of HF Digital Radio Systems		5. Publication Date October 1979	6. Performing Organization Code NTIA/ITS
7. AUTHOR(S) Clark C. Watterson		9. Project/Task/Work Unit No. 9103560	
8. PERFORMING ORGANIZATION NAME AND ADDRESS Institute for Telecommunication Sciences, National Telecommunications and Information Administration, Boulder, Colorado 80303		10. Contract/Grant No. CCC-PO-14-78	
11. Sponsoring Organization Name and Address U.S. Army Communications-Electronics Engineering Installation Agency, Fort Huachuca, Arizona 85613		12. Type of Report and Period Covered Final Report	
14. SUPPLEMENTARY NOTES		13.	
15. ABSTRACT (A 200-word or less factual summary of most significant information. If document includes a significant bibliography of literature survey, mention it here.)  The bit-error-probability performances of HF digital radio systems with respect to channel and equipment additive, multiplicative, and nonlinear distortions are evaluated with respect to the nine system design features that affect the performances. The system design features are the fundamental pulse waveform, the keying method (ASK, PSK, APSK, FSK, and CPK), the multiplexing method (frequency and concentric multiplexing), the type of demodulator filter (matched and nonmatched nonadaptive filters and quasi-static and dynamic adaptive filters), the detection method (coherent, partially coherent, differentially coherent, and noncoherent), the transmitter power, the antennas, diversity, and error coding. Spectral efficiency (information rate/signal bandwidth) is also evaluated. The best combination of design features is determined.			
16. Key Words (Alphabetical order, separated by semicolons)  Adaptive filtering; additive distortion; APSK; ASK; bit error probability; bit error rate; channel model; coding; coherent; CPK; detection; differentially coherent; digital; distortion; diversity; error rate; fading; FSK; HF; ionosphere; keying; modem, multipath; multiplexing; multiplicative distortion; noncoherent; nonlinear distortion; partially coherent; performance; PSK; radio; spectral efficiency.			
17. AVAILABILITY STATEMENT  <input checked="" type="checkbox"/> UNLIMITED.  <input type="checkbox"/> FOR OFFICIAL DISTRIBUTION.		18. Security Class (This report) Unclassified	20. Number of pages 138
		19. Security Class (This page) Unclassified	21. Price:

